

A Novel Method of Estimating GRB Peak Energies Beyond the *Swift*/BAT Limit

LIANG LI^{1, 2, 3} AND YU WANG^{4, 5, 3}

¹ Institute of Fundamental Physics and Quantum Technology, Ningbo University, Ningbo, Zhejiang 315211, People's Republic of China

² School of Physical Science and Technology, Ningbo University, Ningbo, Zhejiang 315211, People's Republic of China

³ INAF – Osservatorio Astronomico d'Abruzzo, Via M. Maggini snc, I-64100, Teramo, Italy

⁴ ICRA and Dipartimento di Fisica, Università di Roma “La Sapienza”, Piazzale Aldo Moro 5, I-00185 Roma, Italy

⁵ ICRA Net, Piazza della Repubblica 10, I-65122 Pescara, Italy

(Received ddmmyyyy; Revised December 12, 2024; Accepted ddmmyyyy; Published ddmmyyyy)

ABSTRACT

The *Swift* Burst Alert Telescope (BAT), operating in the 15–150 keV energy band, struggles to detect the peak energy (E_p) of gamma-ray bursts (GRBs), as most GRBs have E_p values typically distributed between 200–300 keV, exceeding BAT's upper limit. To address this, we develop an innovative method to robustly estimate the lower limit of E_p for GRBs with $E_p > 150$ keV. This approach relies on the intrinsic curvature of GRB spectra, which is already evident within the BAT energy range for such GRBs. By fitting BAT spectra with a cutoff power-law model and extrapolating the spectral curvature beyond BAT's range, we, therefore, can estimate the cutoff energy (E'_c) beyond 150 keV and the corresponding peak energy (E'_p). We applied this method to 17 GRBs, categorizing them into two main groups. Group I (10 bursts) maintains α within a typical range (from ~ -0.8 to ~ -1.20) with increasing E_c ; Group II (2 bursts) maintains E_c within a typical range (300–500 keV) but with varying α . Our results show that for $E_c \lesssim 1000$ keV, the estimated E'_c aligns well with observed values. Moreover, the reliability of E'_c also depends on α : bursts with harder α (e.g., $\alpha \gtrsim -2/3$) show reduced accuracy, while bursts with softer α (e.g., $\alpha \lesssim -2/3$) yield more precise estimates. In conclusion, this method is well-suited for GRB spectra with moderately observed E_c (E_p) values and α indices that are not too hard.

Keywords: Gamma-ray bursts (629); Astronomy data analysis (1858); Time domain astronomy (2109)

1. INTRODUCTION

Gamma-ray bursts (GRBs) are among the most energetic events in the Universe, characterized by brief yet intense emissions of high-energy emission (mostly in γ -ray). Understanding the spectral properties of GRBs is essential for uncovering the physical mechanisms driving these events (e.g., Preece et al. 2000; Kaneko et al. 2006; Goldstein et al. 2012, 2013; Gruber et al. 2014; Yu et al. 2016; Acuner & Ryde 2018; Li 2019a,b; Li et al. 2019; Li & Zhang 2021; Li 2023, and references therein). The photon spectrum of a GRB provides critical insights into the energy distribution of the radiation, with several models proposed to characterize the

observed spectra (e.g., Preece et al. 1998; Lloyd & Petrosian 2000; Geng et al. 2018; Ryde et al. 2019; Acuner et al. 2020). Based on observational data, one of the most frequently used spectral models in the GRB spectral study is the Band function (Band et al. 1993), an empirical model effectively fits the photon spectra across a wide energy range. Phenomenologically, the photon number spectrum of the Band function is defined as

$$N_{\text{Band}}(E) = A \times \begin{cases} \left(\frac{E}{E_{\text{piv}}}\right)^{\alpha} \exp\left(-\frac{E}{E_0}\right), & E < (\alpha - \beta)E_0 \\ \left[\frac{(\alpha - \beta)E_0}{E_{\text{piv}}}\right]^{(\alpha - \beta)} \exp(\beta - \alpha)\left(\frac{E}{E_{\text{piv}}}\right)^{\beta}, & E \geq (\alpha - \beta)E_0 \end{cases}$$

where A is the normalization factor in units of $\text{ph cm}^{-2}\text{keV}^{-1}\text{s}^{-1}$, E_{piv} is the pivot energy always fixed at 100 keV, α and β are the low- and high-energy asymptotic power-law photon indices, respectively, E_0 is the characteristic break energy correlated with the peak energy of νF_{ν} spectrum (assuming $\beta < -2$) by

Corresponding author: Liang Li, Yu Wang
 liliang@nbu.edu.cn; yu.wang@icranet.org

$E_p = (2 + \alpha)E_0$, representing the turning point at which the spectral shape changes from one form to another.

According to the definition, the Band model includes a four-free model parameter (A , α , E_p , and β). Observationally, the spectral indices (α and β) and the peak energy (E_p) are typically distributed around $\alpha \simeq -0.8$ (below the break energy), $\beta \simeq -2.2$ (above the break energy), and $E_p \simeq 220$ keV, respectively (e.g., Preece et al. 2000; Goldstein et al. 2013; Gruber et al. 2014; Yu et al. 2019; Li et al. 2021; Li 2022; Li et al. 2023). It provides a phenomenological fit to GRBs' photon spectra, capturing the emission's complex behavior across different energy ranges and characterizes two distinct spectral regimes: a low-energy power-law component with a photon index α and a high-energy power-law tail with a photon index β , which are smoothly connected at a characteristic break energy, $(\alpha - \beta)E_0$. This smooth transition ensures continuity in the spectrum while fitting the photon spectra across a wide energy range. The model has proven highly effective in describing the emission spectra of the majority of observed GRBs, capturing essential features without assuming specific physical mechanisms (e.g., Yu et al. 2019; Li 2022).

In some cases, the Band function can be replaced by a simpler cutoff power-law function (CPL), which describes a power law with an exponential cutoff. This is particularly useful when the high-energy power-law index (β) is poorly constrained. The CPL function (the first portion of the Band function) is given by

$$N_{\text{CPL}}(E) = A \left(\frac{E}{E_{\text{civ}}} \right)^\alpha \exp\left(-\frac{E}{E_c}\right), \quad (2)$$

where E_c is the cut-off energies, which defines the energy at which the photon spectrum transitions from the low-energy power law to the high-energy exponential cutoff, and correlated with the peak energy E_p of the νF_ν spectrum through $E_p = (2 + \alpha)E_c$.

Observationally, GRB prompt emission is well known to have strong spectral evolution (e.g., Yu et al. 2019; Li et al. 2019, 2021, 2023, and references therein). The Band model is often preferred for time-integrated spectral analysis, as it accumulates more high-energy photons, ensuring that the high-energy segment can be better constrained. Conversely, the CPL model is frequently used for time-resolved spectral analysis, as short timescales often lack sufficient high-energy photons for robust fitting. Both models are standard tools for characterizing the observed spectra, providing nearly equivalent fits to observational data and being widely adopted in nearly all GRB studies (e.g., Kaneko et al. 2006; Goldstein et al. 2012; Gruber et al. 2014; Li 2019a, 2022, 2023, and references therein).

The peak energy, E_p , refers to the energy at which the photon spectrum reaches its maximum in the νF_ν representation, represents the energy at which most of the energy of the selected spectrum (time-resolved analysis) or the entire burst (time-integrated analysis) is released. Therefore, E_p may holds important information and clues for understanding the radiation mechanism of GRBs. Here, we discuss the potential physical meaning of E_p and its relevance to GRB studies.

- Distinguishing radiation mechanisms. For synchrotron radiation, E_p is typically in the range of a few hundred keV, emitted by relativistic electrons in a magnetic field. In contrast, inverse Compton scattering, where these relativistic electrons upscatter lower-energy seed photons, shifts E_p to tens to hundreds of MeV range (Piran 2004).
- Dynamical properties of the relativistic jet. The observed value of E_p is affected Doppler boosting depending on the Lorentz factor of the jet. A larger Lorentz factor results in a higher observed E_p , making it a key diagnostic of the jet's velocity (Lithwick & Sari 2001).
- Differentiating thermal and non-thermal components. Thermal emission, typically associated with the GRB photosphere, produces a well-defined Planck-like peak near E_p , reflecting the characteristic temperature of the emitting region. In contrast, non-thermal processes, such as synchrotron radiation from relativistic particles, produce a broader and more complex spectral shapes around E_p (Pe'er & Ryde 2011).
- GRB classification. SGRBs, typically resulting from compact object mergers (Eichler et al. 1989; Berger 2014; Abbott et al. 2017), exhibit higher E_p values compared to LGRBs, which are associated with the collapse of massive stars (Woosley 1993; MacFadyen & Woosley 1999; Hjorth et al. 2003). This difference is attributed to the jet properties: SGRB jets are generally less baryon-rich and are launched with higher Lorentz factors, leading to more energetic photons and a higher E_p . By contrast, LGRBs, with slower jets and more massive outflows, tend to produce lower E_p values (Kouveliotou et al. 1993).
- Redshift and cosmological implications (standard candle). The empirical correlation between E_p and the isotropic energy $E_{\gamma,\text{iso}}$, known as the Amati relation (Amati et al. 2002), along with similar correlations such as the Yonetoku relation between E_p and the peak luminosity (Yonetoku et al.

2004), establishes GRBs as tool for measuring the redshifts. These relations highlight the potential of GRBs as standard candles, similar to Type Ia supernovae, for probing the universe's expansion history by the observational quantities (Nava et al. 2011).

Since 2004, NASA's *Swift* satellite has revolutionized GRB studies (Gehrels et al. 2004; Burrows et al. 2005; Berger et al. 2005; Campana et al. 2006). It enabled rapid localization and multi-wavelength observations of these events. Major breakthroughs include the discovery of GRB afterglows and confirming distinct origins for long and short GRBs. *Swift* also advanced research on supernovae, black hole formation, and high-redshift cosmology (Gehrels et al. 2009). The satellite carries three instruments: the Burst Alert Telescope (BAT; Barthelmy et al. 2005), the X-Ray Telescope (XRT; Burrows et al. 2005), and the UV-Optical Telescope (UVOT; Roming et al. 2005). The *Swift*/BAT (15-350 keV) instrument¹, while highly effective in detecting and localizing GRBs, has limitations in its energy range, which is restricted to 15-150 keV. This constraint makes it less sensitive to higher-energy emissions, necessitating complementary data from other instruments like Fermi/GBM (Meegan et al. 2009) for broader spectral coverage.

Observational data from multiple satellites with a wider spectral window (e.g., Fermi/GBM) have revealed that the E_p distribution of GRBs covers at least 3 orders of magnitude, with peak values typically falling within the range of 200-300 keV. Consequently, for most GRBs, the typical E_p exceeds the upper limit of the effective energy range (15-150 keV) observed by the *Swift*/BAT. This situation implies that many GRBs detected by *Swift* do not have their E_p measured within the BAT energy band, leading to challenges such as uncertainties in spectral k -corrections (1-10⁴ keV) and accurate calculations of isotropic total release energy $E_{\gamma,\text{iso}}$. To estimate a E_p for *Swift*/BAT GRBs, several attempt has been made by many authors. For instance, Sakamoto et al. (2009) has employed a simple empirical correlation ($\Gamma_{\text{BAT}} - E_p$) between the photon index Γ_{BAT} and the peak energy (E_p) to provide rough estimates of E_p , where Γ_{BAT} is the photon index derived from the power-law model fit. However, this approach suffers from significant random uncertainties for individual GRBs, which can result in inaccurate estimates. Moreover, some recent studies (Yu et al. 2019; Li et al. 2021) have suggested that the $\alpha - E_p$ correlation may not al-

ways exhibit strong consistency if we consider that Γ_{BAT} measured from *Swift*/BAT is the same as α obtained from *Fermi*/GBM; variations in correlation have been observed across different samples and even among distinct bursts.

In practice, when analyzing a GRB spectrum within a relatively narrow energy band (e.g., *Swift*/BAT GRBs)-especially when the upper limit of the observed energy range is much lower than E_p -the spectrum may only be adequately fit by a single power-law function, which can be defined as $N(E) = A(E/E_{\text{piv}})^{-\Gamma}$. However, the intrinsic GRB spectrum is likely curved across a broader energy range. Due to the limitations imposed by the narrow observational band, E_p and significant non-linear spectral features may go undetected. Consequently, the relationship $\Gamma \neq \alpha$ may arise. This discrepancy may helps to explain the inconsistencies observation between the typical Γ values obtained from *Swift*/BAT and the typical α values from *Fermi*/GBM, with the former typically yielding softer spectral indices compared to the latter.

Following these lines of argument, well-determined E_p of *Swift*/BAT GRBs is important for both the GRB physics and observation. Together with XRT and UVOT instruments, one can provide a full data analysis of multi-wavelength observation covering both prompt emission and afterglow emission from the same satellite and therefore ensure a consistency data analysis. On the other hand, we cannot rule out the possibility that, although some statistical criteria to assess the goodness-of-fit, such as reduced chi-squared χ^2_r (GBM Band) is better than χ^2_r (BAT PL), when we perform model fitting, the intrinsic spectral data may contribute more weight to the fitting in the high-energy range (>150 keV).

In this paper, we develop a novel method (spectral shape curvature extrapolation method) to search GRB peak energies E_p beyond the *Swift*/BAT limit. Further, we also compare several other possible approaches (e.g., empirical correlation method). The paper is organized as follows. The methodology is presented in Sections 2. The results are presented in Section 3. The discussions are presented in Section 4 and our conclusions are summarized in Section 5. Throughout the paper, the standard Λ -CDM cosmology with the parameters $H_0 = 67.4 \text{ kms}^{-1} \text{ Mpc}^{-1}$, $\Omega_M = 0.315$, and $\Omega_\Lambda = 0.685$ are adopted (Planck Collaboration et al. 2018).

2. METHODOLOGY

The *Swift*/BAT instrument, with its narrow energy range (15-150 keV), struggles to detect the peak energy (E_p) of GRBs. Some new methods for estimating E_p

¹ The effective energy is 15-150 keV.

beyond the *Swift*/BAT limit, such as the curvature extrapolation method based on spectral shape, can be attempted. The underlying principle is that GRB spectra are intrinsically curved. Therefore, even when the intrinsic E_p of a GRB spectrum is significantly higher than the observational limit of the *Swift*/BAT instrument, a well-defined spectral shape within the BAT energy range may still provide valuable information, such as curvature. By using the properties of this curvature, it is possible to estimate a lower bound for E_p above 150 keV with reasonable accuracy.

2.1. Spectral Model Selection: Band versus Cutoff Power Law

The purpose of this study is to estimate the peak energy (E_p) of GRB spectra for those bursts whose detected by the *Swift*/BAT instrument, where E_p lies beyond the BAT limit, based on the standard GRB spectral model (either Band or CPL model) using an extrapolation method. For the Band model, E_p can be directly measured from the observed spectral data. However, the CPL model provides the cutoff energy (E_c) as the measured parameter, with E_p being closely related to both the low-energy spectral index (α) and the cut-off energies (E_c).

By definition, the Band function consists of two components: the low-energy CPL-function component and the high-energy power-law β -function component. These components are mathematically independent, with no intrinsic connection between their power-law indices. The high-energy β function has minimal influence on the curvature κ and other properties of the low-energy spectrum. Consequently, β contributes little to estimates based on the low-energy component. Observationally, E_p is already estimated from the low-energy component, and the lack of direct observations in the high-energy β regime ($E > E_p$) makes β values even more uncertain. In contrast, the cutoff energy E_c from the CPL model directly reflects the low-energy component and is closely related to parameters like the spectral index α and curvature κ . This connection makes E_c crucial in shaping the low-energy spectrum. In addition, we also test the Band function for estimating E'_p , both with a fixed β and with β as a free parameter, yielded suboptimal results for GRBs 140426A and 090510 (see Appendix). Practically, whether the intrinsic GRB spectrum is CPL-like or Band-like, E_c can be estimated from the spectral curvature of the low-energy component. The peak energy E_p can then be calculated using $E_p = (2 + \alpha)E_c$. Therefore, our primary method relies on the CPL function.

2.2. Sample Selection

Our sample selection primarily relies on the Fermi/GBM burst catalog (Li 2023) for its comprehensive coverage of GRBs with known redshifts and detailed spectral parameters. The detailed selection considerations:

1. All the bursts in our target sample are selected from the Fermi/GBM observation. The Fermi/GBM observational bandwidth encompasses the energy range of *Swift*-BAT, allowing us to select the lower-energy portion corresponding to the BAT energy range to mimic *Swift*-BAT fitting. The higher-energy data are then used to test our method for estimating E_p beyond the BAT energy limit.
2. Since the effective energy range of *Swift*-BAT spans 15–150 keV, our sample excludes bursts with observed E_p values below 150 keV, as these are directly measurable within the BAT energy range.
3. To capture the intrinsic curvature of spectral data within the *Swift*/BAT energy range, we prioritize bright bursts. This is because high-quality spectral data are more readily obtained from bright bursts compared to weaker ones, allowing for a more detailed investigation of the curvature features of the CPL function in the low-energy region below E_p .
4. Previous studies (e.g., Ryde et al. 2010) revealed that a significant fraction of GRBs may exhibit coexisting thermal (Planck function-like) and non-thermal (Band-like) spectral components, with the thermal component typically appearing as a sub-dominant feature on the left shoulder of the spectrum. A recent study (Li 2019b) suggest that the thermal component plays a crucial role in determining the observed Band-like E_p values and low-energy spectral index α . To mitigate contamination from such thermal contributions, we ensure that our sample only includes cases where the CPL (or Band) model is the optimal spectral representation, excluding events like GRB 110721A (e.g., Axelsson et al. 2012; Iyyani et al. 2013), which is characterized by a prominent sub-thermal component.

5. To assess whether the effectiveness of our extrapolation method varies with increasing E_c values, we select 10 GRBs (see the upper-panel of Table 18) from Li (2023) that exhibit gradually increasing observed E_c values and the optimal spectral representation is the CPL model. Moreover, the low-energy spectral index α could also affect E_c estimations, we therefore select α is approximately around -1, with minimal fluctuations, specifically within the range of -0.80 to -1.20. This is because we aimed to ensure that our selected bursts have consistent α values thereby isolating E_c as the primary variable in our analysis. These bursts were incorporated

into the sample and are collectively referred to as Group I in our analysis.

6. Similarly, to evaluate whether the effectiveness of our extrapolation method is influenced by varying α values, we select a subset of GRBs including two interesting events (see the lower-panel of Table 18) from Li (2023) that exhibit a gradual change in observed α values and the optimal spectral representation is the CPL model. As the observed E_p might also affect the accuracy of the estimated E'_p , we focus on GRBs with observed E_p values approximately within 200-400 keV, ensuring minimal fluctuations. These bursts are incorporated into our sample and are collectively referred to as Group II in the subsequent analysis.

7. A similar test is also applied to events where the optimal spectral representation is the Band model, including five interesting bursts (see Table 19). These bursts are included in our sample and are collectively referred to as Group III in the subsequent analysis.

2.3. Modeling Peak Energies Beyond 150 keV

We develop a method that integrates several fixed- E_p spectral fittings, Markov Chain Monte Carlo (MCMC) sampling, and information criterion analysis to explore the parameter space and infer a robust lower limit on E_p when it exceeds the instrument's upper energy threshold. As detailed in Section 2, our approach employs the CPL function, which parametrizes the photon flux $N(E)$ as a combination of a smoothly connected power-law and an exponential decay. Main steps include:

1. To retrieve the original spectral data, we employed 3ML (the Multi-Mission Maximum Likelihood Framework, see Vianello et al. 2015), following to the standard procedures (Li et al. 2019; Li 2019b; Yu et al. 2019; Burgess et al. 2019; Li 2020; Li & Zhang 2021; Li et al. 2021) outlined by the Fermi Science Team. These procedures include the selection of detectors, sources, and background intervals. We rebin the spectral data for each GRB based on its observed characteristics. For bright bursts, we set the photon count per bin to 100 for the NAI detector and 50 for the BGO detector. For relatively weaker bursts, these thresholds were adjusted downward as needed to maintain an acceptable signal to noise ratio (> 3) of each bin, excessively large error bars were addressed by increasing photon counts per bin. This procedure ensures error bars are reasonable and spectral data points are sufficient, which are critical for capturing the intrinsic spectral curvature.

2. To estimate a lower limit on E_c , we fix E_c at a series of values extending beyond the BAT's upper limit (e.g., 22 values from 150 keV to several MeV). For each fixed E_c , we use MCMC sampling to explore the posterior

distributions of the free parameters (A , α , and β). We employ the affine-invariant ensemble sampler (Goodman & Weare 2010), which is efficient for exploring complex parameter spaces. Typically, 20 walkers are used with 6000 iterations per walker. The first 3000 iterations are discarded as burn-in to ensure convergence. This process provides robust posterior estimates for the model parameters.

3. For each fixed E_c , we compute several statistical criteria to assess the goodness-of-fit while accounting for model complexity: Akaike Information Criterion (AIC, Akaike 1974):

$$\text{AIC} = 2k - 2\ln\mathcal{L}, \quad (3)$$

where k is the number of free parameters in the model and \mathcal{L} is the maximized value of the likelihood function for the model. Bayesian Information Criterion (BIC, Schwarz 1978):

$$\text{BIC} = k\ln N - 2\ln\mathcal{L}, \quad (4)$$

where k is the number of model parameters, and N is the number of data points, \mathcal{L} is the maximum likelihood. Deviance Information Criterion (DIC, Spiegelhalter et al. 2002):

$$\text{DIC} = -2\log[p(\text{data} | \hat{\theta})] + 2p_{\text{DIC}}, \quad (5)$$

where $\hat{\theta}$ is the posterior mean of the parameters over the MCMC samples, and p_{DIC} is a term to penalize the more complex model for overfitting (Gelman et al. 2014). Reduced Chi-squared (χ^2_ν):

$$\chi^2_\nu = \frac{1}{\nu} \sum_{i=1}^n \left(\frac{O_i - E_i}{\sigma_i} \right)^2 = \frac{\chi^2}{\text{DOF}}, \quad (6)$$

where O_i and E_i are the observed and expected counts, σ_i are the measurement uncertainties, and $\nu = (n - k)$ is the degrees of freedom (DOF), χ^2 is the sum of squared residuals normalized by the uncertainties, and DOF (degrees of freedom) is the number of data points minus the number of fitted parameters.

4. We analyze how the information criteria vary with changing fixed E_c . As E_c exceeds the true peak or cut-off energy, improvements in fit quality diminish, creating a “bending point” or plateau in the criteria curves (E_c versus Information Criterion). This bending point provides a robust lower limit for E_c . To estimate the uncertainty in this lower limit, we examine the spread of bending points across different criteria. Additionally, the posterior distributions from MCMC sampling provide credible intervals for A and α at each fixed E_c .

5. To quantitatively evaluate the quality of the model comparisons, we primarily adopt DIC and also referred

to Reduced Chi-squared statistic (χ^2_r) for supplementary insight. The choice of DIC as the main criterion is motivated by the full application of Bayesian analysis and MCMC sampling in this study. The difference in DIC values between two models is defined as $\Delta\text{DIC} = \text{DIC}_1 - \text{DIC}_2$ and serves an indicator of model preference. Four levels are commonly used to interpret ΔDIC .

- Level 1 ($\Delta\text{DIC} < 2$): The two models are statistically indistinguishable.
- Level 2 ($2 \leq \Delta\text{DIC} < 5$): Model 2 is weakly preferred over Model 1.
- Level 3 ($5 \leq \Delta\text{DIC} < 10$): Model 2 is significantly better than Model 1
- Level 4 ($\Delta\text{DIC} \geq 10$): Model 2 is strongly favored over Model 1. A difference of $\Delta\text{DIC} \geq 10$ is often considered robust evidence favoring one model over another.

These thresholds are consistent with the principles of other model selection criteria, such as AIC and BIC, and are well-supported by Bayesian model selection theory (Spiegelhalter et al. 2002; Burnham & Anderson 2004). The advantage of DIC lies in its ability to handle hierarchical models and account for model complexity through (p_D).

Additionally, the reduced chi-squared statistic (χ^2_r) is a commonly used measure of model fit in observational sciences and the absolute value of χ^2_r should be considered. Ideally, $\chi^2_r \approx 1$, indicating that the residuals are consistent with the assumed uncertainties. However, the interpretation of χ^2_r depends on factors such as dataset size and the uncertainty estimation. For instance, a χ^2_r slightly above 1 may be acceptable for datasets with high degrees of freedom. Typical interpretation of χ^2_r include: $\chi^2_r \approx 1$: The model fit well, with residuals appropriately reflecting uncertainties. $\chi^2_r < 1$: The model may be overfitting the data, potentially overestimating complexity or uncertainty. $\chi^2_r > 1$: The model may be underfitting, failing to capture the observed variance.

When comparing two fits, the difference in reduced chi-squared values, denoted as $|\Delta\chi^2_r|$, can provide insights into model preference. For statistical equivalence between two models, $|\Delta\chi^2_r|$ should be close to 0. The χ^2 statistic follows a chi-squared distribution, allowing the calculation of a corresponding p -value to assess the model's compatibility with the data. A p -value < 0.05 suggests that the model does not adequately describe the observations, implying the null hypothesis (that the model fits the data) is unlikely. This dual consideration

of χ^2_r and p -value provides a comprehensive framework for evaluating model fits and comparing alternatives in a statistically rigorous manner.

3. RESULTS

Existing catalogs of GRB spectral parameters from wide-bandwidth satellites, such as BATSE (Preece et al. 2000; Goldstein et al. 2013) and GBM (Goldstein et al. 2012; Gruber et al. 2014), reveal that the typical peak energy E_p distribution lies around 200-300 keV. This value significantly exceeds 150 keV, indicating that for a substantial fraction of GRBs observed by *Swift*, their E_p values cannot be determined using *Swift* data alone.

Figure 1 shows the E_p distribution for the complete Fermi/GBM burst catalog, available at the NASA/HEASARC database². This catalog (represented by the grey shaded area) includes a total of 3762 bursts (as of May 2024). The E_p distribution is fitted with a log-normal distribution, $N(\mu, \sigma^2)$, where μ and σ represent the mean and standard deviation, respectively. The best-fit parameters yield $N(2.24, 0.44^2)$, shown by the red line in Figure 1.

To estimate the fraction of bursts with E_p observed within the *Swift*/BAT energy range (15-150 keV) based on the full Fermi/GBM burst sample, we define two separation lines respectively corresponding to $E_p = 15$ keV and $E_p = 150$ keV, and the area enclosed by the two lines represents the BAT energy range (highlighted by the red slash-shaded region in Figure 1). The cumulative distribution for the BAT energy range, denoted as $F(E) = P_{(15\text{keV} \leq E_p \leq 150\text{keV})}$, is calculated to be $F(E) = 0.43$. This result indicates that only approximately 43% of the GBM-detected bursts have their E_p values falling within the BAT energy range, while the remaining 57% have their E_p values located outside this range.

3.1. Simulation Results

GRB spectra often exhibit curvature, a key feature requiring quantitative investigation. To study this, we conducted a series of simulations using the CPL model. First, a synthetic CPL spectrum was generated with typical parameters: normalization $\hat{A} = 1$, photon index $\hat{\alpha} = -1$, and cutoff energy $\hat{E}_{\text{cut}} = 300$ keV. Using these baseline parameters, we simulated 500 spectral data points within the *Swift*/BAT energy range (15-150 keV), adding Gaussian noise with a standard deviation of 10% of the intrinsic values. To assess the effect of varying E_{cut} , we fixed A and α and generated CPL spectra for E_{cut} values of 100, 120, 150, 200, 300, 500, and

² <https://heasarc.gsfc.nasa.gov/W3Browse/fermigbrst.html>

1000 keV, producing seven spectra. To account for amplitude differences, A was normalized for each E_{cut} to ensure comparability (details in Appendix). For each case, we calculated the spectral ratio (data-to-model ratio) and the corresponding residuals to examine deviations from the model.

Figure 2 shows the simulation results. In the top panels of Fig. 2a and Fig. 2b, the red scatter points represent the 500 simulated data points in the 15–150 keV range based on the CPL model using typical model parameters, while the solid curves of various colors depict CPL spectra corresponding to different E_{cut} values across the broader 1–10,000 keV range. The gray dashed line indicates a power-law function with the same A and α values as the CPL model, providing a comparative baseline. The BAT energy range is highlighted by the red slash-shaded region.

The lower panels of Figure 2a present the ratio evolution for $E_{\text{cut}} = 100, 120, 150, 200, 300, 500$, and 1000 keV, respectively. For each E_{cut} , at low energies (near 15 keV), the ratios for all E_{cut} values converge to approximately 1, indicating a good agreement between the data and the model. However, at higher energies (close to 150 keV), significant deviations emerge. For $E_{\text{cut}} < \hat{E}_{\text{cut}}$ (e.g., $E_{\text{cut}} = 100$ keV), the ratio increases above 1 as energy increases, reflecting a systematic overestimation of the data by the model. When $E_{\text{cut}} = \hat{E}_{\text{cut}}$, the ratio remains near 1 across the entire energy range, with minimal fluctuation. Conversely, for $E_{\text{cut}} > \hat{E}_{\text{cut}}$ (e.g., $E_{\text{cut}} = 1000$ keV), the ratio decreases below 1 at higher energies, indicating an underestimation of the data. These trends underline the sensitivity of spectral ratios to variations in E_{cut} , providing a diagnostic tool for identifying the most physically representative model parameters.

The lower panels of Figure 2(b) show the residual evolution for the same E_{cut} values. Notably, the scatter of residuals is larger at low energies (near 15 keV) compared to high energies (near 150 keV), particularly for smaller E_{cut} values (e.g., $E_{\text{cut}} = 100$ keV). This behavior may reflect the combined effects of statistical noise and intrinsic model limitations at lower energy ranges. For $E_{\text{cut}} < \hat{E}_{\text{cut}}$, the residuals predominantly reside in the positive domain, implying systematic mismatches between the data and the model. When $E_{\text{cut}} = \hat{E}_{\text{cut}}$, the residuals fluctuate near zero, signifying excellent model agreement. For $E_{\text{cut}} > \hat{E}_{\text{cut}}$, the residuals are mostly negative, indicating systematic underfitting of the data by the model.

This methodology allows us to constrain E_c even when it exceeds the instrument's energy range. The MCMC approach offers a full probabilistic characterization of

the parameters. However, it is important to note that this method normally provides a lower limit for E_c , rather than an exact value. Its precision depends on factors such as the signal-to-noise ratio of the data and how much the true E_c exceeds the instrument's capabilities.

3.2. Application to Observational Data

When applying our method to real observational data, we address the following critical questions: How well does the E'_c obtained via the extrapolation method correlate with the observed E_c ? Does E'_c evolve with changes in E_c ? If so, what is the nature of this evolution? Does different α values affect the E'_c results? To explore these questions, we conducted targeted data analysis as outlined below. In our analysis, we employ a two-step approach to determine the spectral peak energy (E_p) and associated parameters: preliminary estimation and refined estimation.

3.2.1. Preliminary Estimation of E'_c

When analyzing the spectrum of a BAT-detected GRB, the true value of E_c is unknown. Moreover, given that the distribution of E_c spans at least three orders of magnitude, preliminary estimation must be performed over a wide energy range with relatively large intervals between selected E_c values. We therefore selected 22 E_c values ranging from 100 keV to 5000 keV for a preliminary estimation. These values are 100 keV, 120 keV, 150 keV, 180 keV, 200 keV, 220 keV, 250 keV, 300 keV, 400 keV, 500 keV, 600 keV, 700 keV, 800 keV, 900 keV, 1000 keV, 1200 keV, 1500 keV, 1800 keV, 2000 keV, 3000 keV, 4000 keV, and 5000 keV.

This preliminary step enables an efficient and straightforward determination of a rough E_c value. However, the downside is that the estimation may have a relatively large uncertainty. Once a rough E_c value is obtained, the next step involves a refined estimation by focusing on this value and exploring a narrower range with smaller intervals. This refined process allows for a more accurate determination of E_c within a smaller margin of error.

Another critical factor influencing the results is the selection criterion for the DIC. In our analysis, there exists a global minimum DIC value corresponding to the best-fit model. The difference between the DIC value of other models and this global minimum, ΔDIC , provides an intuitive measure of the relative quality of model selection. If the selection criterion is too loose (e.g., $5 < \Delta\text{DIC} \leq 10$), the estimated E'_c derived from the selected model might be significantly lower than the true observed value E_c , resulting in reduced estimation accuracy. Conversely, if the criterion is too stringent (e.g.,

$0 < \Delta\text{DIC} \leq 2$), the selected model becomes statistically indistinguishable from the best-fit model. While this improves accuracy, it undermines the conservative estimation of the lower limit of E_c , as the selected E'_c might even exceed the true observed E_c . Therefore, we adopted an intermediate criterion, choosing the first model satisfying $2 < \Delta\text{DIC} \leq 5$ to determine E'_c , which serves as a reliable lower limit estimation for E_c .

To eliminate the potential influence of variations in α on the results, we selected 10 bursts from the GBM catalog, where α remained relatively constant within a typical and narrow range (~ 0.80 to ~ 1.20), and the E_c gradually increased from 150 keV up to several MeV with a large change. Figures 3-12 present the preliminary estimation results of the spectral cutoff energy (E'_c) for 10 bursts, whose intrinsic spectra follow a CPL-like model. The intrinsic E_c values of these GRBs range from 173 keV to 2837 keV, corresponding to GRB 140703A, GRB 150301B, GRB 160629A, GRB 090529, GRB 091003, GRB 140606B, GRB 120624B, GRB 090328, GRB 120711A, and GRB 130215A, respectively, in the order shown in the Figures.

In the top panel of each figure, we show the raw spectral data for each analyzed burst alongside the CPL function fitted using the extrapolation method with fixed E'_c values. The vertical axis represents photon flux density ($\text{photons cm}^{-2} \cdot \text{s}^{-1} \cdot \text{keV}^{-1}$), as defined in the CPL model. The gray, red, and blue data points represent spectral data from three distinct energy ranges: E_{below} (below the BAT energy band, $E < 15$ keV), E_{BAT} (within the BAT band, $15 \text{ keV} \leq E \leq 150 \text{ keV}$), and E_{above} (above the BAT band, $E > 150$ keV), respectively. The colored curves correspond to the best-fit CPL models for fixed E'_c values of 100 keV, 120 keV, 150 keV, 180 keV, 200 keV, 220 keV, 250 keV, 300 keV, 400 keV, 500 keV, 600 keV, 700 keV, 800 keV, 900 keV, 1000 keV, 1200 keV, 1500 keV, 1800 keV, 2000 keV, 3000 keV, 4000 keV, and 5000 keV. It is important to note that, to simulate the scenario where only *Swift*/BAT data is available, we used only the raw spectral data from the GBM energy range overlapping with BAT. Detailed data analysis and fitting methods are described in Section §2.3. For each fixed E'_c , we derived the CPL model parameters A and α , along with statistical criteria to evaluate goodness-of-fit, such as χ^2 , degrees of freedom (DOF), reduced χ^2 , AIC, BIC, DIC, and p_{DIC} . These results are summarized in Tables 1-16.

In the middle panel of each figure, we plot the statistical criteria (AIC, BIC, DIC, and χ^2) and their deviations from the minimum value (ΔDIC , and $\Delta\chi^2$) as a function of E'_c . These curves generally fall into two categories: (1) “U”-shaped curves with a distinct minimum

(e.g., GRB 140703A, GRB 160629A, and GRB 091003), where the optimal fit function and the corresponding E'_c can be easily identified by identifying the minimum value of the curve; (2) monotonic decreasing curves resembling a “slide” (GRB 150301B, GRB 090529, GRB 140606B, GRB 120624B, GRB 090328, GRB 120711A, and GRB 130215A), where the statistical criteria decrease as E'_c increases, eventually reaching a bending point or plateau. The E'_c at this bending point provides a robust lower limit for the true E_c . To quantitatively identify the bending point, we define thresholds of $\Delta\text{DIC} \leq 5$ and $\chi_r^2 \leq 0.5$. The value of the first E_c value below these threshold is the value we used. Four horizontal red dashed lines in the figures mark these thresholds ($\Delta\text{DIC} \leq 5$ and $\chi_r^2 \leq 0.5$).

In the bottom panel of each figure, we present the preliminary estimation of E'_c in the νF_ν space. The solid green curve represents the best-fit model derived using the full GBM energy range ($E_{\text{below}} + E_{\text{BAT}} + E_{\text{above}}$), from which the true observed E_c is extracted. The four dashed lines of different colors represent the E'_c values determined using various statistical criteria, with vertical dashed lines marking these corresponding E'_c . Comparing different thresholds, we find that the criterion $\text{DIC}=2$ yields E'_c values that are closest to the true E'_c .

To test the applicability of our extrapolation method for estimating the peak energy (E_p) of GRBs with Band-like spectra, we selected five GRBs with intrinsic Band spectral models (Figures 15-19 and Tables 10-17). Their true E_p values range from 280 keV to 5200 keV. Figures 15-19 present the preliminary E_p estimation results for these bursts. The data analysis procedure is identical to that used for CPL-like GRBs, with the primary distinction appearing in the bottom panels of the figures. In the bottom panels, the green solid lines represent the best-fit Band models derived from the GBM energy range, rather than CPL models. Additionally, the estimated E'_c obtained via the extrapolation method is converted to an E_p estimate using the relation, here we define $E'_p = (2+\alpha)E'_c$.

Another important question to address is whether the variation in α values, as measured within the BAT energy range, has a significant impact on the resulting cut-off energy, E'_c .

Similarly, to exclude the potential influence of variations in E_c on the results, we selected two GRBs from the GBM catalog, where E_c remained relatively stable within a typical and narrow range (200 keV to 400 keV), while α gradually increased from -1.9 to -0.4 with a large change (see the lower-panel of Table 18). The data analysis procedure is identical to that used for CPL-like GRBs. Figures 13-14 present the preliminary estima-

tion results of the spectral cutoff energy (E_c) for the two bursts, whose intrinsic spectra follow a CPL-like model. The intrinsic E_c values of these GRBs are $E_c = 418^{+21}_{-20}$ and $E_c = 315^{+19}_{-18}$, and the intrinsic α values of these GRBs range from $-0.51^{+0.02}_{-0.02}$ to $-1.70^{+0.01}_{-0.01}$, corresponding to GRB 100414A, and GRB 180728A, respectively.

We observed that when the low-energy spectral index α is either very hard (e.g., GRB 100414A with $-0.51^{+0.02}_{-0.02}$) or very soft (e.g., GRB 180728A with $-1.70^{+0.01}_{-0.01}$), the E'_c values obtained through the extrapolation method tend to be higher than the true observed E'_c , showing a noticeable deviation. This deviation is particularly pronounced in cases with a harder α (e.g., GRB 100414A). To quantitatively assess these deviations, we define the ratio $k_\xi \equiv (E'_c/E_c)$ as the value of E'_c obtained through the extrapolation method divided by the true observed E'_c . For GRB 100414A, we find $k_\xi = 12.7$ (the statistical criteria $\Delta\text{DIC} \leq 2$ are used), while for GRB 180728A, $k_\xi = 1.6$ ($\Delta\text{DIC} \leq 2$). The results indicate that both GRBs have k_ξ values significantly greater than 1, with k_ξ for GRB 100414A being much higher than that for GRB 180728A. This demonstrates that the deviation for GRB 100414A is considerably larger than that for GRB 180728A.

3.2.2. Refined Estimation of E'_c

We obtained a relatively coarse value of E'_c from the preliminary estimation. These E'_c values, derived through the extrapolation method, are consistent with the true observed values for most GRBs. If the precision requirement for E_c estimation is low, the preliminary estimation suffices. However, for higher precision demands, a refined estimation can be conducted based on the initial E_c results, aiming to confine the uncertainty to a smaller range. The process of refined estimation involves the following steps:

From the preliminary estimation, we found that the statistical criterion $\Delta\text{DIC} \leq 5$ effectively identifies E_c . Thus, we take the E_c value obtained under $\Delta\text{DIC} \leq 5$ as the starting point for refined estimation. For each GRB with $E_c \leq 500$ keV, we select 10 additional E_c values at uniform intervals before the starting point and 5 additional E_c values after it. The interval i is determined as follows: $i=10$ for $E_c \leq 500$ keV, $i=25$ for $500 \text{ keV} \leq E_c \leq 1000$ keV, and $i=50$ for $E_c \geq 1000$ keV.

We repeat all data analysis steps from the preliminary estimation to obtain a finer set of E_c results with smaller intervals and reduced uncertainties. The fitting results (e.g., A , α , χ^2 , DOF, χ^2_r , AIC, BIC, DIC, and p_{DIC}) are summarized in the lower-panel of Tables 1-13. Three GRBs were excluded from this refined analysis because the E_c values obtained from the preliminary estimation

differed significantly from their observed values, rendering further detailed estimation meaningless.

Combining the preliminary and refined estimations, we find that among the 10 GRBs in Group I, 8 GRBs have their estimated E'_c values closely matching the observed E_c . Only two GRBs (GRB 120711A and GRB 130215A) show significant deviation between the estimated E'_c and their observed E_c values, both of which have $E_c > 1000$ keV, far exceeding the upper energy limit of the BAT instrument (150 keV). For the two GRBs in Group II, one (GRB 180728A) exhibits an estimated E'_c that matches the observed value closely, albeit slightly higher. This GRB is characterized by a very soft intrinsic α index (-1.70 ± 0.01). In contrast, the other burst (GRB 100414A) shows a large deviation between its estimated E'_c and observed E_c , with the intrinsic α index being notably hard (-0.52 ± 0.02).

4. DISCUSSIONS

4.1. Curvature in the CPL function within the *Swift*/BAT Energy Range

The curvature of a curve is defined as the measure of its deviation from a straight line, providing a quantitative description of the degree of bending. In the context of gamma-ray burst spectral analysis, curvature can be utilized to examine the bending behavior of the CPL function within the energy range observed by *Swift*-BAT (15-150 keV). This analysis is particularly relevant for evaluating how well the CPL function captures spectral features in this energy band, especially when the intrinsic spectral shape exhibits significant deviation from linearity. We, therefore, use **curvature** to describe the degree of bending of a curve at a point, reflecting how rapidly its geometric shape changes. The formula for curvature in two-dimensional space is given by:

$$\kappa = \frac{|f''(E)|}{\left(1 + (f'(E))^2\right)^{3/2}} \quad (7)$$

where $f(E)$ is the function value corresponding to energy E (e.g., the photon spectrum density in the CPL or Band model), $f'(E)$ is the first derivative of $f(E)$ with respect to E , $f''(E)$ is the second derivative of $f(E)$ with respect to E .

The total curvature is computed using the following integral expression:

$$C = \int_{E_{\min}}^{E_{\max}} \kappa(E) dE \quad (8)$$

where $\kappa(E) = \frac{|f''(E)|}{\left(1 + (f'(E))^2\right)^{3/2}}$ is the curvature at energy E , E_{\min} and E_{\max} are the lower and upper bounds of the energy range (e.g., 15 keV and 150 keV).

This expression is numerically evaluated using the trapezoidal rule, implemented in Python with the `np.trapz` function, which approximates the integral by summing the areas of trapezoids formed under the curve.

To quantitatively evaluate the impact of changes in the cut-off energy E_c on the curvature of the CPL function within the BAT energy range (15-150 keV), we conducted the following analysis. First, we fixed two parameters, the normalization ($A = 1$) and the low-energy spectral index ($\alpha = -1$), at typical values. We then allowed E_c to vary, selecting several representative observational values ranging from 150 keV to 10,000 keV (see the upper-left panel of Figure 20). For each E_c , we calculated the total curvature C (see the upper-right panel of Figure 20) and the corresponding curvature radius ρ (see the lower-right panel of Figure 20). Our results indicate that the total curvature decreases as E_c increases. This suggests that when the intrinsical E_c of a CPL spectrum approaches the upper limit of the BAT energy range (150 keV), the extrapolated curvature provides a more reliable estimate of the E_c , even though the decrease in curvature with increasing E_c is not particularly steep.

Similarly, we analyzed the effect of changes in the low-energy spectral index α on the curvature of the CPL function in the BAT energy band. For this analysis, we fixed $A = 1$ and E_c keV as typical values and allowed α to vary. We selected several representative observational values for α ranging from -1.9 to -0.4 (see the lower-left panel of Figure 20). For each α , we calculated the total curvature C (see the left-panel of Figure 20) and the corresponding curvature radius ρ (see the lower-right panel of Figure 20). We found that the total curvature decreases as α becomes harder, indicating that when the intrinsically α of a CPL spectrum is harder, the extrapolated curvature method yields a more reliable estimate of the true peak energy E_p .

The general effects of each parameter on the curvature of the CPL function based on theory: (1) Normalization A : Typically, the curvature remains nearly unaffected by changes in A because it scales the amplitude of the function without altering the overall shape. (2) Low-energy spectral index α : Changing α often has a noticeable effect on curvature, especially at lower energies, as it alters the slope of the function in this region. (3) Peak energy E_p : Modifying E_p shifts the spectrum's peak, which can significantly affect the curvature, particularly around the peak's location in the energy band. (4) High-energy spectral index β : Variations in β influence the curvature at higher energies, though their impact on curvature in the 15-150 keV range might be

less prominent unless the spectrum has significant high-energy contributions.

4.2. Comparison with Other Methods

[Sakamoto et al. \(2009\)](#) proposed a correlation between the peak energy (E_p) in the νF_ν spectrum and the photon index Γ derived from a simple power-law (SPL) model, expressed as: $\log E_p = 3.258 - 0.829\Gamma$, ($1.3 \leq \Gamma \leq 2.3$). To evaluate this method in comparison to ours, we applied the SPL model to fit the spectral data in the BAT energy range. The fitted photon index Γ and the E_{p1} values derived using the above relation are summarized in Columns 3 and 11 of Table 20. Moreover, we identified 9 GRBs observed simultaneously by both GBM and BAT. For these bursts, we collected fitting results provided by the *Swift* Science Team. It is worth noting that almost all these GRBs were poorly fitted by the SPL model, yet the SPL model was still reported as the best-fitting model on the *Swift* Science Data Centre website³.

We compared several methods for estimating the E_p of *Swift* GRBs, and the results are presented in Figure 21. In the figure, the solid circles represent the true observed E_p values (obtained from GBM data), the stars indicate the E_p values estimated using our spectral curvature extrapolation method, the triangles represent the E_p values derived from the empirical relation proposed by [Sakamoto et al. \(2009\)](#), and the squares denote the E_p values provided by the Science Data Centre website⁴ based on BAT data fitting.

The comparison reveals that the E_p values provided by the *Swift* Science Team show the poorest agreement with the true observed values (GBM data). When compared to the method of [Sakamoto et al. \(2009\)](#), our extrapolation method yields significantly better E_p estimates for nine GRBs. However, for three bursts (GRB 090510, GRB 120711A, and GRB 130215A) neither method performs well. Notably, the true E_p values of these three bursts are exceptionally high ($E_p > 1000$ keV), likely exceeding the applicable range of both methods.

Interestingly, only one burst (GRB 100414A) shows better E_p estimation using the method described in [Sakamoto et al. \(2009\)](#) compared to ours. This exception may be attributed to the harder spectral index (α) of this GRB. Based on this result, we suggest that the method in [Sakamoto et al. \(2009\)](#) might be more reliable for GRBs with harder α values, whereas our curvature

³ <https://swift.gsfc.nasa.gov/results/batgrbcat/>

⁴ <https://swift.gsfc.nasa.gov/sdc/>

extrapolation method is generally more effective for the majority of GRBs.

5. CONCLUSIONS

The *Swift* Burst Alert Telescope (BAT), operating in the 15–150 keV energy band, has significantly advanced our understanding of nature of gamma-ray bursts, in both theory and observation aspects (Gehrels et al. 2009). However, its limited energy coverage poses challenges when analyzing bursts whose spectral peak energies exceed 150 keV, as most GRBs have E_p values typically distributed between 200–300 keV, exceeding BAT’s upper limit. Given that *Swift*/BAT operates within the 15–150 keV energy band, most GRBs with peak energies exceeding 150 keV present a significant challenge for precise E_p estimation. In this paper, we developed an innovative method to reliably estimate the cut-off energy (E'_c) and peak energy (E_p) of GRB spectra observed by the *Swift*/BAT satellite, particularly when the E_c (or E_p) lies above the instrument’s observational energy range (>150 keV).

We selected 17 bright GRBs for performing such a test. In order to perform a self-consistency check, all the bursts are selected from the GBM observations, which provides a broader energy observation window covering both the BAT energy range and higher energy bands beyond BAT’s upper limit. Using the intrinsic curvature of the CPL spectrum within the BAT range, we extrapolated the E'_c values for energies beyond BAT’s range. To examine whether the estimated E'_c values are influenced by the true observed E_c and the low-energy spectral index α , we divided the sample into three Groups. Group I: Consists of 10 GRBs with α values consistently within the typical range, while E_c varies significantly from 150 keV to several MeV. Group II: Includes 2 GRBs with E_c approximately fixed within the typical distribution range but with α values varying significantly. Group III: Includes 5 GRBs where the optimal spectral model is the Band model, providing an additional test for consistency.

We then performed a two-step estimation process for these samples: preliminary estimation and refined estimation. We selected 22 reasonably spaced and gradually increasing E_c values ranging from 150 keV to several MeV. For each GRB in the sample, we fixed E_c and used the CPL model to fit the spectral data within the BAT energy range. Using a statistical criterion of $\Delta\text{DIC} \leq 5$, we preliminarily selected a rough E_c estimate. Based on the results of the preliminary estimation, we then selected a narrower range of E'_c values for each GRB and conducted refined estimation. The number of E'_c values chosen for refinement varied depending on the pre-

liminary results. In Group I, 8 GRBs showed excellent agreement between the extrapolated E'_c and the true observed values. These GRBs all had observed E_c values within a moderate range (150–1000 keV). However, two bursts (GRB 120711A and GRB 130215A) with significantly mismatched E_c estimates had observed E_c values exceeding 1000 keV, far beyond BAT’s upper energy limit. In Group II, one burst (GRB 180728A) showed good agreement between the estimated E'_c and observed E_c , with its α index being relatively soft. In contrast, the other burst (GRB 100414A), characterized by a very hard α index, exhibited a significant mismatch between the estimated E'_c and observed E_c . In Group III, which included GRBs with intrinsic Band-like spectra, the results were consistent with the findings from Groups I and II. These findings align with our simulation results discussed earlier. High E_c values and hard α indices correspond to less pronounced curvature within the BAT energy range, leading to greater uncertainty in E_c estimates derived from this method. Conversely, GRBs with moderate E_c values (150–1000 keV) and α indices near typical values yield reliable extrapolated E_c estimates.

Overall, our analysis indicates that when E_c lies within a moderate range ($150 \text{ keV} < E_c \lesssim 1000 \text{ keV}$) and the intrinsic α index is not too hard ($\alpha \gtrsim -2/3$), the extrapolated E'_c values obtained through this curvature method are consistent with their observed E_c values. Conversely, when E_c is excessively high ($E_c > 1000$ keV) or α is too hard (e.g., beyond the synchrotron radiation death line, Preece et al. 1998, $\alpha = -2/3$), significant deviation arise between the estimated E'_c and observed E_c values. In general, our method achieves higher accuracy compared to directly fitting the spectrum or estimating E_c (or E_p) through empirical relations.

ACKNOWLEDGMENTS

This work is supported by the Natural Science Foundation of China (grant No. 11874033), the KC Wong Magna Foundation at Ningbo University, and made use of the High Energy Astrophysics Science Archive Research Center (HEASARC) Online Service at the NASA/Goddard Space Flight Center (GSFC). The computations were supported by the high performance computing center at Ningbo University.

Facilities: *Fermi*/GBM

Software: 3ML (Vianello et al. 2015), matplotlib (Hunter 2007), NumPy (Harris et al. 2020; van der Walt et al. 2011), SciPy (Virtanen et al. 2020), lmfit

(Newville et al. 2016), `astropy` (Astropy Collaboration et al. 2013), `pandas` (Reback et al. 2022), `emcee`

(Foreman-Mackey et al. 2013), `seaborn` (Waskom et al. 2017)

REFERENCES

- Abbott, B. P., Abbott, R., Abbott, T. D., et al. 2017, ApJL, 848, L13, doi: [10.3847/2041-8213/aa920c](https://doi.org/10.3847/2041-8213/aa920c)
- Acuner, Z., & Ryde, F. 2018, MNRAS, 475, 1708, doi: [10.1093/mnras/stx3106](https://doi.org/10.1093/mnras/stx3106)
- Acuner, Z., Ryde, F., Pe'er, A., Mortlock, D., & Ahlgren, B. 2020, ApJ, 893, 128, doi: [10.3847/1538-4357/ab80c7](https://doi.org/10.3847/1538-4357/ab80c7)
- Akaike, H. 1974, IEEE Transactions on Automatic Control, 19, 716
- Amati, L., Frontera, F., Tavani, M., et al. 2002, A&A, 390, 81, doi: [10.1051/0004-6361:20020722](https://doi.org/10.1051/0004-6361:20020722)
- Astropy Collaboration, Robitaille, T. P., Tollerud, E. J., et al. 2013, A&A, 558, A33, doi: [10.1051/0004-6361/201322068](https://doi.org/10.1051/0004-6361/201322068)
- Axelsson, M., Baldini, L., Barbiellini, G., et al. 2012, The Astrophysical Journal Letters, 757, L31, doi: [10.1088/2041-8205/757/2/L31](https://doi.org/10.1088/2041-8205/757/2/L31)
- Band, D., Matteson, J., Ford, L., et al. 1993, The Astrophysical Journal, 413, 281, doi: [10.1086/172995](https://doi.org/10.1086/172995)
- Barthelmy, S. D., Barbier, L. M., Cummings, J. R., et al. 2005, SSRv, 120, 143, doi: [10.1007/s11214-005-5096-3](https://doi.org/10.1007/s11214-005-5096-3)
- Berger, E. 2014, ARA&A, 52, 43, doi: [10.1146/annurev-astro-081913-035926](https://doi.org/10.1146/annurev-astro-081913-035926)
- Berger, E., Price, P. A., Cenko, S. B., et al. 2005, Nature, 438, 988, doi: [10.1038/nature04238](https://doi.org/10.1038/nature04238)
- Burgess, J. M., Greiner, J., Bégué, D., & Berlato, F. 2019, MNRAS, 490, 927, doi: [10.1093/mnras/stz2589](https://doi.org/10.1093/mnras/stz2589)
- Burnham, K. P., & Anderson, D. R. 2004, Sociological methods & research, 33, 261
- Burrows, D. N., Romano, P., Falcone, A., et al. 2005, Science, 309, 1833, doi: [10.1126/science.1116168](https://doi.org/10.1126/science.1116168)
- Burrows, D. N., Hill, J. E., Nosek, J. A., et al. 2005, Space Science Reviews, 120, 165
- Campana, S., Mangano, V., Blustin, A. J., et al. 2006, Nature, 442, 1008, doi: [10.1038/nature04892](https://doi.org/10.1038/nature04892)
- Eichler, D., Livio, M., Piran, T., & Schramm, D. N. 1989, Nature, 340, 126, doi: [10.1038/340126a0](https://doi.org/10.1038/340126a0)
- Foreman-Mackey, D., Hogg, D. W., Lang, D., & Goodman, J. 2013, PASP, 125, 306, doi: [10.1086/670067](https://doi.org/10.1086/670067)
- Gehrels, N., Ramirez-Ruiz, E., & Fox, D. B. 2009, ARA&A, 47, 567, doi: [10.1146/annurev.astro.46.060407.145147](https://doi.org/10.1146/annurev.astro.46.060407.145147)
- Gehrels, N., Chincarini, G., Giommi, P., et al. 2004, ApJ, 611, 1005, doi: [10.1086/422091](https://doi.org/10.1086/422091)
- Gelman, A., Hwang, J., & Vehtari, A. 2014, STATISTICS AND COMPUTING, 24, 997, doi: [10.1007/s11222-013-9416-2](https://doi.org/10.1007/s11222-013-9416-2)
- Geng, J.-J., Huang, Y.-F., Wu, X.-F., Zhang, B., & Zong, H.-S. 2018, ApJS, 234, 3, doi: [10.3847/1538-4365/aa9e84](https://doi.org/10.3847/1538-4365/aa9e84)
- Goldstein, A., Preece, R. D., Mallozzi, R. S., et al. 2013, ApJS, 208, 21, doi: [10.1088/0067-0049/208/2/21](https://doi.org/10.1088/0067-0049/208/2/21)
- Goldstein, A., Burgess, J. M., Preece, R. D., et al. 2012, The Astrophysical Journals, 199, 19, doi: [10.1088/0067-0049/199/1/19](https://doi.org/10.1088/0067-0049/199/1/19)
- Goodman, J., & Weare, J. 2010, Communications in Applied Mathematics and Computational Science, 5, 65, doi: [10.2140/camcos.2010.5.65](https://doi.org/10.2140/camcos.2010.5.65)
- Gruber, D., Goldstein, A., Weller von Ahlefeld, V., et al. 2014, ApJS, 211, 12, doi: [10.1088/0067-0049/211/1/12](https://doi.org/10.1088/0067-0049/211/1/12)
- Harris, C. R., Millman, K. J., van der Walt, S. J., et al. 2020, Nature, 585, 357, doi: [10.1038/s41586-020-2649-2](https://doi.org/10.1038/s41586-020-2649-2)
- Hjorth, J., Sollerman, J., Møller, P., et al. 2003, Nature, 423, 847, doi: [10.1038/nature01750](https://doi.org/10.1038/nature01750)
- Hunter, J. D. 2007, Computing in Science and Engineering, 9, 90, doi: [10.1109/MCSE.2007.55](https://doi.org/10.1109/MCSE.2007.55)
- Iyyani, S., Ryde, F., Axelsson, M., et al. 2013, MNRAS, 433, 2739, doi: [10.1093/mnras/stt863](https://doi.org/10.1093/mnras/stt863)
- Kaneko, Y., Preece, R. D., Briggs, M. S., et al. 2006, ApJS, 166, 298, doi: [10.1086/505911](https://doi.org/10.1086/505911)
- Kouveliotou, C., Meegan, C. A., Fishman, G. J., et al. 1993, ApJL, 413, L101, doi: [10.1086/186969](https://doi.org/10.1086/186969)
- Li, L. 2019a, ApJS, 242, 16, doi: [10.3847/1538-4365/ab1b78](https://doi.org/10.3847/1538-4365/ab1b78)
- . 2019b, ApJS, 245, 7, doi: [10.3847/1538-4365/ab42de](https://doi.org/10.3847/1538-4365/ab42de)
- . 2020, ApJ, 894, 100, doi: [10.3847/1538-4357/ab8014](https://doi.org/10.3847/1538-4357/ab8014)
- . 2022, ApJ, 941, 27, doi: [10.3847/1538-4357/ac3d89](https://doi.org/10.3847/1538-4357/ac3d89)
- . 2023, ApJS, 266, 31, doi: [10.3847/1538-4365/acc867](https://doi.org/10.3847/1538-4365/acc867)
- Li, L., Ryde, F., Pe'er, A., Yu, H.-F., & Acuner, Z. 2021, ApJS, 254, 35, doi: [10.3847/1538-4365/abee2a](https://doi.org/10.3847/1538-4365/abee2a)
- Li, L., & Zhang, B. 2021, ApJS, 253, 43, doi: [10.3847/1538-4365/abded1](https://doi.org/10.3847/1538-4365/abded1)
- Li, L., Geng, J.-J., Meng, Y.-Z., et al. 2019, ApJ, 884, 109, doi: [10.3847/1538-4357/ab40b9](https://doi.org/10.3847/1538-4357/ab40b9)
- Li, L., Wang, Y., Ryde, F., et al. 2023, ApJL, 944, L57, doi: [10.3847/2041-8213/acb99d](https://doi.org/10.3847/2041-8213/acb99d)
- Lithwick, Y., & Sari, R. 2001, ApJ, 555, 540, doi: [10.1086/321455](https://doi.org/10.1086/321455)
- Lloyd, N. M., & Petrosian, V. 2000, ApJ, 543, 722, doi: [10.1086/317125](https://doi.org/10.1086/317125)
- MacFadyen, A. I., & Woosley, S. E. 1999, ApJ, 524, 262, doi: [10.1086/307790](https://doi.org/10.1086/307790)
- Meegan, C., Lichti, G., Bhat, P. N., et al. 2009, ApJ, 702, 791, doi: [10.1088/0004-637X/702/1/791](https://doi.org/10.1088/0004-637X/702/1/791)

- Nava, L., Ghirlanda, G., Ghisellini, G., & Celotti, A. 2011, *A&A*, 530, A21, doi: [10.1051/0004-6361/201016270](https://doi.org/10.1051/0004-6361/201016270)
- Newville, M., Stensitzki, T., Allen, D. B., et al. 2016, *ascl*, *ascl*
- Pe'er, A., & Ryde, F. 2011, *The Astrophysical Journal*, 732, 49, doi: [10.1088/0004-637X/732/1/49](https://doi.org/10.1088/0004-637X/732/1/49)
- Piran, T. 2004, *Reviews of Modern Physics*, 76, 1143, doi: [10.1103/RevModPhys.76.1143](https://doi.org/10.1103/RevModPhys.76.1143)
- Planck Collaboration, Aghanim, N., Akrami, Y., et al. 2018, arXiv e-prints, arXiv:1807.06209. <https://arxiv.org/abs/1807.06209>
- Preece, R. D., Briggs, M. S., Mallozzi, R. S., et al. 1998, *The Astrophysical Journal Letters*, 506, L23, doi: [10.1086/311644](https://doi.org/10.1086/311644)
- . 2000, *ApJS*, 126, 19, doi: [10.1086/313289](https://doi.org/10.1086/313289)
- Reback, J., jbrockmendel, McKinney, W., et al. 2022, *pandas-dev/pandas: Pandas 1.4.2, v1.4.2*, Zenodo, Zenodo, doi: [10.5281/zenodo.3509134](https://doi.org/10.5281/zenodo.3509134)
- Roming, P. W. A., Kennedy, T. E., Mason, K. O., et al. 2005, *SSRv*, 120, 95, doi: [10.1007/s11214-005-5095-4](https://doi.org/10.1007/s11214-005-5095-4)
- Ryde, F., Yu, H.-F., Dereli-Bégué, H., et al. 2019, *MNRAS*, 484, 1912, doi: [10.1093/mnras/stz083](https://doi.org/10.1093/mnras/stz083)
- Ryde, F., Axelsson, M., Zhang, B. B., et al. 2010, *The Astrophysical Journal Letters*, 709, L172, doi: [10.1088/2041-8205/709/2/L172](https://doi.org/10.1088/2041-8205/709/2/L172)
- Sakamoto, T., Sato, G., Barbier, L., et al. 2009, *ApJ*, 693, 922, doi: [10.1088/0004-637X/693/1/922](https://doi.org/10.1088/0004-637X/693/1/922)
- Schwarz, G. 1978, *Annals of Statistics*, 6, 461
- Spiegelhalter, D. J., Best, N. G., Carlin, B. P., & Van Der Linde, A. 2002, *Journal of the royal statistical society: Series b (statistical methodology)*, 64, 583
- van der Walt, S., Colbert, S. C., & Varoquaux, G. 2011, *Computing in Science and Engineering*, 13, 22, doi: [10.1109/MCSE.2011.37](https://doi.org/10.1109/MCSE.2011.37)
- Vianello, G., Lauer, R. J., Younk, P., et al. 2015, arXiv e-prints. <https://arxiv.org/abs/1507.08343>
- Virtanen, P., Gommers, R., Oliphant, T. E., et al. 2020, *Nature Methods*, 17, 261, doi: [10.1038/s41592-019-0686-2](https://doi.org/10.1038/s41592-019-0686-2)
- Waskom, M., Botvinnik, O., O'Kane, D., et al. 2017, *Mwaskom/Seaborn: V0.8.1* (September 2017), v0.8.1, Zenodo, Zenodo, doi: [10.5281/zenodo.883859](https://doi.org/10.5281/zenodo.883859)
- Woosley, S. E. 1993, *ApJ*, 405, 273, doi: [10.1086/172359](https://doi.org/10.1086/172359)
- Yonetoku, D., Murakami, T., Nakamura, T., et al. 2004, *ApJ*, 609, 935, doi: [10.1086/421285](https://doi.org/10.1086/421285)
- Yu, H.-F., Dereli-Bégué, H., & Ryde, F. 2019, *ApJ*, 886, 20, doi: [10.3847/1538-4357/ab488a](https://doi.org/10.3847/1538-4357/ab488a)
- Yu, H.-F., Preece, R. D., Greiner, J., et al. 2016, *A&A*, 588, A135, doi: [10.1051/0004-6361/201527509](https://doi.org/10.1051/0004-6361/201527509)

Table 1. Results of GRB 140703A

E_c	Level	A (Fixed) (Estimation) ($\text{ph.s}^{-1}.\text{cm}^{-2}\text{keV}^{-1}$)	α	χ^2	DOF	χ^2_r	AIC	BIC	DIC	pDIC
(1)	(2)	(3)	(4)	(5)	(6)	(7)	(8)	(9)	(10)	(11)
Preliminary estimation										
100	Preliminary	1.08×10^{-2}	0.90	36.2	26	1.39	40.2	42.8	40.2	4.05
120	Preliminary	9.71×10^{-3}	0.99	33.1	26	1.27	37.1	39.7	37.1	4.02
150	Preliminary	8.70×10^{-3}	1.09	31.7	26	1.22	35.7	38.3	35.6	3.98
180	Preliminary	8.09×10^{-3}	1.14	31.7	26	1.22	35.7	38.3	35.7	4.01
200	Preliminary	7.80×10^{-3}	1.18	31.9	26	1.23	35.9	38.6	35.9	4.00
220	Preliminary	7.57×10^{-3}	1.20	32.3	26	1.24	36.3	39.0	36.3	4.04
250	Preliminary	7.29×10^{-3}	1.23	32.9	26	1.27	36.9	39.6	36.9	4.04
300	Preliminary	6.98×10^{-3}	1.27	33.9	26	1.30	37.9	40.5	37.9	4.07
400	Preliminary	6.60×10^{-3}	1.31	35.4	26	1.36	39.4	42.1	39.5	4.03
500	Preliminary	6.38×10^{-3}	1.34	36.6	26	1.41	40.6	43.2	40.6	4.02
600	Preliminary	6.24×10^{-3}	1.36	37.4	26	1.44	41.4	44.1	41.4	4.01
700	Preliminary	6.14×10^{-3}	1.37	38.0	26	1.46	42.0	44.7	42.1	4.04
800	Preliminary	6.07×10^{-3}	1.38	38.6	26	1.48	42.6	45.2	42.5	3.99
900	Preliminary	6.01×10^{-3}	1.39	39.0	26	1.50	43.0	45.6	42.9	3.97
1000	Preliminary	5.97×10^{-3}	1.40	39.3	26	1.51	43.3	45.9	43.3	4.02
1200	Preliminary	5.90×10^{-3}	1.41	39.8	26	1.53	43.8	46.5	43.8	3.98
1500	Preliminary	5.83×10^{-3}	1.41	40.3	26	1.55	44.3	47.0	44.3	4.01
1800	Preliminary	5.79×10^{-3}	1.42	40.7	26	1.56	44.7	47.3	44.7	4.01
2000	Preliminary	5.76×10^{-3}	1.42	40.9	26	1.57	44.9	47.5	44.8	3.99
3000	Preliminary	5.70×10^{-3}	1.43	41.4	26	1.59	45.4	48.1	45.4	4.00
4000	Preliminary	5.67×10^{-3}	1.44	41.7	26	1.60	45.7	48.3	45.7	4.04
5000	Preliminary	5.65×10^{-3}	1.44	41.9	26	1.61	45.9	48.5	45.8	3.98
Refined estimation										
50	Refined	2.02×10^{-2}	0.37	89.5	26	3.44	93.5	96.2	93.5	3.95
60	Refined	1.65×10^{-2}	0.55	65.3	26	2.51	69.3	71.9	69.2	3.94
70	Refined	1.42×10^{-2}	0.67	51.9	26	1.99	55.9	58.5	55.8	3.96
80	Refined	1.27×10^{-2}	0.77	44.0	26	1.69	48.0	50.6	47.9	3.89
90	Refined	1.16×10^{-2}	0.84	39.2	26	1.51	43.2	45.8	43.2	4.01
110	Refined	1.02×10^{-2}	0.95	34.3	26	1.32	38.3	40.9	38.2	3.95
130	Refined	9.31×10^{-3}	1.03	32.3	26	1.24	36.3	39.0	36.3	3.99
140	Refined	8.98×10^{-3}	1.06	31.9	26	1.23	35.9	38.6	35.8	3.93
160	Refined	8.47×10^{-3}	1.11	31.6	26	1.21	35.6	38.2	35.5	3.96
170	Refined	8.26×10^{-3}	1.13	31.6	26	1.21	35.6	38.3	35.6	3.98
190	Refined	7.94×10^{-3}	1.16	31.8	26	1.22	35.8	38.4	35.7	3.89
210	Refined	7.67×10^{-3}	1.19	32.1	26	1.23	36.1	38.8	36.0	3.93
230	Refined	7.46×10^{-3}	1.21	32.5	26	1.25	36.5	39.2	36.5	4.00
240	Refined	7.37×10^{-3}	1.22	32.7	26	1.26	36.7	39.4	36.6	3.93
260	Refined	7.22×10^{-3}	1.24	33.1	26	1.27	37.1	39.8	37.1	4.00
270	Refined	7.15×10^{-3}	1.25	33.3	26	1.28	37.3	40.0	37.3	3.96
280	Refined	7.09×10^{-3}	1.26	33.5	26	1.29	37.5	40.1	37.5	3.97
290	Refined	7.03×10^{-3}	1.26	33.7	26	1.30	37.7	40.3	37.6	3.94

Table 2. Results of GRB 160629A

E_c	Level	A (Fixed) (Estimation) (ph.s $^{-1}$.cm $^{-2}$ keV $^{-1}$)	α	χ^2	DOF	χ_r^2	AIC	BIC	DIC	pDIC
(1)	(2)	(3)	(4)	(5)	(6)	(7)	(8)	(9)	(10)	(11)
Preliminary estimation										
100	Preliminary	1.76×10^{-2}	0.63	19.9	13	1.53	23.9	25.3	23.8	3.96
120	Preliminary	1.59×10^{-2}	0.72	15.4	13	1.18	19.4	20.8	19.3	3.93
150	Preliminary	1.44×10^{-2}	0.80	12.1	13	0.93	16.1	17.5	16.0	3.90
180	Preliminary	1.34×10^{-2}	0.86	10.5	13	0.81	14.5	16.0	14.5	3.96
200	Preliminary	1.30×10^{-2}	0.89	10.0	13	0.77	14.0	15.4	14.0	3.98
220	Preliminary	1.26×10^{-2}	0.92	9.6	13	0.74	13.6	15.0	13.6	4.00
250	Preliminary	1.22×10^{-2}	0.94	9.3	13	0.71	13.3	14.7	13.2	3.92
300	Preliminary	1.17×10^{-2}	0.98	9.1	13	0.70	13.1	14.5	13.0	3.95
400	Preliminary	1.11×10^{-2}	1.02	9.1	13	0.70	13.1	14.5	13.1	3.96
500	Preliminary	1.08×10^{-2}	1.05	9.3	13	0.71	13.3	14.7	13.2	3.89
600	Preliminary	1.06×10^{-2}	1.07	9.5	13	0.73	13.5	14.9	13.4	3.95
700	Preliminary	1.04×10^{-2}	1.08	9.6	13	0.74	13.6	15.0	13.6	3.97
800	Preliminary	1.03×10^{-2}	1.09	9.7	13	0.75	13.7	15.2	13.7	3.98
900	Preliminary	1.02×10^{-2}	1.10	9.9	13	0.76	13.9	15.3	13.8	3.95
1000	Preliminary	1.01×10^{-2}	1.11	10.0	13	0.77	14.0	15.4	13.9	3.99
1200	Preliminary	1.00×10^{-2}	1.11	10.1	13	0.78	14.1	15.5	14.1	3.96
1500	Preliminary	9.93×10^{-3}	1.12	10.3	13	0.79	14.3	15.7	14.2	3.93
1800	Preliminary	9.88×10^{-3}	1.13	10.4	13	0.80	14.4	15.8	14.4	4.02
2000	Preliminary	9.83×10^{-3}	1.13	10.5	13	0.81	14.5	15.9	14.4	3.98
3000	Preliminary	9.72×10^{-3}	1.14	10.7	13	0.82	14.7	16.1	14.7	4.00
4000	Preliminary	9.66×10^{-3}	1.15	10.8	13	0.83	14.8	16.2	14.8	3.98
5000	Preliminary	9.64×10^{-3}	1.15	10.8	13	0.83	14.8	16.2	14.8	4.00
Refined estimation										
110	Refined	1.66×10^{-2}	0.67	17.3	13	1.33	21.3	22.7	21.3	3.98
130	Refined	1.53×10^{-2}	0.75	14.0	13	1.08	18.0	19.4	18.0	4.04
140	Refined	1.48×10^{-2}	0.78	12.9	13	0.99	16.9	18.3	16.8	3.92
160	Refined	1.40×10^{-2}	0.83	11.4	13	0.88	15.4	16.9	15.4	4.00
170	Refined	1.37×10^{-2}	0.84	10.9	13	0.84	14.9	16.4	15.0	4.02
190	Refined	1.32×10^{-2}	0.88	10.2	13	0.79	14.2	15.6	14.2	3.93
210	Refined	1.28×10^{-2}	0.91	9.8	13	0.75	13.8	15.2	13.7	3.98
230	Refined	1.25×10^{-2}	0.93	9.5	13	0.73	13.5	14.9	13.5	3.98
240	Refined	1.23×10^{-2}	0.94	9.4	13	0.72	13.4	14.8	13.3	3.97
260	Refined	1.21×10^{-2}	0.95	9.2	13	0.71	13.2	14.6	13.1	3.92
270	Refined	1.20×10^{-2}	0.96	9.2	13	0.71	13.2	14.6	13.2	4.01
280	Refined	1.19×10^{-2}	0.97	9.1	13	0.70	13.1	14.6	13.2	4.02
290	Refined	1.18×10^{-2}	0.97	9.1	13	0.70	13.1	14.5	13.1	3.95
310	Refined	1.16×10^{-2}	0.99	9.1	13	0.70	13.1	14.5	13.0	3.94
320	Refined	1.16×10^{-2}	0.99	9.1	13	0.70	13.1	14.5	13.1	4.01
330	Refined	1.15×10^{-2}	1.00	9.1	13	0.70	13.1	14.5	13.0	3.96
340	Refined	1.14×10^{-2}	1.00	9.1	13	0.70	13.1	14.5	13.0	3.94
350	Refined	1.14×10^{-2}	1.01	9.1	13	0.70	13.1	14.5	13.0	3.93
360	Refined	1.13×10^{-2}	1.01	9.1	13	0.70	13.1	14.5	13.1	3.98
370	Refined	1.13×10^{-2}	1.01	9.1	13	0.70	13.1	14.5	13.0	3.95
380	Refined	1.12×10^{-2}	1.02	9.1	13	0.70	13.1	14.5	13.0	3.96
390	Refined	1.12×10^{-2}	1.02	9.1	13	0.70	13.1	14.5	13.1	3.98

Table 3. Results of GRB 090529

E_c	Level	A (Fixed) (Estimation) ($\text{ph.s}^{-1}.\text{cm}^{-2}\text{keV}^{-1}$)	α	χ^2	DOF	χ_r^2	AIC	BIC	DIC	pDIC
(1)	(2)	(3)	(4)	(5)	(6)	(7)	(8)	(9)	(10)	(11)
Preliminary estimation										
100	Preliminary	5.83×10^{-2}	0.75	195.7	62	3.16	199.7	204.0	199.6	3.95
120	Preliminary	5.28×10^{-2}	0.84	175.3	62	2.83	179.3	183.6	179.3	3.96
150	Preliminary	4.78×10^{-2}	0.93	158.8	62	2.56	162.8	167.1	162.7	3.92
180	Preliminary	4.47×10^{-2}	0.99	149.9	62	2.42	153.9	158.2	153.9	3.98
200	Preliminary	4.33×10^{-2}	1.02	146.2	62	2.36	150.2	154.5	150.1	3.95
220	Preliminary	4.20×10^{-2}	1.04	143.4	62	2.31	147.4	151.8	147.3	3.88
250	Preliminary	4.07×10^{-2}	1.07	140.6	62	2.27	144.6	148.9	144.5	3.90
300	Preliminary	3.91×10^{-2}	1.11	137.7	62	2.22	141.7	146.0	141.6	3.93
400	Preliminary	3.71×10^{-2}	1.16	135.1	62	2.18	139.1	143.4	139.0	3.96
500	Preliminary	3.60×10^{-2}	1.18	134.0	62	2.16	138.0	142.4	138.1	4.02
600	Preliminary	3.53×10^{-2}	1.20	133.6	62	2.15	137.6	141.9	137.5	3.90
700	Preliminary	3.48×10^{-2}	1.21	133.3	62	2.15	137.3	141.6	137.3	3.93
800	Preliminary	3.44×10^{-2}	1.22	133.2	62	2.15	137.2	141.5	137.2	3.98
900	Preliminary	3.41×10^{-2}	1.23	133.2	62	2.15	137.2	141.5	137.1	3.92
1000	Preliminary	3.39×10^{-2}	1.24	133.1	62	2.15	137.1	141.5	137.1	3.93
1200	Preliminary	3.35×10^{-2}	1.25	133.1	62	2.15	137.1	141.5	137.1	3.93
1500	Preliminary	3.32×10^{-2}	1.26	133.2	62	2.15	137.2	141.5	137.2	3.98
1800	Preliminary	3.30×10^{-2}	1.26	133.3	62	2.15	137.3	141.6	137.2	3.92
2000	Preliminary	3.29×10^{-2}	1.27	133.3	62	2.15	137.3	141.6	137.3	3.96
3000	Preliminary	3.25×10^{-2}	1.28	133.4	62	2.15	137.4	141.8	137.4	3.95
4000	Preliminary	3.23×10^{-2}	1.28	133.5	62	2.15	137.5	141.9	137.4	3.88
5000	Preliminary	3.22×10^{-2}	1.28	133.6	62	2.15	137.6	141.9	137.5	3.95
Refined estimation										
210	Refined	4.26×10^{-2}	1.03	144.7	62	2.33	148.7	153.0	148.7	3.97
230	Refined	4.15×10^{-2}	1.05	142.4	62	2.30	146.4	150.7	146.3	3.99
240	Refined	4.11×10^{-2}	1.07	141.4	62	2.28	145.4	149.7	145.4	3.98
260	Refined	4.03×10^{-2}	1.08	139.9	62	2.26	143.9	148.2	143.8	3.98
270	Refined	4.00×10^{-2}	1.09	139.2	62	2.25	143.2	147.5	143.2	4.02
280	Refined	3.96×10^{-2}	1.10	138.7	62	2.24	142.7	147.0	142.6	3.99
290	Refined	3.93×10^{-2}	1.10	138.1	62	2.23	142.1	146.5	142.1	3.99
310	Refined	3.88×10^{-2}	1.12	137.3	62	2.21	141.3	145.6	141.3	4.01
320	Refined	3.86×10^{-2}	1.12	136.9	62	2.21	140.9	145.3	141.0	4.01
330	Refined	3.83×10^{-2}	1.13	136.6	62	2.20	140.6	144.9	140.7	4.05
340	Refined	3.82×10^{-2}	1.13	136.3	62	2.20	140.3	144.7	140.4	4.05
350	Refined	3.79×10^{-2}	1.14	136.1	62	2.19	140.1	144.4	140.0	3.97
360	Refined	3.78×10^{-2}	1.14	135.8	62	2.19	139.8	144.2	139.8	3.99
370	Refined	3.76×10^{-2}	1.15	135.6	62	2.19	139.6	143.9	139.6	4.02
380	Refined	3.74×10^{-2}	1.15	135.4	62	2.18	139.4	143.7	139.4	3.98
390	Refined	3.73×10^{-2}	1.15	135.2	62	2.18	139.2	143.6	139.2	3.96
410	Refined	3.70×10^{-2}	1.16	134.9	62	2.18	138.9	143.3	138.9	3.95
420	Refined	3.69×10^{-2}	1.16	134.8	62	2.17	138.8	143.1	138.7	3.94
430	Refined	3.67×10^{-2}	1.17	134.7	62	2.17	138.7	143.0	138.6	3.98
440	Refined	3.66×10^{-2}	1.17	134.6	62	2.17	138.6	142.9	138.6	4.00
450	Refined	3.65×10^{-2}	1.17	134.4	62	2.17	138.4	142.8	138.4	3.97

Table 4. Results of GRB 091003

E_c	Level	A (Fixed) (Estimation) ($\text{ph.s}^{-1}.\text{cm}^{-2}\text{keV}^{-1}$)	α	χ^2	DOF	χ_r^2	AIC	BIC	DIC	pDIC
(1)	(2)	(3)	(4)	(5)	(6)	(7)	(8)	(9)	(10)	(11)
Preliminary estimation										
100	Preliminary	7.90×10^{-2}	0.60	211.3	60	3.52	215.3	219.5	215.3	4.03
120	Preliminary	7.17×10^{-2}	0.70	156.8	60	2.61	160.8	165.1	160.8	4.01
150	Preliminary	6.50×10^{-2}	0.80	114.6	60	1.91	118.6	122.9	118.6	3.98
180	Preliminary	6.09×10^{-2}	0.86	93.6	60	1.56	97.6	101.9	97.6	4.02
200	Preliminary	5.89×10^{-2}	0.90	85.3	60	1.42	89.3	93.6	89.3	4.00
220	Preliminary	5.73×10^{-2}	0.92	79.7	60	1.33	83.7	87.9	83.7	4.01
250	Preliminary	5.55×10^{-2}	0.96	74.2	60	1.24	78.2	82.5	78.2	4.01
300	Preliminary	5.33×10^{-2}	1.00	69.6	60	1.16	73.6	77.8	73.6	4.02
400	Preliminary	5.06×10^{-2}	1.04	66.9	60	1.12	70.9	75.2	71.0	4.07
500	Preliminary	4.91×10^{-2}	1.07	67.1	60	1.12	71.1	75.3	71.1	3.99
600	Preliminary	4.82×10^{-2}	1.09	67.9	60	1.13	71.9	76.1	71.9	4.04
700	Preliminary	4.74×10^{-2}	1.11	68.8	60	1.15	72.8	77.1	72.8	3.98
800	Preliminary	4.69×10^{-2}	1.12	69.7	60	1.16	73.7	78.0	73.8	4.08
900	Preliminary	4.65×10^{-2}	1.13	70.6	60	1.18	74.6	78.8	74.6	3.99
1000	Preliminary	4.62×10^{-2}	1.13	71.3	60	1.19	75.3	79.6	75.3	3.98
1200	Preliminary	4.58×10^{-2}	1.14	72.5	60	1.21	76.5	80.8	76.6	4.05
1500	Preliminary	4.53×10^{-2}	1.15	73.9	60	1.23	77.9	82.1	77.9	4.00
1800	Preliminary	4.50×10^{-2}	1.16	74.9	60	1.25	78.9	83.1	78.9	3.99
2000	Preliminary	4.48×10^{-2}	1.16	75.4	60	1.26	79.4	83.7	79.5	4.05
3000	Preliminary	4.44×10^{-2}	1.17	77.1	60	1.28	81.1	85.3	81.1	4.03
4000	Preliminary	4.41×10^{-2}	1.18	78.0	60	1.30	82.0	86.2	82.0	4.05
5000	Preliminary	4.40×10^{-2}	1.18	78.5	60	1.31	82.5	86.8	82.5	4.00
Refined estimation										
210	Refined	5.80×10^{-2}	0.91	82.2	60	1.37	86.2	90.5	86.3	4.09
230	Refined	5.66×10^{-2}	0.94	77.5	60	1.29	81.5	85.8	81.5	4.03
240	Refined	5.60×10^{-2}	0.95	75.7	60	1.26	79.7	84.0	79.8	4.04
260	Refined	5.49×10^{-2}	0.96	72.9	60	1.22	76.9	81.2	76.9	3.98
270	Refined	5.45×10^{-2}	0.97	71.9	60	1.20	75.9	80.1	75.9	4.03
280	Refined	5.40×10^{-2}	0.98	71.0	60	1.18	75.0	79.2	75.0	4.09
290	Refined	5.36×10^{-2}	0.99	70.2	60	1.17	74.2	78.5	74.3	4.09
310	Refined	5.29×10^{-2}	1.00	69.0	60	1.15	73.0	77.3	73.1	4.11
320	Refined	5.26×10^{-2}	1.01	68.6	60	1.14	72.6	76.8	72.6	4.05
330	Refined	5.23×10^{-2}	1.01	68.2	60	1.14	72.2	76.4	72.3	4.08
340	Refined	5.20×10^{-2}	1.02	67.9	60	1.13	71.9	76.1	71.9	4.04
350	Refined	5.18×10^{-2}	1.02	67.6	60	1.13	71.6	75.9	71.7	4.06
360	Refined	5.15×10^{-2}	1.03	67.4	60	1.12	71.4	75.7	71.5	4.07
370	Refined	5.13×10^{-2}	1.03	67.2	60	1.12	71.2	75.5	71.3	4.10
380	Refined	5.11×10^{-2}	1.04	67.1	60	1.12	71.1	75.4	71.2	4.07
390	Refined	5.08×10^{-2}	1.04	67.0	60	1.12	71.0	75.3	71.1	4.10
410	Refined	5.05×10^{-2}	1.05	66.9	60	1.11	70.9	75.1	70.9	4.06
420	Refined	5.03×10^{-2}	1.05	66.8	60	1.11	70.8	75.1	71.0	4.11
430	Refined	5.01×10^{-2}	1.06	66.8	60	1.11	70.8	75.1	70.9	4.10
440	Refined	5.00×10^{-2}	1.06	66.8	60	1.11	70.8	75.1	70.9	4.06
450	Refined	4.98×10^{-2}	1.06	66.8	60	1.11	70.8	75.1	70.9	4.09

Table 5. Results of GRB 140606B

E_c	Level	A (Fixed) (Estimation) (ph.s $^{-1}$.cm $^{-2}$ keV $^{-1}$)	α	χ^2	DOF	χ_r^2	AIC	BIC	DIC	pDIC
(1)	(2)	(3)	(4)	(5)	(6)	(7)	(8)	(9)	(10)	(11)
Preliminary estimation										
100	Preliminary	4.07×10^{-2}	0.70	102.6	47	2.18	106.6	110.3	106.6	4.07
120	Preliminary	3.70×10^{-2}	0.80	89.0	47	1.89	93.0	96.7	93.0	4.02
150	Preliminary	3.36×10^{-2}	0.89	77.2	47	1.64	81.2	85.0	81.3	4.03
180	Preliminary	3.15×10^{-2}	0.95	70.5	47	1.50	74.5	78.3	74.5	3.97
200	Preliminary	3.05×10^{-2}	0.98	67.5	47	1.44	71.5	75.3	71.6	4.04
220	Preliminary	2.97×10^{-2}	1.01	65.2	47	1.39	69.2	73.0	69.3	4.02
250	Preliminary	2.87×10^{-2}	1.04	62.7	47	1.33	66.7	70.5	66.8	4.06
300	Preliminary	2.76×10^{-2}	1.08	59.9	47	1.28	63.9	67.7	64.0	4.06
400	Preliminary	2.63×10^{-2}	1.12	57.0	47	1.21	61.0	64.7	61.0	4.02
500	Preliminary	2.55×10^{-2}	1.15	55.5	47	1.18	59.5	63.2	59.5	4.05
600	Preliminary	2.50×10^{-2}	1.17	54.6	47	1.16	58.6	62.3	58.6	4.02
700	Preliminary	2.47×10^{-2}	1.18	54.0	47	1.15	58.0	61.8	58.0	4.02
800	Preliminary	2.44×10^{-2}	1.19	53.6	47	1.14	57.6	61.4	57.6	4.05
900	Preliminary	2.42×10^{-2}	1.20	53.3	47	1.13	57.3	61.1	57.4	4.09
1000	Preliminary	2.40×10^{-2}	1.21	53.1	47	1.13	57.1	60.8	57.1	4.06
1200	Preliminary	2.38×10^{-2}	1.22	52.7	47	1.12	56.7	60.5	56.8	4.05
1500	Preliminary	2.36×10^{-2}	1.23	52.4	47	1.12	56.4	60.2	56.5	4.02
1800	Preliminary	2.34×10^{-2}	1.23	52.3	47	1.11	56.3	60.0	56.3	4.04
2000	Preliminary	2.33×10^{-2}	1.24	52.2	47	1.11	56.2	60.0	56.2	4.00
3000	Preliminary	2.31×10^{-2}	1.24	51.9	47	1.10	55.9	59.7	56.0	4.04
4000	Preliminary	2.30×10^{-2}	1.25	51.8	47	1.10	55.8	59.6	55.8	4.00
5000	Preliminary	2.29×10^{-2}	1.25	51.7	47	1.10	55.7	59.5	55.8	4.02
Refined estimation										
275	Refined	2.81×10^{-2}	1.06	61.2	47	1.30	65.2	68.9	65.1	3.95
325	Refined	2.72×10^{-2}	1.09	59.0	47	1.25	63.0	66.7	62.9	3.94
350	Refined	2.69×10^{-2}	1.10	58.2	47	1.24	62.2	66.0	62.2	3.99
375	Refined	2.66×10^{-2}	1.11	57.5	47	1.22	61.5	65.3	61.5	3.98
425	Refined	2.61×10^{-2}	1.13	56.5	47	1.20	60.5	64.3	60.5	4.03
450	Refined	2.59×10^{-2}	1.14	56.1	47	1.19	60.1	63.9	60.1	4.00
475	Refined	2.57×10^{-2}	1.15	55.8	47	1.19	59.8	63.5	59.7	4.00
525	Refined	2.54×10^{-2}	1.16	55.2	47	1.17	59.2	63.0	59.2	3.96
550	Refined	2.52×10^{-2}	1.16	55.0	47	1.17	59.0	62.7	58.9	3.97
575	Refined	2.52×10^{-2}	1.16	55.0	47	1.17	59.0	62.7	58.9	3.97
625	Refined	2.49×10^{-2}	1.17	54.4	47	1.16	58.4	62.2	58.4	4.00
650	Refined	2.48×10^{-2}	1.18	54.2	47	1.15	58.2	62.0	58.2	4.01
675	Refined	2.48×10^{-2}	1.18	54.1	47	1.15	58.1	61.9	58.1	3.99
725	Refined	2.46×10^{-2}	1.19	53.9	47	1.15	57.9	61.6	57.9	3.99
750	Refined	2.45×10^{-2}	1.19	53.8	47	1.14	57.8	61.5	57.7	3.96
775	Refined	2.45×10^{-2}	1.19	53.7	47	1.14	57.7	61.4	57.6	3.97
825	Refined	2.44×10^{-2}	1.19	53.5	47	1.14	57.5	61.3	57.5	4.03
850	Refined	2.43×10^{-2}	1.20	53.4	47	1.14	57.4	61.2	57.4	3.95
875	Refined	2.43×10^{-2}	1.20	53.3	47	1.13	57.3	61.1	57.3	4.01

Table 6. Results of GRB 120624B

E_c	Level	A (Fixed) (Estimation) ($\text{ph.s}^{-1}.\text{cm}^{-2}\text{keV}^{-1}$)	α	χ^2	DOF	χ^2_r	AIC	BIC	DIC	pDIC
(1)	(2)	(3)	(4)	(5)	(6)	(7)	(8)	(9)	(10)	(11)
Preliminary estimation										
100	Preliminary	4.54×10^{-2}	0.40	181.2	34	5.33	185.2	188.3	185.2	4.00
120	Preliminary	4.14×10^{-2}	0.51	144.5	34	4.25	148.5	151.7	148.5	3.98
150	Preliminary	3.78×10^{-2}	0.62	113.5	34	3.34	117.5	120.7	117.5	4.01
180	Preliminary	3.55×10^{-2}	0.69	96.1	34	2.83	100.1	103.3	100.1	4.02
200	Preliminary	3.44×10^{-2}	0.73	88.5	34	2.60	92.5	95.6	92.5	4.00
220	Preliminary	3.35×10^{-2}	0.76	82.7	34	2.43	86.7	89.9	86.8	4.03
250	Preliminary	3.25×10^{-2}	0.79	76.5	34	2.25	80.5	83.6	80.4	3.95
300	Preliminary	3.13×10^{-2}	0.84	69.8	34	2.05	73.8	77.0	73.7	3.90
400	Preliminary	2.98×10^{-2}	0.89	63.0	34	1.85	67.0	70.2	67.0	3.98
500	Preliminary	2.90×10^{-2}	0.92	59.7	34	1.76	63.7	66.9	63.7	3.95
600	Preliminary	2.84×10^{-2}	0.94	57.9	34	1.70	61.9	65.1	62.0	4.06
700	Preliminary	2.80×10^{-2}	0.96	56.8	34	1.67	60.8	64.0	60.8	3.98
800	Preliminary	2.77×10^{-2}	0.97	56.0	34	1.65	60.0	63.2	60.0	4.01
900	Preliminary	2.75×10^{-2}	0.98	55.5	34	1.63	59.5	62.7	59.5	4.02
1000	Preliminary	2.73×10^{-2}	0.99	55.1	34	1.62	59.1	62.3	59.1	3.96
1200	Preliminary	2.71×10^{-2}	1.00	54.6	34	1.61	58.6	61.8	58.6	3.94
1500	Preliminary	2.68×10^{-2}	1.01	54.2	34	1.59	58.2	61.3	58.2	3.99
1800	Preliminary	2.67×10^{-2}	1.02	53.9	34	1.59	57.9	61.1	57.9	4.00
2000	Preliminary	2.66×10^{-2}	1.02	53.8	34	1.58	57.8	61.0	57.8	3.95
3000	Preliminary	2.63×10^{-2}	1.03	53.5	34	1.57	57.5	60.7	57.5	3.97
4000	Preliminary	2.62×10^{-2}	1.04	53.4	34	1.57	57.4	60.6	57.4	3.99
5000	Preliminary	2.61×10^{-2}	1.04	53.3	34	1.57	57.3	60.5	57.3	3.96
Refined estimation										
425	Refined	2.96×10^{-2}	0.90	62.0	34	1.82	66.0	69.1	65.9	3.98
450	Refined	2.93×10^{-2}	0.91	61.1	34	1.80	65.1	68.3	65.1	3.99
475	Refined	2.91×10^{-2}	0.92	60.4	34	1.78	64.4	67.5	64.4	4.05
525	Refined	2.88×10^{-2}	0.93	59.2	34	1.74	63.2	66.3	63.2	4.01
550	Refined	2.87×10^{-2}	0.94	58.7	34	1.73	62.7	65.9	62.7	4.01
575	Refined	2.85×10^{-2}	0.94	58.3	34	1.71	62.3	65.4	62.3	4.01
625	Refined	2.83×10^{-2}	0.95	57.6	34	1.69	61.6	64.7	61.6	4.02
650	Refined	2.82×10^{-2}	0.95	57.3	34	1.68	61.3	64.5	61.4	4.12
675	Refined	2.81×10^{-2}	0.96	57.0	34	1.68	61.0	64.2	61.1	4.03
725	Refined	2.79×10^{-2}	0.96	56.6	34	1.66	60.6	63.7	60.6	4.00
750	Refined	2.79×10^{-2}	0.97	56.4	34	1.66	60.4	63.5	60.4	3.98
775	Refined	2.78×10^{-2}	0.97	56.2	34	1.65	60.2	63.4	60.2	4.03
825	Refined	2.77×10^{-2}	0.97	55.9	34	1.64	59.9	63.1	59.9	4.04
850	Refined	2.76×10^{-2}	0.98	55.8	34	1.64	59.8	62.9	59.8	4.08
875	Refined	2.76×10^{-2}	0.98	55.6	34	1.64	59.6	62.8	59.7	4.06

Table 7. Results of GRB 090328

E_c	Level	A (Fixed) (Estimation) ($\text{ph.s}^{-1}.\text{cm}^{-2}\text{keV}^{-1}$)	α	χ^2	DOF	χ_r^2	AIC	BIC	DIC	pDIC
(1)	(2)	(3)	(4)	(5)	(6)	(7)	(8)	(9)	(10)	(11)
Preliminary estimation										
100	Preliminary	3.32×10^{-2}	0.65	150.3	29	5.18	154.3	157.1	154.3	4.00
120	Preliminary	3.01×10^{-2}	0.74	118.1	29	4.07	122.1	124.9	122.1	4.03
150	Preliminary	2.73×10^{-2}	0.84	91.1	29	3.14	95.1	98.0	95.1	3.98
180	Preliminary	2.55×10^{-2}	0.90	76.2	29	2.63	80.2	83.0	80.2	4.00
200	Preliminary	2.47×10^{-2}	0.93	69.6	29	2.40	73.6	76.5	73.6	3.97
220	Preliminary	2.40×10^{-2}	0.96	64.7	29	2.23	68.7	71.6	68.8	4.02
250	Preliminary	2.33×10^{-2}	0.99	59.5	29	2.05	63.5	66.3	63.4	3.98
300	Preliminary	2.23×10^{-2}	1.03	53.9	29	1.86	57.9	60.7	57.9	4.03
400	Preliminary	2.13×10^{-2}	1.08	48.2	29	1.66	52.2	55.1	52.2	4.01
500	Preliminary	2.06×10^{-2}	1.11	45.6	29	1.57	49.6	52.4	49.5	3.96
600	Preliminary	2.02×10^{-2}	1.12	44.1	29	1.52	48.1	51.0	48.1	3.97
700	Preliminary	1.99×10^{-2}	1.14	43.2	29	1.49	47.2	50.1	47.2	4.01
800	Preliminary	1.97×10^{-2}	1.15	42.6	29	1.47	46.6	49.5	46.6	4.03
900	Preliminary	1.95×10^{-2}	1.16	42.2	29	1.45	46.2	49.1	46.2	4.01
1000	Preliminary	1.94×10^{-2}	1.16	41.9	29	1.44	45.9	48.8	45.9	4.05
1200	Preliminary	1.92×10^{-2}	1.17	41.5	29	1.43	45.5	48.4	45.6	4.06
1500	Preliminary	1.90×10^{-2}	1.18	41.2	29	1.42	45.2	48.0	45.2	4.00
1800	Preliminary	1.89×10^{-2}	1.19	41.0	29	1.41	45.0	47.9	45.0	3.99
2000	Preliminary	1.88×10^{-2}	1.19	40.9	29	1.41	44.9	47.8	44.9	4.00
3000	Preliminary	1.86×10^{-2}	1.20	40.7	29	1.40	44.7	47.6	44.7	4.01
4000	Preliminary	1.85×10^{-2}	1.21	40.6	29	1.40	44.6	47.5	44.6	4.03
5000	Preliminary	1.85×10^{-2}	1.21	40.6	29	1.40	44.6	47.4	44.6	4.01
Refined estimation										
275	Refined	2.28×10^{-2}	1.01	56.3	29	1.94	60.3	63.2	60.2	3.95
325	Refined	2.20×10^{-2}	1.04	52.0	29	1.79	56.0	58.8	55.9	3.95
350	Refined	2.17×10^{-2}	1.06	50.5	29	1.74	54.5	57.3	54.4	3.93
375	Refined	2.15×10^{-2}	1.07	49.2	29	1.70	53.2	56.1	53.2	3.93
425	Refined	2.11×10^{-2}	1.09	47.4	29	1.63	51.4	54.2	51.4	3.99
450	Refined	2.09×10^{-2}	1.09	46.7	29	1.61	50.7	53.5	50.6	3.92
475	Refined	2.07×10^{-2}	1.10	46.1	29	1.59	50.1	52.9	50.0	3.97
525	Refined	2.05×10^{-2}	1.11	45.1	29	1.56	49.1	52.0	49.1	3.96
550	Refined	2.04×10^{-2}	1.12	44.7	29	1.54	48.7	51.6	48.7	3.98
550	Refined	2.04×10^{-2}	1.12	44.7	29	1.54	48.7	51.6	48.7	3.95
575	Refined	2.03×10^{-2}	1.12	44.4	29	1.53	48.4	51.3	48.3	3.91
625	Refined	2.01×10^{-2}	1.13	43.8	29	1.51	47.8	50.7	47.8	3.93
650	Refined	2.00×10^{-2}	1.13	43.6	29	1.50	47.6	50.5	47.5	3.92
675	Refined	2.00×10^{-2}	1.14	43.4	29	1.50	47.4	50.2	47.3	3.92
725	Refined	1.98×10^{-2}	1.14	43.0	29	1.48	47.0	49.9	47.0	4.00
750	Refined	1.98×10^{-2}	1.14	42.9	29	1.48	46.9	49.7	46.8	3.95
775	Refined	1.97×10^{-2}	1.15	42.7	29	1.47	46.7	49.6	46.7	3.93
825	Refined	1.96×10^{-2}	1.15	42.5	29	1.46	46.5	49.4	46.4	3.94
850	Refined	1.96×10^{-2}	1.15	42.4	29	1.46	46.4	49.2	46.3	3.94
875	Refined	1.96×10^{-2}	1.16	42.3	29	1.46	46.3	49.1	46.2	3.97

Table 8. Results of GRB 150301B

E_c	Level	A (Fixed) (Estimation) (ph.s $^{-1}$.cm $^{-2}$ keV $^{-1}$)	α	χ^2	DOF	χ_r^2	AIC	BIC	DIC	pDIC
(1)	(2)	(3)	(4)	(5)	(6)	(7)	(8)	(9)	(10)	(11)
Preliminary estimation										
100	Preliminary	2.25×10^{-2}	0.78	30.1	18	1.67	34.1	36.1	34.1	3.96
120	Preliminary	2.04×10^{-2}	0.88	27.0	18	1.50	31.0	33.0	31.0	4.04
150	Preliminary	1.85×10^{-2}	0.98	24.3	18	1.35	28.3	30.3	28.3	3.98
180	Preliminary	1.73×10^{-2}	1.04	22.9	18	1.27	26.9	28.9	26.9	3.98
200	Preliminary	1.67×10^{-2}	1.07	22.3	18	1.24	26.3	28.3	26.2	3.99
220	Preliminary	1.63×10^{-2}	1.10	21.8	18	1.21	25.8	27.8	25.8	3.98
250	Preliminary	1.58×10^{-2}	1.13	21.3	18	1.18	25.3	27.3	25.3	3.98
300	Preliminary	1.52×10^{-2}	1.17	20.8	18	1.15	24.8	26.8	24.7	3.97
400	Preliminary	1.44×10^{-2}	1.22	20.2	18	1.12	24.2	26.2	24.2	3.97
500	Preliminary	1.40×10^{-2}	1.25	20.0	18	1.11	24.0	26.0	24.0	4.01
600	Preliminary	1.37×10^{-2}	1.27	19.9	18	1.10	23.9	25.9	23.9	3.97
700	Preliminary	1.35×10^{-2}	1.28	19.8	18	1.10	23.8	25.8	23.7	3.94
800	Preliminary	1.34×10^{-2}	1.29	19.8	18	1.10	23.8	25.8	23.7	3.99
900	Preliminary	1.33×10^{-2}	1.30	19.7	18	1.10	23.7	25.7	23.7	3.98
1000	Preliminary	1.32×10^{-2}	1.31	19.7	18	1.09	23.7	25.7	23.7	4.01
1200	Preliminary	1.30×10^{-2}	1.32	19.7	18	1.09	23.7	25.7	23.6	3.95
1500	Preliminary	1.29×10^{-2}	1.33	19.7	18	1.09	23.7	25.7	23.6	3.96
1800	Preliminary	1.28×10^{-2}	1.34	19.6	18	1.09	23.6	25.6	23.6	3.98
2000	Preliminary	1.28×10^{-2}	1.34	19.6	18	1.09	23.6	25.6	23.6	3.94
3000	Preliminary	1.26×10^{-2}	1.35	19.6	18	1.09	23.6	25.6	23.6	3.97
4000	Preliminary	1.26×10^{-2}	1.35	19.6	18	1.09	23.6	25.6	23.6	4.02
5000	Preliminary	1.25×10^{-2}	1.36	19.6	18	1.09	23.6	25.6	23.6	4.00
Refined estimation										
110	Refined	2.13×10^{-2}	0.83	28.3	18	1.57	32.3	34.3	32.3	3.98
130	Refined	1.96×10^{-2}	0.92	25.9	18	1.44	29.9	31.9	29.9	4.00
140	Refined	1.90×10^{-2}	0.95	25.0	18	1.39	29.0	31.0	29.0	3.99
160	Refined	1.80×10^{-2}	1.00	23.8	18	1.32	27.8	29.8	27.7	3.98
170	Refined	1.76×10^{-2}	1.02	23.3	18	1.29	27.3	29.3	27.3	4.00
190	Refined	1.70×10^{-2}	1.06	22.5	18	1.25	26.5	28.5	26.5	3.93
210	Refined	1.65×10^{-2}	1.09	22.0	18	1.22	26.0	28.0	25.9	3.93
230	Refined	1.61×10^{-2}	1.11	21.6	18	1.20	25.6	27.6	25.6	4.00
240	Refined	1.60×10^{-2}	1.12	21.4	18	1.19	25.4	27.4	25.4	3.95
260	Refined	1.57×10^{-2}	1.14	21.2	18	1.18	25.2	27.2	25.2	3.99
270	Refined	1.55×10^{-2}	1.15	21.0	18	1.17	25.0	27.0	25.1	4.04
280	Refined	1.54×10^{-2}	1.16	20.9	18	1.16	24.9	26.9	24.9	3.95
290	Refined	1.53×10^{-2}	1.16	20.9	18	1.16	24.9	26.8	24.8	3.97
310	Refined	1.51×10^{-2}	1.18	20.7	18	1.15	24.7	26.7	24.6	3.94
320	Refined	1.50×10^{-2}	1.19	20.6	18	1.15	24.6	26.6	24.6	3.96
330	Refined	1.49×10^{-2}	1.19	20.6	18	1.14	24.6	26.6	24.6	4.00
340	Refined	1.48×10^{-2}	1.19	20.5	18	1.14	24.5	26.5	24.4	3.93
350	Refined	1.48×10^{-2}	1.20	20.5	18	1.14	24.5	26.4	24.4	3.96
360	Refined	1.47×10^{-2}	1.20	20.4	18	1.13	24.4	26.4	24.4	3.99
370	Refined	1.46×10^{-2}	1.21	20.4	18	1.13	24.4	26.4	24.3	3.93
380	Refined	1.45×10^{-2}	1.21	20.3	18	1.13	24.3	26.3	24.2	3.91
390	Refined	1.45×10^{-2}	1.22	20.3	18	1.13	24.3	26.3	24.3	3.98

Table 9. Results of GRB 180728A

E_c	Level	A (Fixed) (Estimation) (ph.s $^{-1}$.cm $^{-2}$ keV $^{-1}$)	α	χ^2	DOF	χ_r^2	AIC	BIC	DIC	pDIC
(1)	(2)	(3)	(4)	(5)	(6)	(7)	(8)	(9)	(10)	(11)
Preliminary estimation										
100	Preliminary	3.02×10^{-1}	1.40	410.7	47	8.74	414.7	418.5	414.7	3.99
120	Preliminary	2.74×10^{-1}	1.47	319.9	47	6.81	323.9	327.7	323.9	3.94
150	Preliminary	2.49×10^{-1}	1.55	247.2	47	5.26	251.2	255.0	251.1	3.91
180	Preliminary	2.33×10^{-1}	1.60	209.3	47	4.45	213.3	217.1	213.2	3.90
200	Preliminary	2.26×10^{-1}	1.62	193.6	47	4.12	197.6	201.4	197.5	3.93
220	Preliminary	2.20×10^{-1}	1.64	182.4	47	3.88	186.4	190.2	186.4	3.93
250	Preliminary	2.13×10^{-1}	1.67	171.1	47	3.64	175.1	178.8	175.0	3.96
300	Preliminary	2.04×10^{-1}	1.70	160.2	47	3.41	164.2	168.0	164.1	3.94
400	Preliminary	1.95×10^{-1}	1.74	151.3	47	3.22	155.3	159.1	155.3	3.92
500	Preliminary	1.89×10^{-1}	1.76	148.7	47	3.16	152.7	156.4	152.6	3.92
600	Preliminary	1.85×10^{-1}	1.78	147.9	47	3.15	151.9	155.7	152.0	4.01
700	Preliminary	1.83×10^{-1}	1.79	148.0	47	3.15	152.0	155.8	151.9	3.90
800	Preliminary	1.81×10^{-1}	1.80	148.3	47	3.16	152.3	156.1	152.3	3.99
900	Preliminary	1.79×10^{-1}	1.80	148.8	47	3.16	152.8	156.5	152.7	3.98
1000	Preliminary	1.78×10^{-1}	1.81	149.2	47	3.17	153.2	157.0	153.2	4.01
1200	Preliminary	1.76×10^{-1}	1.82	150.1	47	3.19	154.1	157.9	154.1	3.96
1500	Preliminary	1.74×10^{-1}	1.82	151.2	47	3.22	155.2	159.0	155.1	3.95
1800	Preliminary	1.73×10^{-1}	1.83	152.1	47	3.24	156.1	159.8	156.1	4.01
2000	Preliminary	1.73×10^{-1}	1.83	152.5	47	3.25	156.5	160.3	156.5	3.97
3000	Preliminary	1.71×10^{-1}	1.84	154.1	47	3.28	158.1	161.9	158.1	3.99
4000	Preliminary	1.70×10^{-1}	1.84	154.9	47	3.30	158.9	162.7	158.9	3.96
5000	Preliminary	1.70×10^{-1}	1.85	155.5	47	3.31	159.5	163.3	159.5	3.96
Refined estimation										
260	Refined	2.11×10^{-1}	1.68	168.2	47	3.58	172.2	176.0	172.2	3.99
270	Refined	2.09×10^{-1}	1.68	165.8	47	3.53	169.8	173.6	169.8	3.99
280	Refined	2.07×10^{-1}	1.69	163.7	47	3.48	167.7	171.5	167.7	4.07
290	Refined	2.06×10^{-1}	1.69	161.8	47	3.44	165.8	169.6	165.8	3.97
310	Refined	2.03×10^{-1}	1.70	158.7	47	3.38	162.7	166.5	162.8	4.02
320	Refined	2.02×10^{-1}	1.71	157.5	47	3.35	161.5	165.2	161.5	4.01
330	Refined	2.01×10^{-1}	1.71	156.3	47	3.33	160.3	164.1	160.4	4.02
340	Refined	2.00×10^{-1}	1.72	155.4	47	3.31	159.4	163.1	159.3	4.00
350	Refined	1.99×10^{-1}	1.72	154.5	47	3.29	158.5	162.3	158.4	3.97
360	Refined	1.98×10^{-1}	1.73	153.7	47	3.27	157.7	161.5	157.7	4.04
370	Refined	1.97×10^{-1}	1.73	153.0	47	3.26	157.0	160.8	157.1	4.05
380	Refined	1.96×10^{-1}	1.73	152.4	47	3.24	156.4	160.2	156.4	3.99
390	Refined	1.95×10^{-1}	1.74	151.8	47	3.23	155.8	159.6	155.8	3.95
410	Refined	1.94×10^{-1}	1.74	150.9	47	3.21	154.9	158.7	154.9	3.94
420	Refined	1.93×10^{-1}	1.74	150.5	47	3.20	154.5	158.3	154.6	4.02
430	Refined	1.93×10^{-1}	1.75	150.2	47	3.20	154.2	158.0	154.2	4.00
440	Refined	1.92×10^{-1}	1.75	149.9	47	3.19	153.9	157.7	153.9	4.04
450	Refined	1.91×10^{-1}	1.75	149.6	47	3.18	153.6	157.4	153.6	4.03
460	Refined	1.91×10^{-1}	1.75	149.4	47	3.18	153.4	157.1	153.4	4.07
470	Refined	1.90×10^{-1}	1.76	149.2	47	3.17	153.2	156.9	153.1	3.97
480	Refined	1.90×10^{-1}	1.76	149.0	47	3.17	153.0	156.7	153.0	4.05
490	Refined	1.89×10^{-1}	1.76	148.8	47	3.17	152.8	156.6	152.8	4.01

Table 10. Results of GRB 140206A

E_c	Level	A (Fixed) (Estimation) (ph.s $^{-1}$.cm $^{-2}$ keV $^{-1}$)	α	χ^2	DOF	χ_r^2	AIC	BIC	DIC	pDIC
(1)	(2)	(3)	(4)	(5)	(6)	(7)	(8)	(9)	(10)	(11)
Preliminary estimation										
100	Preliminary	1.20×10^{-1}	0.59	424.9	59	7.20	428.9	433.1	429.0	4.10
120	Preliminary	1.09×10^{-1}	0.69	317.6	59	5.38	321.6	325.9	321.6	3.98
150	Preliminary	9.86×10^{-2}	0.78	232.4	59	3.94	236.4	240.7	236.5	4.08
180	Preliminary	9.22×10^{-2}	0.84	188.4	59	3.19	192.4	196.6	192.4	4.02
200	Preliminary	8.92×10^{-2}	0.88	170.3	59	2.89	174.3	178.5	174.3	4.03
220	Preliminary	8.68×10^{-2}	0.90	157.5	59	2.67	161.5	165.7	161.5	4.02
250	Preliminary	8.40×10^{-2}	0.93	144.5	59	2.45	148.5	152.7	148.6	4.10
300	Preliminary	8.07×10^{-2}	0.97	132.2	59	2.24	136.2	140.4	136.2	4.02
400	Preliminary	7.67×10^{-2}	1.02	122.4	59	2.08	126.4	130.6	126.5	4.03
500	Preliminary	7.44×10^{-2}	1.05	119.6	59	2.03	123.6	127.8	123.7	4.05
600	Preliminary	7.29×10^{-2}	1.07	119.0	59	2.02	123.0	127.3	123.1	4.04
700	Preliminary	7.19×10^{-2}	1.08	119.2	59	2.02	123.2	127.5	123.3	4.03
800	Preliminary	7.11×10^{-2}	1.09	119.7	59	2.03	123.7	128.0	123.8	4.00
900	Preliminary	7.05×10^{-2}	1.10	120.3	59	2.04	124.3	128.6	124.4	4.03
1000	Preliminary	7.00×10^{-2}	1.10	121.0	59	2.05	125.0	129.2	125.0	4.03
1200	Preliminary	6.93×10^{-2}	1.11	122.1	59	2.07	126.1	130.3	126.1	4.05
1500	Preliminary	6.86×10^{-2}	1.12	123.5	59	2.09	127.5	131.7	127.6	4.09
1800	Preliminary	6.81×10^{-2}	1.13	124.6	59	2.11	128.6	132.8	128.7	4.10
2000	Preliminary	6.79×10^{-2}	1.13	125.1	59	2.12	129.1	133.4	129.2	4.07
3000	Preliminary	6.72×10^{-2}	1.14	127.1	59	2.15	131.1	135.3	131.1	4.04
4000	Preliminary	6.69×10^{-2}	1.15	128.1	59	2.17	132.1	136.3	132.2	4.04
5000	Preliminary	6.66×10^{-2}	1.15	128.8	59	2.18	132.8	137.0	132.8	4.04
Refined estimation										
260	Refined	8.32×10^{-2}	0.94	141.3	59	2.39	145.3	149.5	145.3	3.99
270	Refined	8.25×10^{-2}	0.95	138.5	59	2.35	142.5	146.7	142.5	3.94
280	Refined	8.19×10^{-2}	0.96	136.1	59	2.31	140.1	144.3	140.1	4.01
290	Refined	8.13×10^{-2}	0.96	134.0	59	2.27	138.0	142.2	138.0	3.97
310	Refined	8.02×10^{-2}	0.98	130.6	59	2.21	134.6	138.8	134.5	3.98
320	Refined	7.97×10^{-2}	0.98	129.1	59	2.19	133.1	137.4	133.1	4.00
330	Refined	7.92×10^{-2}	0.99	127.9	59	2.17	131.9	136.1	131.8	3.91
340	Refined	7.88×10^{-2}	0.99	126.8	59	2.15	130.8	135.0	130.8	4.01
350	Refined	7.84×10^{-2}	1.00	125.8	59	2.13	129.8	134.1	129.8	4.01
360	Refined	7.80×10^{-2}	1.00	125.0	59	2.12	129.0	133.2	129.0	4.02
370	Refined	7.77×10^{-2}	1.01	124.2	59	2.11	128.2	132.4	128.2	4.01
380	Refined	7.73×10^{-2}	1.01	123.5	59	2.09	127.5	131.8	127.5	3.95
390	Refined	7.70×10^{-2}	1.01	123.0	59	2.08	127.0	131.2	126.9	3.99
410	Refined	7.64×10^{-2}	1.02	122.0	59	2.07	126.0	130.2	125.9	3.99
420	Refined	7.62×10^{-2}	1.02	121.6	59	2.06	125.6	129.8	125.5	3.97
430	Refined	7.59×10^{-2}	1.03	121.2	59	2.05	125.2	129.4	125.2	4.00
440	Refined	7.57×10^{-2}	1.03	120.9	59	2.05	124.9	129.1	124.9	4.02
450	Refined	7.54×10^{-2}	1.03	120.6	59	2.04	124.6	128.8	124.6	3.97
460	Refined	7.52×10^{-2}	1.04	120.3	59	2.04	124.3	128.6	124.3	3.95
470	Refined	7.50×10^{-2}	1.04	120.1	59	2.04	124.1	128.3	124.1	3.99
480	Refined	7.48×10^{-2}	1.04	119.9	59	2.03	123.9	128.2	123.9	3.99
490	Refined	7.46×10^{-2}	1.04	119.8	59	2.03	123.8	128.0	123.8	4.00

Table 11. Results of GRB 110731A

E_c	Level	A (Fixed) (Estimation) (ph.s $^{-1}$.cm $^{-2}$ keV $^{-1}$)	α	χ^2	DOF	χ_r^2	AIC	BIC	DIC	pDIC
(1)	(2)	(3)	(4)	(5)	(6)	(7)	(8)	(9)	(10)	(11)
Preliminary estimation										
100	Preliminary	1.34×10^{-1}	0.46	142.8	40	3.57	146.8	150.3	146.9	4.08
120	Preliminary	1.22×10^{-1}	0.56	116.7	40	2.92	120.7	124.2	120.8	4.14
150	Preliminary	1.11×10^{-1}	0.66	94.5	40	2.36	98.5	102.0	98.6	4.16
180	Preliminary	1.04×10^{-1}	0.73	82.0	40	2.05	86.0	89.5	86.1	4.13
200	Preliminary	1.00×10^{-1}	0.76	76.4	40	1.91	80.4	83.9	80.6	4.12
220	Preliminary	9.78×10^{-2}	0.79	72.3	40	1.81	76.3	79.8	76.4	4.13
250	Preliminary	9.47×10^{-2}	0.82	67.7	40	1.69	71.7	75.2	71.8	4.07
300	Preliminary	9.10×10^{-2}	0.86	62.8	40	1.57	66.8	70.3	66.9	4.09
400	Preliminary	8.66×10^{-2}	0.91	57.7	40	1.44	61.7	65.2	61.8	4.11
500	Preliminary	8.40×10^{-2}	0.94	55.2	40	1.38	59.2	62.7	59.3	4.06
600	Preliminary	8.24×10^{-2}	0.96	53.8	40	1.35	57.8	61.3	58.0	4.14
700	Preliminary	8.12×10^{-2}	0.98	52.9	40	1.32	56.9	60.4	57.0	4.09
800	Preliminary	8.04×10^{-2}	0.99	52.3	40	1.31	56.3	59.8	56.5	4.13
900	Preliminary	7.97×10^{-2}	1.00	51.9	40	1.30	55.9	59.4	56.0	4.08
1000	Preliminary	7.92×10^{-2}	1.00	51.6	40	1.29	55.6	59.0	55.6	4.04
1200	Preliminary	7.84×10^{-2}	1.01	51.1	40	1.28	55.1	58.6	55.2	4.05
1500	Preliminary	7.76×10^{-2}	1.02	50.7	40	1.27	54.7	58.2	54.8	4.08
1800	Preliminary	7.71×10^{-2}	1.03	50.5	40	1.26	54.5	58.0	54.7	4.15
2000	Preliminary	7.68×10^{-2}	1.03	50.4	40	1.26	54.4	57.9	54.5	4.12
3000	Preliminary	7.60×10^{-2}	1.04	50.1	40	1.25	54.1	57.6	54.2	4.10
4000	Preliminary	7.57×10^{-2}	1.05	50.0	40	1.25	54.0	57.5	54.1	4.11
5000	Preliminary	7.54×10^{-2}	1.05	49.9	40	1.25	53.9	57.4	54.1	4.11
Refined estimation										
275	Refined	9.27×10^{-2}	0.85	64.9	40	1.62	68.9	72.4	68.9	4.00
325	Refined	8.97×10^{-2}	0.88	61.1	40	1.53	65.1	68.6	65.1	4.01
350	Refined	8.85×10^{-2}	0.89	59.7	40	1.49	63.7	67.2	63.8	4.05
375	Refined	8.75×10^{-2}	0.90	58.6	40	1.47	62.6	66.1	62.7	4.03
425	Refined	8.59×10^{-2}	0.92	56.9	40	1.42	60.9	64.4	61.0	4.02
450	Refined	8.52×10^{-2}	0.93	56.3	40	1.41	60.3	63.8	60.3	4.01
475	Refined	8.46×10^{-2}	0.94	55.7	40	1.39	59.7	63.2	59.8	4.04
525	Refined	8.36×10^{-2}	0.95	54.8	40	1.37	58.8	62.3	58.8	4.02
550	Refined	8.31×10^{-2}	0.95	54.4	40	1.36	58.4	61.9	58.5	4.07
575	Refined	8.31×10^{-2}	0.95	54.4	40	1.36	58.4	61.9	58.5	4.07
625	Refined	8.21×10^{-2}	0.97	53.6	40	1.34	57.6	61.0	57.6	4.02
650	Refined	8.17×10^{-2}	0.97	53.3	40	1.33	57.3	60.8	57.4	4.04
675	Refined	8.15×10^{-2}	0.97	53.1	40	1.33	57.1	60.6	57.1	4.03
725	Refined	8.10×10^{-2}	0.98	52.7	40	1.32	56.7	60.2	56.8	4.02
750	Refined	8.08×10^{-2}	0.98	52.6	40	1.31	56.6	60.1	56.6	4.03
775	Refined	8.06×10^{-2}	0.99	52.5	40	1.31	56.5	59.9	56.5	4.04
825	Refined	8.02×10^{-2}	0.99	52.2	40	1.31	56.2	59.7	56.2	4.05
850	Refined	8.00×10^{-2}	0.99	52.1	40	1.30	56.1	59.6	56.1	4.03
875	Refined	7.98×10^{-2}	0.99	52.0	40	1.30	56.0	59.5	56.0	4.05

Table 12. Results of GRB 180720B

E_c (Fixed)	Level (Estimation)	A (ph.s $^{-1}$.cm $^{-2}$ keV $^{-1}$)	α	χ^2	DOF	χ_r^2	AIC	BIC	DIC	pDIC
(1)	(2)	(3)	(4)	(5)	(6)	(7)	(8)	(9)	(10)	(11)
Preliminary estimation										
100	Preliminary	2.40×10^{-1}	0.59	772.5	110	7.02	776.5	781.9	776.4	3.91
120	Preliminary	2.18×10^{-1}	0.69	591.8	110	5.38	595.8	601.3	595.8	3.92
150	Preliminary	1.98×10^{-1}	0.79	442.4	110	4.02	446.4	451.9	446.4	3.96
180	Preliminary	1.85×10^{-1}	0.85	361.0	110	3.28	365.0	370.4	364.9	3.95
200	Preliminary	1.79×10^{-1}	0.88	325.9	110	2.96	329.9	335.3	329.8	3.94
220	Preliminary	1.74×10^{-1}	0.91	300.0	110	2.73	304.0	309.5	304.0	3.96
250	Preliminary	1.69×10^{-1}	0.94	272.5	110	2.48	276.5	281.9	276.4	3.96
300	Preliminary	1.62×10^{-1}	0.98	243.9	110	2.22	247.9	253.3	247.8	3.95
400	Preliminary	1.54×10^{-1}	1.03	216.3	110	1.97	220.3	225.7	220.2	3.92
500	Preliminary	1.50×10^{-1}	1.06	204.1	110	1.86	208.1	213.6	208.1	3.99
600	Preliminary	1.47×10^{-1}	1.08	197.9	110	1.80	201.9	207.3	201.8	3.94
700	Preliminary	1.45×10^{-1}	1.09	194.3	110	1.77	198.3	203.8	198.3	3.94
800	Preliminary	1.43×10^{-1}	1.10	192.2	110	1.75	196.2	201.6	196.1	3.94
900	Preliminary	1.42×10^{-1}	1.11	190.8	110	1.73	194.8	200.2	194.7	3.91
1000	Preliminary	1.41×10^{-1}	1.12	189.9	110	1.73	193.9	199.3	193.8	3.96
1200	Preliminary	1.39×10^{-1}	1.13	188.8	110	1.72	192.8	198.2	192.7	3.94
1500	Preliminary	1.38×10^{-1}	1.14	188.1	110	1.71	192.1	197.6	192.1	3.96
1800	Preliminary	1.37×10^{-1}	1.14	187.9	110	1.71	191.9	197.3	191.8	3.93
2000	Preliminary	1.37×10^{-1}	1.15	187.8	110	1.71	191.8	197.3	191.7	3.85
3000	Preliminary	1.35×10^{-1}	1.16	187.9	110	1.71	191.9	197.3	191.9	3.96
4000	Preliminary	1.34×10^{-1}	1.16	188.1	110	1.71	192.1	197.5	192.0	3.91
5000	Preliminary	1.34×10^{-1}	1.16	188.2	110	1.71	192.2	197.7	192.3	4.01
Refined estimation										
275	Refined	1.65×10^{-1}	0.96	256.2	110	2.33	260.2	265.6	260.1	3.94
325	Refined	1.60×10^{-1}	1.00	234.4	110	2.13	238.4	243.9	238.4	3.93
350	Refined	1.58×10^{-1}	1.01	227.0	110	2.06	231.0	236.4	231.0	3.96
375	Refined	1.56×10^{-1}	1.02	221.1	110	2.01	225.1	230.5	225.1	3.99
425	Refined	1.53×10^{-1}	1.04	212.4	110	1.93	216.4	221.8	216.3	3.94
450	Refined	1.52×10^{-1}	1.05	209.1	110	1.90	213.1	218.6	213.1	3.93
475	Refined	1.51×10^{-1}	1.05	206.4	110	1.88	210.4	215.9	210.3	3.92
525	Refined	1.49×10^{-1}	1.06	202.2	110	1.84	206.2	211.6	206.2	3.99
550	Refined	1.48×10^{-1}	1.07	200.5	110	1.82	204.5	210.0	204.5	3.95
575	Refined	1.48×10^{-1}	1.07	200.5	110	1.82	204.5	210.0	204.5	4.01
625	Refined	1.47×10^{-1}	1.07	199.1	110	1.81	203.1	208.5	203.1	3.97
650	Refined	1.46×10^{-1}	1.08	196.8	110	1.79	200.8	206.2	200.7	3.94
675	Refined	1.45×10^{-1}	1.09	195.9	110	1.78	199.9	205.3	199.8	3.93
725	Refined	1.45×10^{-1}	1.09	195.0	110	1.77	199.0	204.5	199.0	3.95
750	Refined	1.44×10^{-1}	1.10	193.7	110	1.76	197.7	203.1	197.7	3.99
775	Refined	1.44×10^{-1}	1.10	193.1	110	1.76	197.1	202.5	197.1	3.98
825	Refined	1.43×10^{-1}	1.11	191.8	110	1.74	195.8	201.2	195.8	4.02
850	Refined	1.42×10^{-1}	1.11	191.4	110	1.74	195.4	200.8	195.4	3.96
875	Refined	1.42×10^{-1}	1.11	191.1	110	1.74	195.1	200.5	195.1	3.99

Table 13. Results of GRB 190530A

E_c	Level	A (Fixed) (Estimation) ($\text{ph.s}^{-1} \cdot \text{cm}^{-2} \text{keV}^{-1}$)	α	χ^2	DOF	χ^2_r	AIC	BIC	DIC	pDIC
(1)	(2)	(3)	(4)	(5)	(6)	(7)	(8)	(9)	(10)	(11)
Preliminary estimation										
100	Preliminary	4.54×10^{-1}	0.47	1264.4	91	13.89	1268.4	1273.4	1268.4	4.00
120	Preliminary	4.11×10^{-1}	0.57	925.0	91	10.16	929.0	934.0	929.0	4.03
150	Preliminary	3.72×10^{-1}	0.66	647.8	91	7.12	651.8	656.9	651.8	3.99
180	Preliminary	3.48×10^{-1}	0.72	499.2	91	5.49	503.2	508.3	503.3	4.02
200	Preliminary	3.36×10^{-1}	0.76	436.1	91	4.79	440.1	445.2	440.1	3.98
220	Preliminary	3.27×10^{-1}	0.78	390.2	91	4.29	394.2	399.2	394.1	3.98
250	Preliminary	3.17×10^{-1}	0.81	341.8	91	3.76	345.8	350.9	345.8	3.99
300	Preliminary	3.04×10^{-1}	0.85	292.9	91	3.22	296.9	302.0	296.9	3.98
400	Preliminary	2.89×10^{-1}	0.90	247.8	91	2.72	251.8	256.9	251.8	4.00
500	Preliminary	2.80×10^{-1}	0.93	229.4	91	2.52	233.4	238.5	233.4	4.01
600	Preliminary	2.74×10^{-1}	0.95	220.8	91	2.43	224.8	229.9	224.9	4.05
700	Preliminary	2.70×10^{-1}	0.96	216.5	91	2.38	220.5	225.5	220.5	4.04
800	Preliminary	2.67×10^{-1}	0.97	214.2	91	2.35	218.2	223.3	218.2	3.96
900	Preliminary	2.65×10^{-1}	0.98	213.0	91	2.34	217.0	222.1	217.1	4.03
1000	Preliminary	2.63×10^{-1}	0.98	212.5	91	2.33	216.5	221.5	216.5	4.04
1200	Preliminary	2.61×10^{-1}	0.99	212.3	91	2.33	216.3	221.3	216.3	4.02
1500	Preliminary	2.58×10^{-1}	1.00	212.8	91	2.34	216.8	221.8	216.8	4.03
1800	Preliminary	2.56×10^{-1}	1.01	213.5	91	2.35	217.5	222.6	217.5	4.01
2000	Preliminary	2.55×10^{-1}	1.01	214.0	91	2.35	218.0	223.1	218.1	4.03
3000	Preliminary	2.53×10^{-1}	1.02	216.1	91	2.37	220.1	225.1	220.1	3.98
4000	Preliminary	2.51×10^{-1}	1.03	217.4	91	2.39	221.4	226.4	221.4	4.07
5000	Preliminary	2.51×10^{-1}	1.03	218.2	91	2.40	222.2	227.3	222.3	4.05
Refined estimation										
425	Refined	2.86×10^{-1}	0.91	241.7	91	2.66	245.7	250.8	245.7	4.03
450	Refined	2.84×10^{-1}	0.91	236.8	91	2.60	240.8	245.8	240.8	3.99
475	Refined	2.82×10^{-1}	0.92	232.7	91	2.56	236.7	241.8	236.8	4.04
525	Refined	2.78×10^{-1}	0.93	226.7	91	2.49	230.7	235.7	230.7	4.01
550	Refined	2.77×10^{-1}	0.94	224.4	91	2.47	228.4	233.4	228.4	4.04
550	Refined	2.77×10^{-1}	0.94	224.4	91	2.47	228.4	233.4	228.4	4.01
575	Refined	2.76×10^{-1}	0.94	222.4	91	2.44	226.4	231.5	226.4	3.98
625	Refined	2.73×10^{-1}	0.95	219.4	91	2.41	223.4	228.5	223.5	4.07
650	Refined	2.72×10^{-1}	0.95	218.3	91	2.40	222.3	227.4	222.3	4.05
675	Refined	2.71×10^{-1}	0.96	217.3	91	2.39	221.3	226.4	221.3	3.98
725	Refined	2.70×10^{-1}	0.96	215.8	91	2.37	219.8	224.8	219.8	4.04
750	Refined	2.69×10^{-1}	0.96	215.2	91	2.36	219.2	224.2	219.2	4.02
775	Refined	2.68×10^{-1}	0.97	214.6	91	2.36	218.6	223.7	218.7	4.03
825	Refined	2.67×10^{-1}	0.97	213.8	91	2.35	217.8	222.9	217.8	3.99
850	Refined	2.66×10^{-1}	0.97	213.5	91	2.35	217.5	222.6	217.5	3.99
875	Refined	2.66×10^{-1}	0.98	213.3	91	2.34	217.3	222.3	217.2	3.97
925	Refined	2.65×10^{-1}	0.98	212.9	91	2.34	216.9	221.9	216.9	3.99
950	Refined	2.64×10^{-1}	0.98	212.7	91	2.34	216.7	221.8	216.7	4.04
975	Refined	2.64×10^{-1}	0.98	212.6	91	2.34	216.6	221.6	216.6	3.99

Table 14. Results of GRB 100414A

E_c	Level	A (Fixed)	α	χ^2	DOF	χ_r^2	AIC	BIC	DIC	pDIC
(1)	(2)	(3)	(4)	(5)	(6)	(7)	(8)	(9)	(10)	(11)
100	Preliminary	6.95×10^{-2}	-0.02	1017.6	118	8.62	1021.6	1027.2	1021.6	4.00
120	Preliminary	6.36×10^{-2}	0.10	816.6	118	6.92	820.6	826.2	820.6	3.95
150	Preliminary	5.81×10^{-2}	0.22	641.3	118	5.44	645.3	650.9	645.3	4.00
180	Preliminary	5.47×10^{-2}	0.29	540.0	118	4.58	544.0	549.5	544.0	4.02
200	Preliminary	5.30×10^{-2}	0.33	494.2	118	4.19	498.2	503.8	498.2	4.01
220	Preliminary	5.17×10^{-2}	0.36	459.2	118	3.89	463.2	468.8	463.3	4.01
250	Preliminary	5.02×10^{-2}	0.40	420.4	118	3.56	424.4	430.0	424.4	4.01
300	Preliminary	4.83×10^{-2}	0.44	377.5	118	3.20	381.5	387.1	381.5	3.98
400	Preliminary	4.61×10^{-2}	0.50	331.4	118	2.81	335.4	340.9	335.4	4.00
500	Preliminary	4.48×10^{-2}	0.53	307.7	118	2.61	311.7	317.3	311.7	3.99
600	Preliminary	4.39×10^{-2}	0.55	293.6	118	2.49	297.6	303.2	297.6	3.97
700	Preliminary	4.34×10^{-2}	0.57	284.5	118	2.41	288.5	294.0	288.4	3.98
800	Preliminary	4.29×10^{-2}	0.58	278.0	118	2.36	282.0	287.6	282.0	3.99
900	Preliminary	4.26×10^{-2}	0.59	273.3	118	2.32	277.3	282.9	277.3	4.00
1000	Preliminary	4.23×10^{-2}	0.60	269.7	118	2.29	273.7	279.3	273.7	4.00
1200	Preliminary	4.19×10^{-2}	0.61	264.6	118	2.24	268.6	274.2	268.6	3.98
1500	Preliminary	4.15×10^{-2}	0.62	259.9	118	2.20	263.9	269.5	263.9	3.99
1800	Preliminary	4.12×10^{-2}	0.62	257.0	118	2.18	261.0	266.5	260.9	3.99
2000	Preliminary	4.11×10^{-2}	0.63	255.5	118	2.17	259.5	265.1	259.6	4.06
3000	Preliminary	4.07×10^{-2}	0.64	251.5	118	2.13	255.5	261.1	255.5	3.99
4000	Preliminary	4.05×10^{-2}	0.64	249.7	118	2.12	253.7	259.2	253.7	4.01
5000	Preliminary	4.04×10^{-2}	0.65	248.6	118	2.11	252.6	258.2	252.6	4.02

Table 15. Results of GRB 120711A

E_c	Level	A (Fixed) (Estimation) (ph.s $^{-1}$.cm $^{-2}$ keV $^{-1}$)	α	χ^2	DOF	χ_r^2	AIC	BIC	DIC	pDIC
(1)	(2)	(3)	(4)	(5)	(6)	(7)	(8)	(9)	(10)	(11)
100	Preliminary	5.28×10^{-2}	0.42	91.9	9	10.22	95.9	96.7	95.9	4.01
120	Preliminary	4.79×10^{-2}	0.53	67.4	9	7.49	71.4	72.2	71.3	3.94
150	Preliminary	4.35×10^{-2}	0.63	47.5	9	5.28	51.5	52.3	51.5	3.99
180	Preliminary	4.08×10^{-2}	0.70	37.0	9	4.12	41.0	41.8	41.0	3.98
200	Preliminary	3.95×10^{-2}	0.74	32.6	9	3.63	36.6	37.4	36.6	3.96
220	Preliminary	3.84×10^{-2}	0.77	29.5	9	3.28	33.5	34.3	33.4	3.96
250	Preliminary	3.72×10^{-2}	0.80	26.2	9	2.91	30.2	31.0	30.2	3.96
300	Preliminary	3.58×10^{-2}	0.84	23.0	9	2.55	27.0	27.8	27.0	3.98
400	Preliminary	3.40×10^{-2}	0.89	20.2	9	2.25	24.2	25.0	24.2	4.00
500	Preliminary	3.30×10^{-2}	0.92	19.2	9	2.13	23.2	24.0	23.2	3.97
600	Preliminary	3.23×10^{-2}	0.94	18.8	9	2.09	22.8	23.6	22.8	3.97
700	Preliminary	3.19×10^{-2}	0.96	18.7	9	2.08	22.7	23.5	22.7	3.96
800	Preliminary	3.15×10^{-2}	0.97	18.7	9	2.07	22.7	23.5	22.6	3.93
900	Preliminary	3.13×10^{-2}	0.98	18.7	9	2.08	22.7	23.5	22.7	3.97
1000	Preliminary	3.11×10^{-2}	0.98	18.7	9	2.08	22.7	23.5	22.7	3.98
1200	Preliminary	3.07×10^{-2}	0.99	18.9	9	2.10	22.9	23.7	22.9	3.98
1500	Preliminary	3.04×10^{-2}	1.00	19.1	9	2.12	23.1	23.8	23.0	3.99
1800	Preliminary	3.02×10^{-2}	1.01	19.2	9	2.13	23.2	24.0	23.2	3.99
2000	Preliminary	3.01×10^{-2}	1.01	19.3	9	2.14	23.3	24.1	23.3	3.99
3000	Preliminary	2.98×10^{-2}	1.02	19.6	9	2.18	23.6	24.4	23.6	4.00
4000	Preliminary	2.97×10^{-2}	1.03	19.8	9	2.20	23.8	24.6	23.7	3.91
5000	Preliminary	2.96×10^{-2}	1.03	19.9	9	2.21	23.9	24.7	23.8	3.97

Table 16. Results of GRB 130215A

E_c	Level	A (Fixed) (Estimation) (ph.s $^{-1}$.cm $^{-2}$ keV $^{-1}$)	α	χ^2	DOF	χ_r^2	AIC	BIC	DIC	pDIC
(1)	(2)	(3)	(4)	(5)	(6)	(7)	(8)	(9)	(10)	(11)
100	Preliminary	1.70×10^{-2}	0.84	17.7	11	1.61	21.7	22.8	21.6	3.94
120	Preliminary	1.55×10^{-2}	0.92	15.2	11	1.38	19.2	20.4	19.2	3.99
150	Preliminary	1.40×10^{-2}	0.99	13.2	11	1.20	17.2	18.3	17.1	3.95
180	Preliminary	1.32×10^{-2}	1.05	12.1	11	1.10	16.1	17.2	16.1	4.03
200	Preliminary	1.27×10^{-2}	1.07	11.6	11	1.05	15.6	16.7	15.6	3.99
220	Preliminary	1.24×10^{-2}	1.10	11.2	11	1.02	15.2	16.3	15.1	3.94
250	Preliminary	1.20×10^{-2}	1.12	10.8	11	0.98	14.8	15.9	14.8	3.99
300	Preliminary	1.16×10^{-2}	1.15	10.3	11	0.94	14.3	15.5	14.2	3.91
400	Preliminary	1.10×10^{-2}	1.19	9.9	11	0.90	13.9	15.0	13.8	3.94
500	Preliminary	1.07×10^{-2}	1.21	9.7	11	0.88	13.7	14.8	13.6	3.98
600	Preliminary	1.05×10^{-2}	1.23	9.5	11	0.87	13.5	14.7	13.5	3.99
700	Preliminary	1.03×10^{-2}	1.24	9.5	11	0.86	13.5	14.6	13.4	3.93
800	Preliminary	1.02×10^{-2}	1.25	9.4	11	0.86	13.4	14.5	13.3	3.94
900	Preliminary	1.01×10^{-2}	1.26	9.4	11	0.85	13.4	14.5	13.3	3.96
1000	Preliminary	1.01×10^{-2}	1.26	9.3	11	0.85	13.3	14.5	13.3	3.94
1200	Preliminary	9.97×10^{-3}	1.27	9.3	11	0.85	13.3	14.4	13.2	3.90
1500	Preliminary	9.87×10^{-3}	1.28	9.3	11	0.84	13.3	14.4	13.2	3.97
1800	Preliminary	9.81×10^{-3}	1.28	9.2	11	0.84	13.2	14.4	13.2	3.99
2000	Preliminary	9.77×10^{-3}	1.29	9.2	11	0.84	13.2	14.4	13.2	3.98
3000	Preliminary	9.67×10^{-3}	1.29	9.2	11	0.84	13.2	14.3	13.2	3.95
4000	Preliminary	9.62×10^{-3}	1.30	9.2	11	0.84	13.2	14.3	13.2	3.97
5000	Preliminary	9.59×10^{-3}	1.30	9.2	11	0.84	13.2	14.3	13.2	3.97

Table 17. Results of GRB 090510

E_c	Level	A (Fixed) (Estimation) ($\text{ph.s}^{-1}.\text{cm}^{-2}\text{keV}^{-1}$)	α	χ^2	DOF	χ_r^2	AIC	BIC	DIC	pDIC
(1)	(2)	(3)	(4)	(5)	(6)	(7)	(8)	(9)	(10)	(11)
100	Preliminary	2.88×10^{-2}	0.35	17.4	20	0.87	21.4	23.6	21.4	4.00
120	Preliminary	2.62×10^{-2}	0.46	16.4	20	0.82	20.4	22.6	20.4	3.95
150	Preliminary	2.38×10^{-2}	0.56	15.7	20	0.78	19.7	21.8	19.6	3.99
180	Preliminary	2.24×10^{-2}	0.63	15.3	20	0.76	19.3	21.4	19.3	4.01
200	Preliminary	2.17×10^{-2}	0.67	15.1	20	0.75	19.1	21.3	19.1	4.01
220	Preliminary	2.12×10^{-2}	0.69	15.0	20	0.75	19.0	21.1	19.0	4.06
250	Preliminary	2.05×10^{-2}	0.73	14.8	20	0.74	18.8	21.0	18.8	3.97
300	Preliminary	1.97×10^{-2}	0.77	14.7	20	0.74	18.7	20.9	18.8	4.03
400	Preliminary	1.88×10^{-2}	0.82	14.6	20	0.73	18.6	20.8	18.7	4.05
500	Preliminary	1.83×10^{-2}	0.85	14.6	20	0.73	18.6	20.8	18.6	4.02
600	Preliminary	1.79×10^{-2}	0.88	14.6	20	0.73	18.6	20.8	18.6	4.03
700	Preliminary	1.76×10^{-2}	0.89	14.6	20	0.73	18.6	20.8	18.6	3.98
800	Preliminary	1.75×10^{-2}	0.90	14.6	20	0.73	18.6	20.8	18.6	4.01
900	Preliminary	1.74×10^{-2}	0.91	14.6	20	0.73	18.6	20.8	18.6	3.99
1000	Preliminary	1.72×10^{-2}	0.92	14.6	20	0.73	18.6	20.8	18.6	3.98
1200	Preliminary	1.71×10^{-2}	0.93	14.6	20	0.73	18.6	20.8	18.6	3.98
1500	Preliminary	1.69×10^{-2}	0.94	14.6	20	0.73	18.6	20.8	18.6	3.98
1800	Preliminary	1.68×10^{-2}	0.94	14.7	20	0.73	18.7	20.8	18.7	4.02
2000	Preliminary	1.68×10^{-2}	0.95	14.7	20	0.73	18.7	20.8	18.7	4.00
3000	Preliminary	1.66×10^{-2}	0.96	14.7	20	0.73	18.7	20.9	18.7	4.06
4000	Preliminary	1.65×10^{-2}	0.96	14.7	20	0.73	18.7	20.9	18.7	3.98
5000	Preliminary	1.65×10^{-2}	0.97	14.7	20	0.73	18.7	20.9	18.7	3.96

Table 18. Results of E'_c Estimation of the CPL model

GRB	Group	Model	E_c	A	α	E_p	E'_c	α'	E'_p	E_c vs. E'_c	Interpretation
			(Observed)	(Observed)	(Observed)	(Observed)	($\Delta\text{DIC} \leq 5$)	($\Delta\text{DIC} \leq 5$)	($\Delta\text{DIC} \leq 5$)	(Match)	(For E_c vs. E'_c)
(1)	(2)	(3)	(4)	(5)	(6)	(7)	(8)	(9)	(10)	(11)	(12)
140703A(026)	I	CPL	173^{+51}_{-38}	$0.8^{+0.3}_{-0.2}$	$-1.16^{+0.11}_{-0.12}$	145^{+47}_{-38}	100	-0.90	110	Nicely	Moderated E_c and α
150301B(818)	I	CPL	239^{+178}_{-100}	$1.5^{+1.5}_{-0.7}$	$-1.16^{+0.21}_{-0.22}$	201^{+158}_{-99}	150	-0.98	153	Nicely	Moderated E_c and α
160629A(930)	I	CPL	212^{+64}_{-49}	$0.5^{+0.2}_{-0.1}$	$-0.91^{+0.12}_{-0.11}$	231^{+74}_{-58}	140	-0.78	171	Nicely	Moderated E_c and α
090529(564)	I	CPL	305^{+66}_{-55}	$3.6^{+0.8}_{-0.6}$	$-1.15^{+0.06}_{-0.06}$	259^{+59}_{-50}	300	-1.11	267	Nicely	Moderated E_c and α
091003(191)	I	CPL	388^{+41}_{-38}	2.9 ± 0.3	-1.03 ± 0.03	376^{+41}_{-39}	280	-0.98	286	Nicely	Moderated E_c and α
140606B(133)	I	CPL	531^{+188}_{-137}	$2.7^{+0.7}_{-0.5}$	-1.19 ± 0.07	430^{+157}_{-117}	425	-1.13	370	Nicely	Moderated E_c and α
120624B(933)	I	CPL	642^{+90}_{-79}	$1.3^{+0.2}_{-0.2}$	-0.98 ± 0.04	655^{+95}_{-85}	575	-0.94	610	Nicely	Moderated E_c and α
090328(401)	I	CPL	759^{+104}_{-95}	1.7 ± 0.1	$-1.13^{+0.03}_{-0.02}$	660^{+93}_{-84}	500	-1.11	445	Nicely	Moderated E_c and α
120711A(115)	I	CPL	1326^{+140}_{-121}	$1.6^{+0.2}_{-0.1}$	-1.01 ± 0.02	1313^{+141}_{-123}	300	-0.84	348	Poorly	E_c too high
130215A(063)	I	CPL	2387^{+1798}_{-970}	2.0 ± 0.3	-1.38 ± 0.04	1480^{+1119}_{-609}	150	-0.99	152	Poorly	E_c too high
100414A(097)	II	CPL	418^{+21}_{-20}	$0.36^{+0.04}_{-0.02}$	-0.52 ± 0.02	619^{+32}_{-31}	3000	-0.63	4110	Poorly	α too hard
180728A(728)	II	CPL	339^{+17}_{-16}	160 ± 10	-1.70 ± 0.01	102^{+6}_{-6}	380	-1.73	103	Nicely	Moderated E_c and α

Table 19. Results of E'_p Estimation of the Band model

GRB	Group	Model	E_p	A	α	β	E'_c	α'	E'_p	E_p vs. E'_p	Interpretation
			(Observed)	(Observed)	(Observed)	(Observed)	($\Delta\text{DIC} \leq 5$)	($\Delta\text{DIC} \leq 5$)	($\Delta\text{DIC} \leq 5$)	(Match)	(For E_p vs. E'_p)
(1)	(2)	(3)	(4)	(5)	(6)	(7)	(8)	(9)	(10)	(11)	(12)
140206A(275)	III	Band	280^{+10}_{-10}	$(4.2 \pm 0.1) \times 10^{-2}$	-0.96 ± 0.16	-2.21 ± 0.05	380	-1.01	376	Nicely	Moderated E_p and α
110731A(465)	III	Band	366^{+27}_{-27}	$(4.8 \pm 0.2) \times 10^{-2}$	-0.90 ± 0.03	-3.00 ± 0.70	525	-0.95	551	Nicely	Moderated E_p and α
180720B(598)	III	Band	511 ± 26	$(7.0 \pm 0.1) \times 10^{-2}$	-1.07 ± 0.01	-2.21 ± 0.03	775	-1.10	697	Nicely	Moderated E_p and α
190530A(430)	III	Band	866^{+13}_{-13}	$(1.3 \pm 0.01) \times 10^{-1}$	-1.01 ± 0.01	-3.63 ± 0.20	700	-0.96	729	Nicely	Moderated E_p and α
090510(016)	III	Band	5200^{+574}_{-584}	$(9.0 \pm 0.4) \times 10^{-3}$	-0.89 ± 0.04	-3.4 ± 1.3	100	-0.34	165	Poorly	E_p too high

Table 20. Results of E'_p Estimation Using the Empirical Relation.

GRB	A	Γ	χ^2	DOF	χ^2_r	AIC	BIC	DIC	pDIC	E'_p	E_p vs. E'_p
(1)	(2)	(3)	(4)	(5)	(6)	(7)	(8)	(9)	(10)	(11)	(12)
090328	$(1.82^{+0.02}_{-0.02}) \times 10^{-2}$	$1.22^{+0.02}_{-0.01}$	40.48	29	1.40	44.48	47.35	44.43	3.95	176 ± 7	Poorly
090510	$(2.27^{+0.11}_{-0.11}) \times 10^{-2}$	$1.00^{+0.07}_{-0.07}$	13.35	28	0.48	17.35	20.15	17.33	3.99	269 ± 36	Poorly
090529	$(3.18^{+0.04}_{-0.04}) \times 10^{-2}$	$1.29^{+0.02}_{-0.02}$	133.88	62	2.16	137.88	142.20	137.88	4.00	154 ± 6	Poorly
091003	$(4.35^{+0.03}_{-0.03}) \times 10^{-2}$	$1.19^{+0.01}_{-0.01}$	80.86	60	1.35	84.86	89.12	84.79	3.93	187 ± 4	Poorly
100414A	$(3.99^{+0.02}_{-0.02}) \times 10^{-2}$	$0.66^{+0.01}_{-0.01}$	244.61	118	2.07	248.61	254.18	248.64	4.03	514 ± 10	Poorly
110731A	$(7.45^{+0.10}_{-0.10}) \times 10^{-2}$	$1.06^{+0.02}_{-0.02}$	49.71	40	1.24	53.71	57.18	53.73	4.02	240 ± 9	Poorly
120624B	$(2.58^{+0.03}_{-0.03}) \times 10^{-2}$	$1.05^{+0.02}_{-0.02}$	53.15	34	1.56	57.15	60.32	57.21	4.05	244 ± 9	Poorly
120711A	$(2.92^{+0.04}_{-0.04}) \times 10^{-2}$	$1.04^{+0.02}_{-0.02}$	20.37	9	2.26	24.37	25.16	24.35	3.98	249 ± 10	Poorly
130215A	$(0.95^{+0.02}_{-0.02}) \times 10^{-2}$	$1.31^{+0.04}_{-0.04}$	9.17	11	0.83	13.17	14.30	13.18	4.01	149 ± 11	Poorly
140206A	$(6.59^{+0.03}_{-0.03}) \times 10^{-2}$	$1.16^{+0.01}_{-0.01}$	131.70	59	2.23	135.70	139.93	135.64	3.94	198 ± 4	Poorly
140606B	$(2.27^{+0.03}_{-0.03}) \times 10^{-2}$	$1.26^{+0.02}_{-0.02}$	51.51	47	1.10	55.51	59.29	55.50	3.99	164 ± 6	Poorly
140703A	$(5.57^{+0.11}_{-0.11}) \times 10^{-3}$	$1.45^{+0.03}_{-0.03}$	42.56	26	1.64	46.56	49.22	46.53	3.98	114 ± 7	Poorly
150301B	$(1.24^{+0.04}_{-0.04}) \times 10^{-2}$	$1.37^{+0.05}_{-0.05}$	19.63	18	1.09	23.63	25.62	23.71	4.08	133 ± 13	Poorly
160629A	$(9.53^{+0.20}_{-0.21}) \times 10^{-3}$	$1.16^{+0.03}_{-0.03}$	11.09	13	0.85	15.09	16.51	15.12	4.03	198 ± 11	Poorly
180720B	$(1.32^{+0.01}_{-0.01}) \times 10^{-1}$	$1.18^{+0.01}_{-0.01}$	189.23	110	1.72	193.23	198.67	193.22	3.99	190 ± 4	Poorly
180728A	$(1.68^{+0.01}_{-0.01}) \times 10^{-1}$	$1.86^{+0.01}_{-0.01}$	157.88	47	3.36	161.88	165.67	161.86	3.98	52 ± 1	Poorly
190530A	$(2.48^{+0.01}_{-0.01}) \times 10^{-1}$	$1.04^{+0.01}_{-0.01}$	222.39	91	2.44	226.39	231.46	226.32	3.92	249 ± 5	Poorly

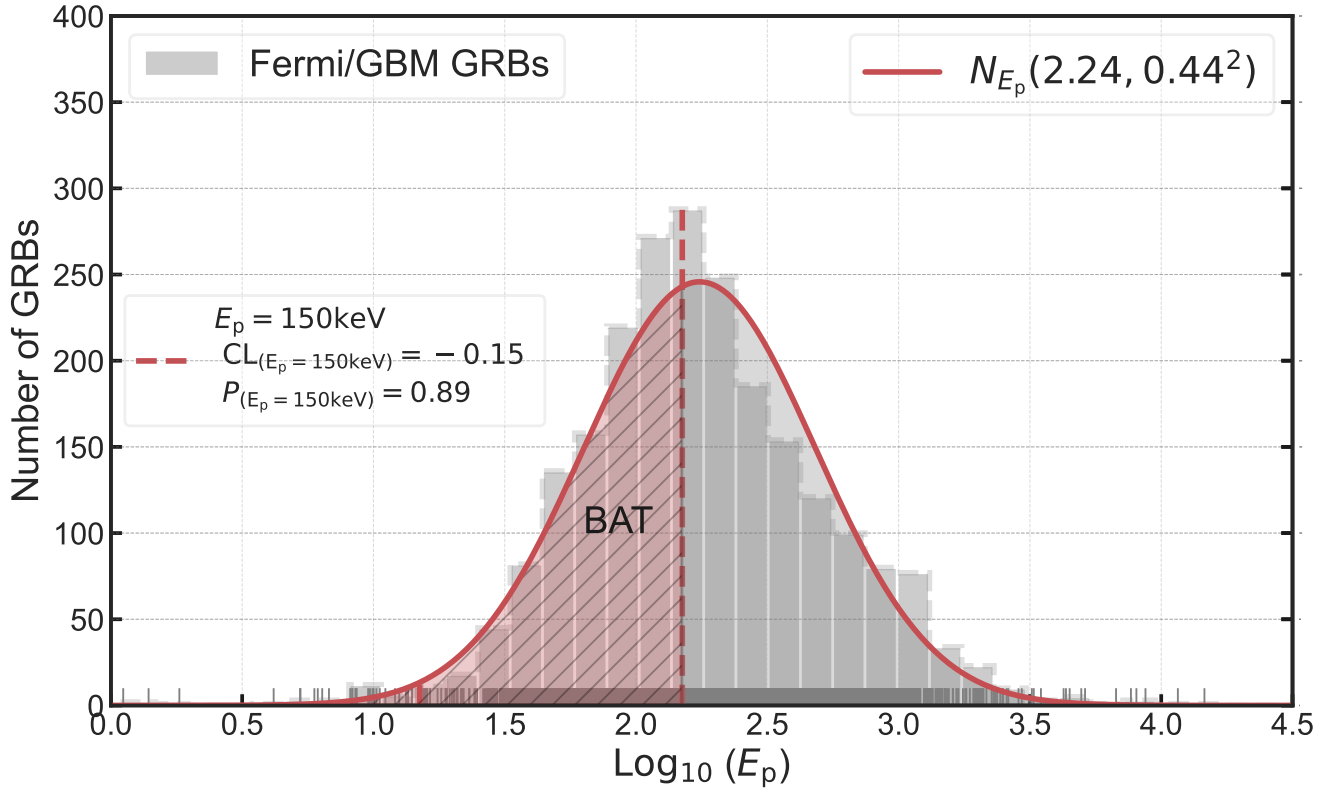


Figure 1. Distribution of E_p for the complete Fermi/GBM burst catalog (grey shaded region). The red solid lines represent its best Gaussian fits. The E_p distribution covers by the BAT energy range is highlighted by the red slash-shaded region.

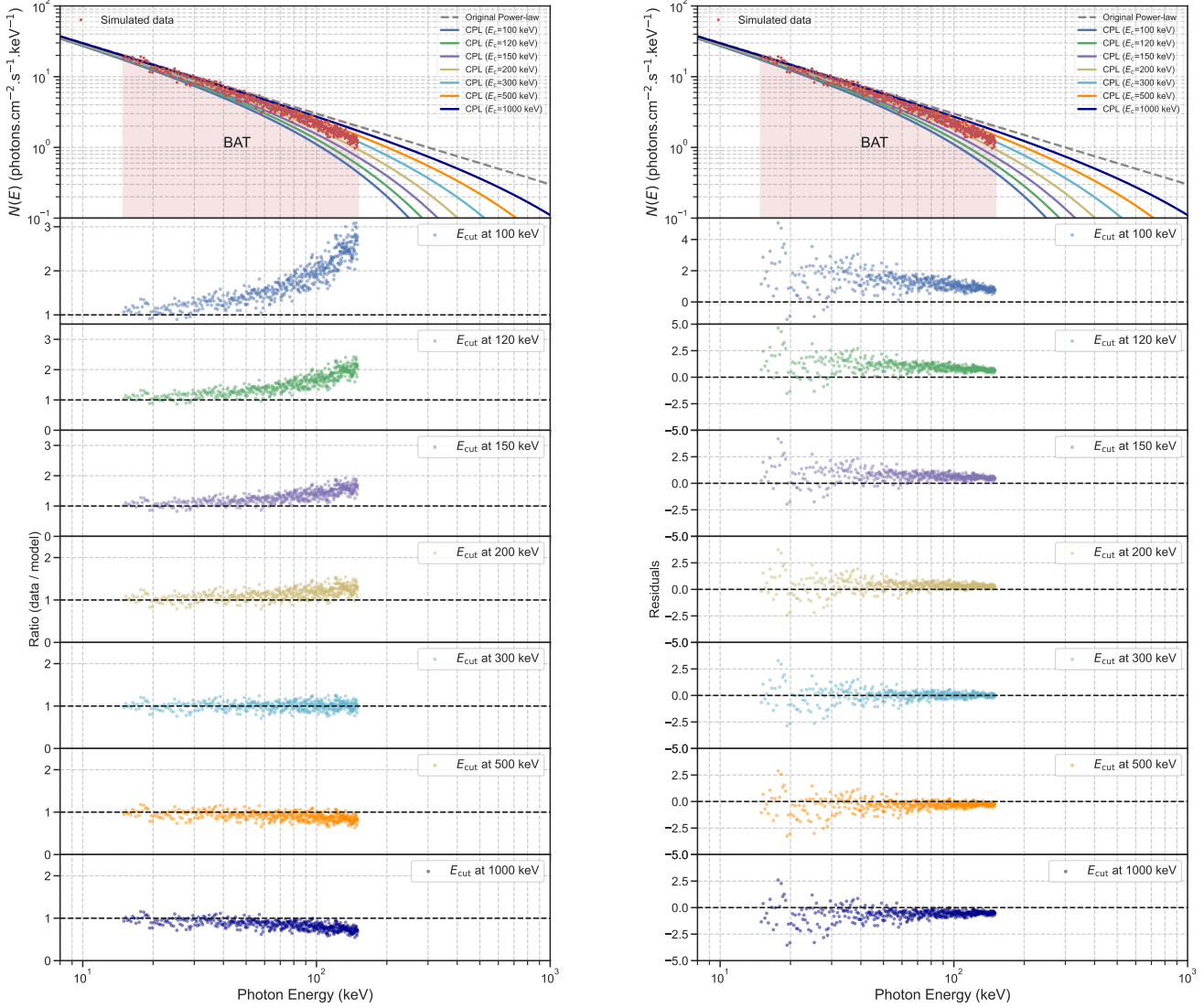


Figure 2. Simulation results for GRB spectra using the CPL model. Left-panel: Top panel shows the simulated data points (red) in the 15–150 keV band, CPL model curves for various E_{cut} values (colored lines), and the power-law baseline (gray dashed line). The lower panels show the ratio evolution for E_{cut} values ranging from 100 keV to 1000 keV. Right-panel: Similar layout, but showing residual evolution for the same E_{cut} values.

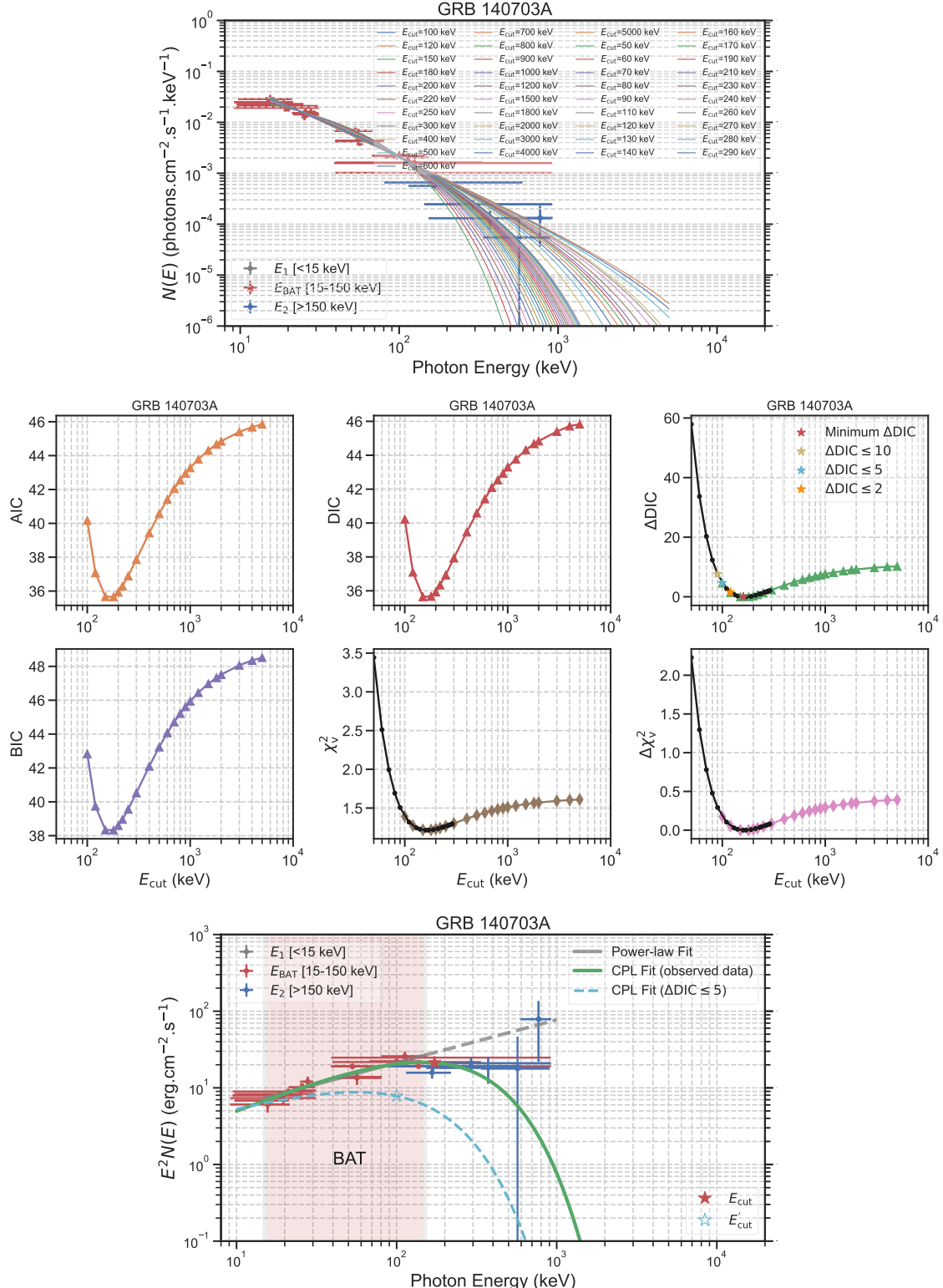


Figure 3. The results of GRB 140703A. **Top panel:** The spectral data obtained from the GBM observation, separated into three distinct energy ranges: E_1 [< 15 keV] (grey), E_{BAT} [15–150 keV] (red), and E_2 [> 150 keV] (blue). Solid colored lines represent the CPL spectral model with varying E_c values (see Table 1). **Middle panel:** The statistical criteria (AIC, BIC, DIC, χ^2) and their deviations (ΔDIC , $\Delta \chi^2$) from the minimum value plotted as function as E_c . Five-pointed stars in different colors denote the locations corresponding to various ΔDIC thresholds used for evaluation on the $\Delta \text{DIC}-E_c$ diagram. The data points indicated by black circles represent the refined estimations, while the others represent the preliminary estimations. **Bottom panel:** The original spectral data from GBM observation (grey, red, and blue points) alongside the best CPL model fit (green solid line), with the fitted model parameters: $E_c=173^{+51}_{-38}$ keV, $A=(7.6^{+3.3}_{-2.3}) \times 10^{-1}$, $\alpha=-1.16^{+0.11}_{-0.12}$. The grey solid and dashed lines represent the best power-law fits to the spectral data within and outside the BAT energy range. Dashed lines in different colors correspond to CPL fit derived from model parameters selected using different ΔDIC thresholds ($\Delta \text{DIC} \leq 10$, $\Delta \text{DIC} \leq 5$, $\Delta \text{DIC} \leq 2$, and minimum ΔDIC).

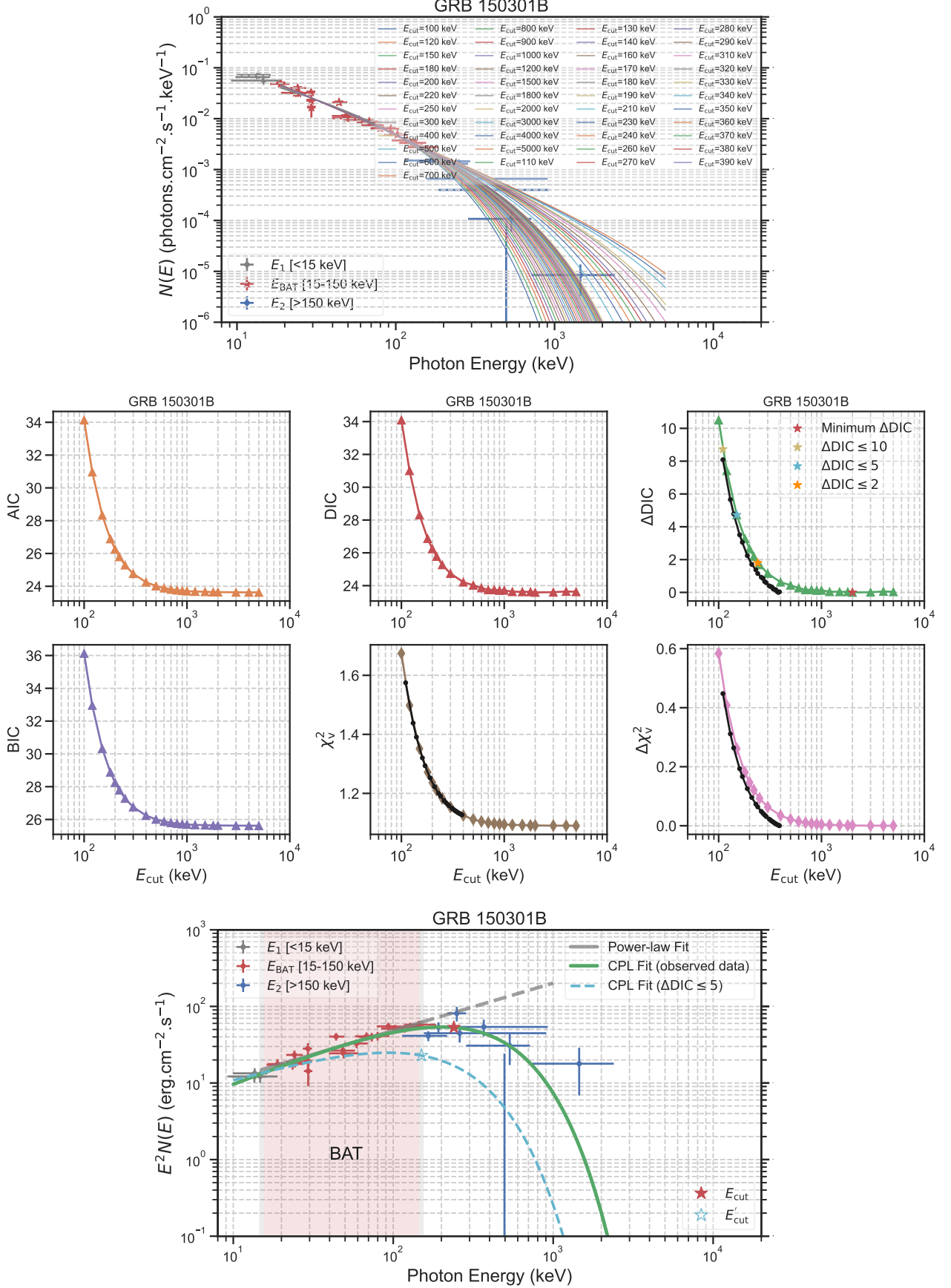


Figure 4. Same as Figure 3 but for GRB 150301B. Note that the best CPL model fit to the original spectral data from GBM observation gives $E_c=239^{+178}_{-100}$ keV, $A=(1.5^{+1.5}_{-0.7})$, $\alpha=-1.16^{+0.21}_{-0.22}$.

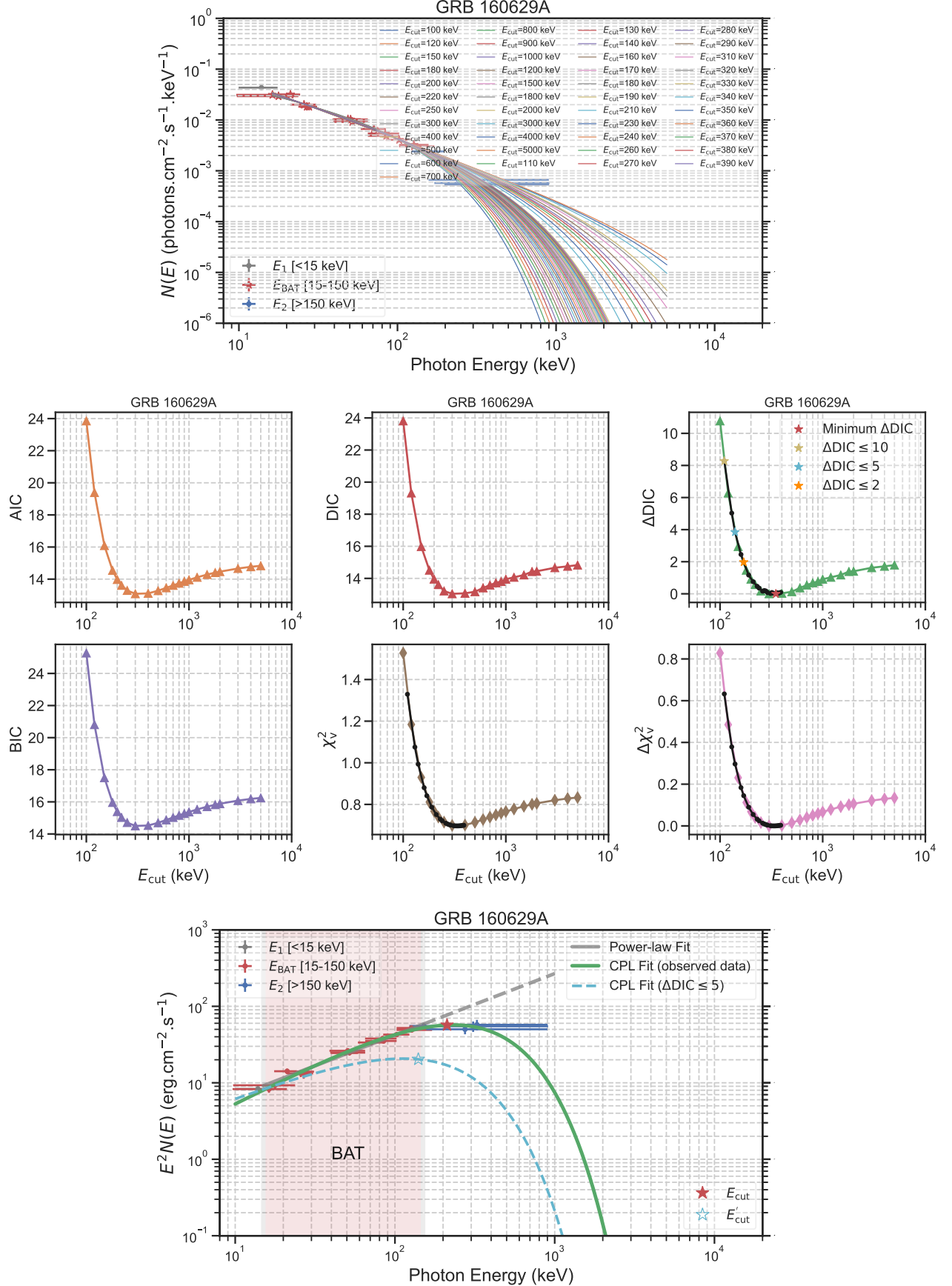


Figure 5. Same as Figure 3 but for GRB 160629A. Note that the best CPL model fit to the original spectral data from GBM observation gives $E_c=212^{+64}_{-49}$ keV, $A=(4.5^{+2.0}_{-1.4})\times 10^{-1}$, $\alpha=-0.91^{+0.12}_{-0.11}$.

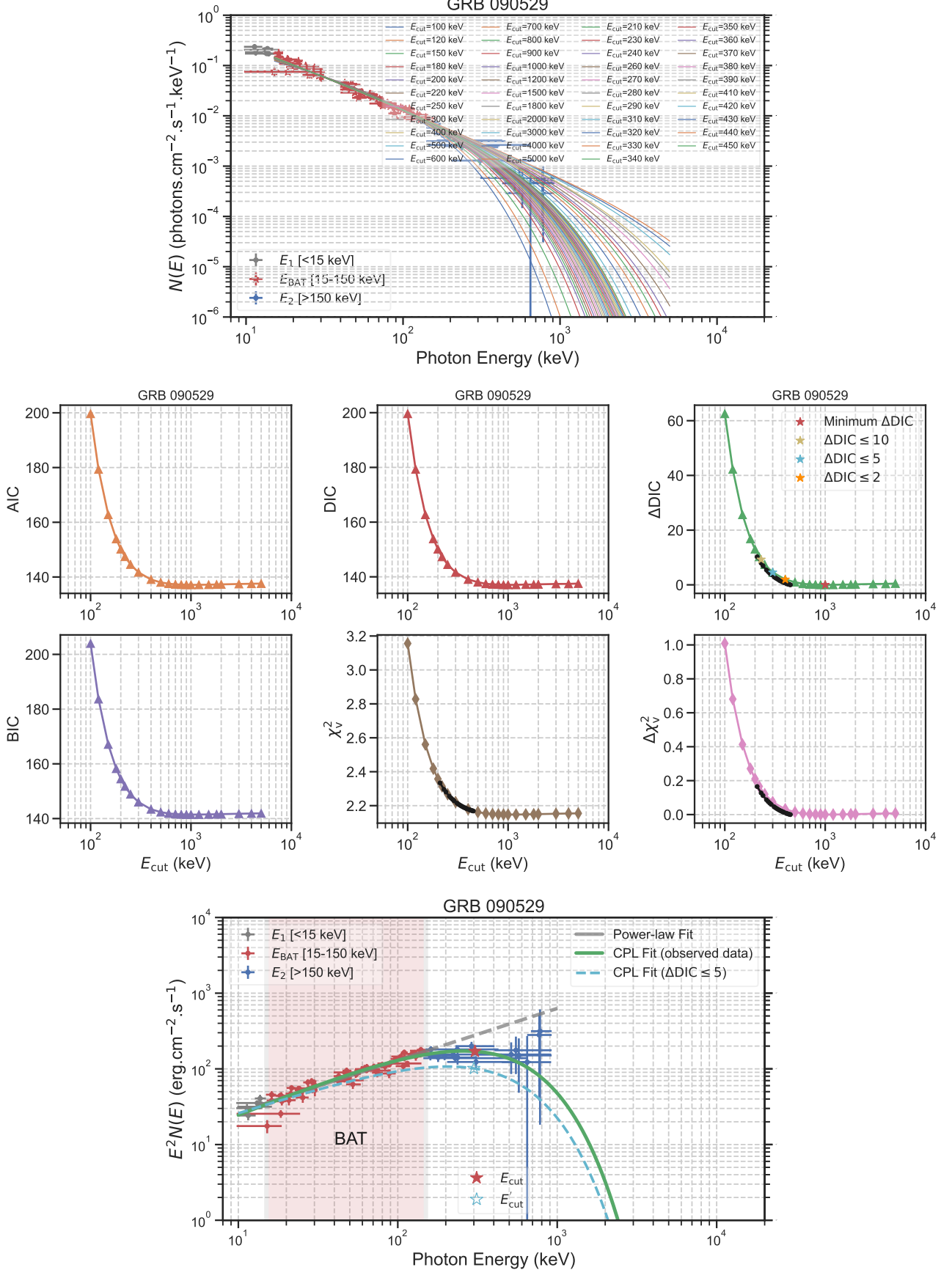


Figure 6. Same as Figure 3 but for GRB 090529. Note that the best CPL model fit to the original spectral data from GBM observation gives $E_c=305^{+66}_{-55}$ keV, $A=(3.6^{+0.8}_{-0.6})$, $\alpha=-1.15^{+0.06}_{-0.06}$.

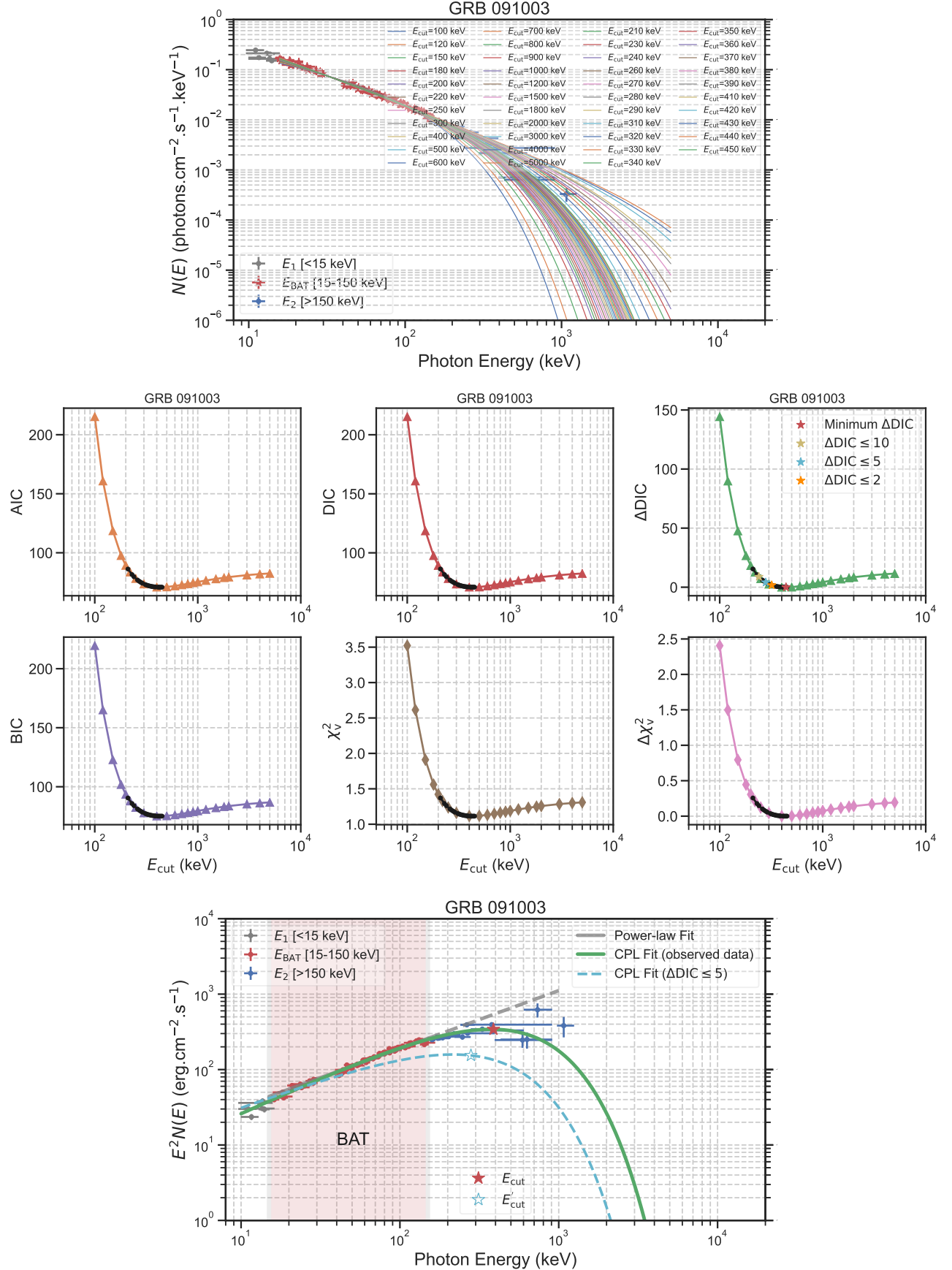


Figure 7. Same as Figure 3 but for GRB 091003. Note that the best CPL model fit to the original spectral data from GBM observation gives $E_c = 388^{+41}_{-38}$ keV, $A = (2.9^{+0.3}_{-0.3})^{+0.03}_{-0.03}$.

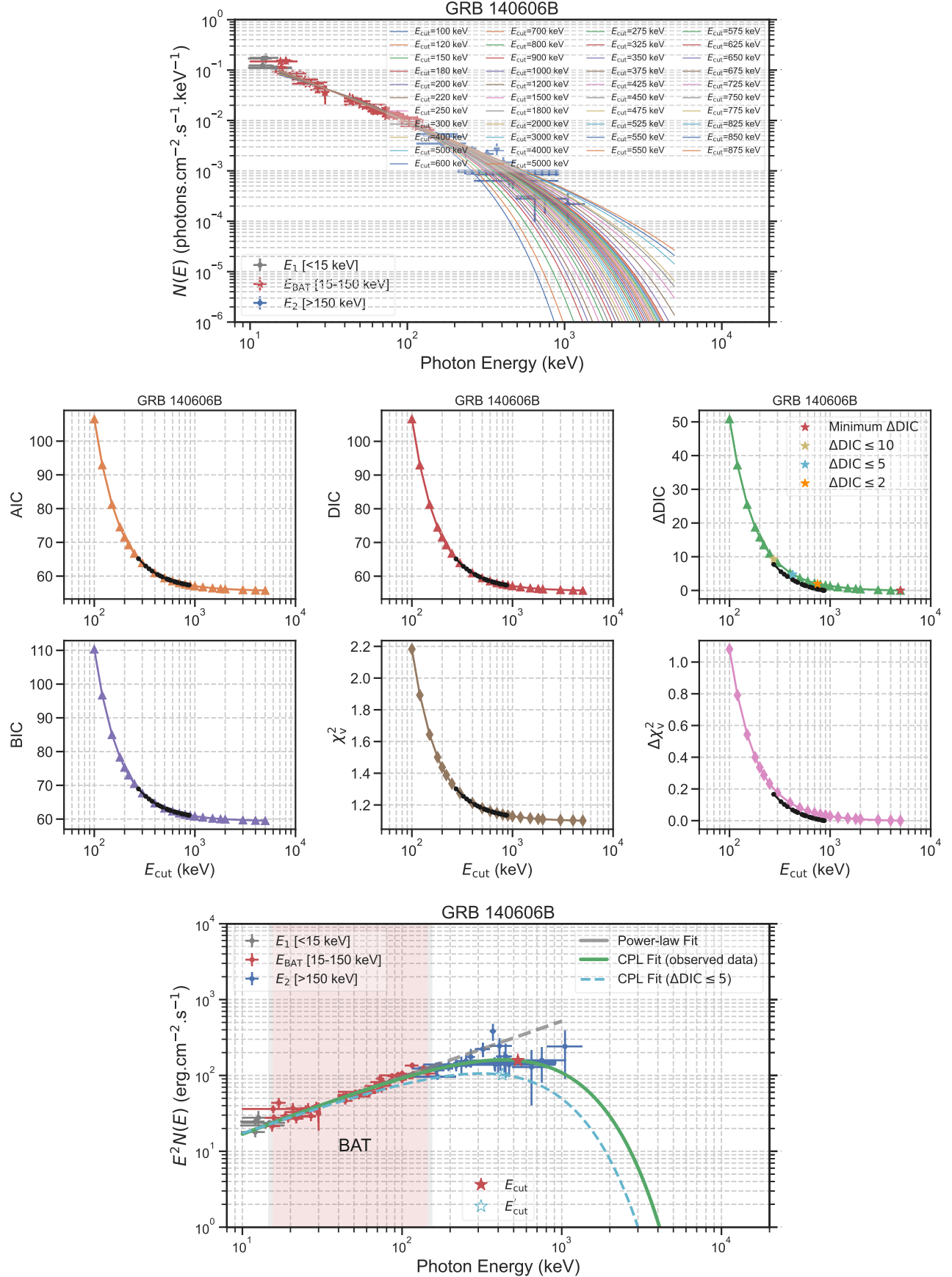


Figure 8. Same as Figure 3 but for GRB 140606B. Note that the best CPL model fit to the original spectral data from GBM observation gives $E_c=531^{+188}_{-136}$ keV, $A=(2.7^{+0.7}_{-0.5})$, $\alpha=-1.19^{+0.07}_{-0.07}$.

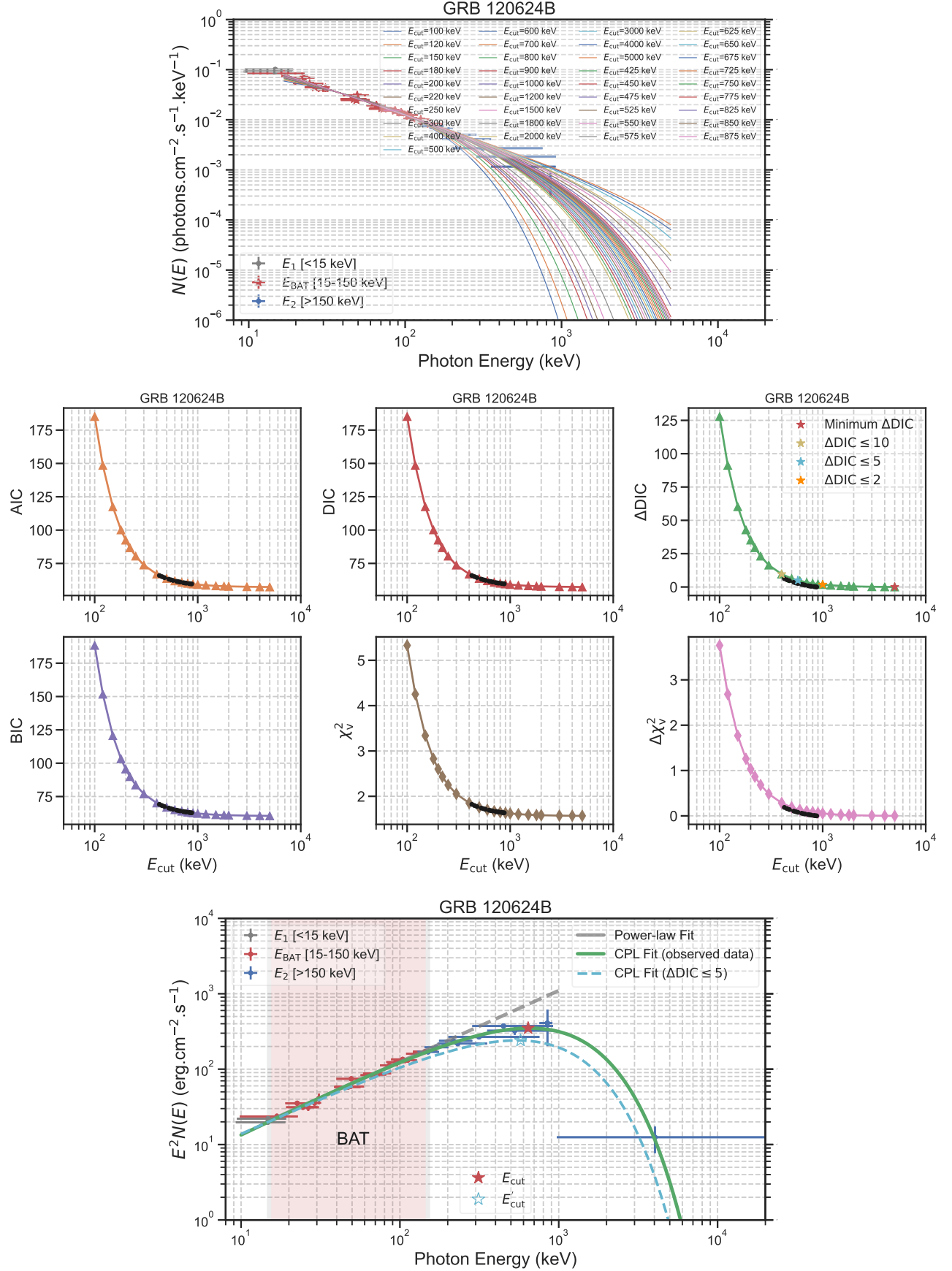


Figure 9. Same as Figure 3 but for GRB 120624B. Note that the best CPL model fit to the original spectral data from GBM observation gives $E_c=626^{+65}_{-60}$ keV, $A=(1.30^{+0.18}_{-0.16})$, $\alpha=-0.98^{+0.04}_{-0.04}$.

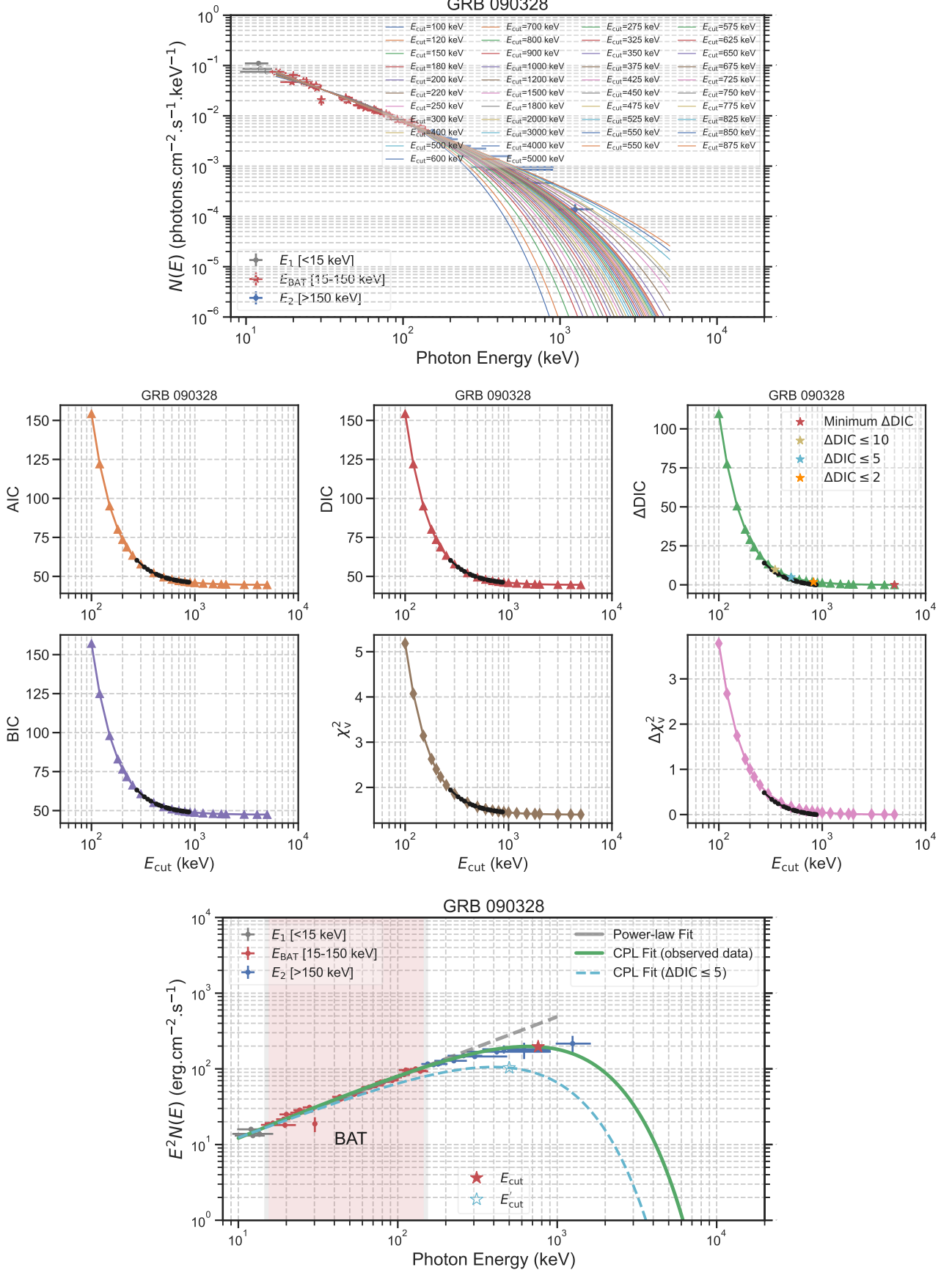


Figure 10. Same as Figure 3 but for GRB 090328. Note that the best CPL model fit to the original spectral data from GBM observation gives $E_c=759^{+104}_{-95}$ keV, $A=(1.7^{+0.1}_{-0.1})$, $\alpha=-1.13^{+0.03}_{-0.02}$.

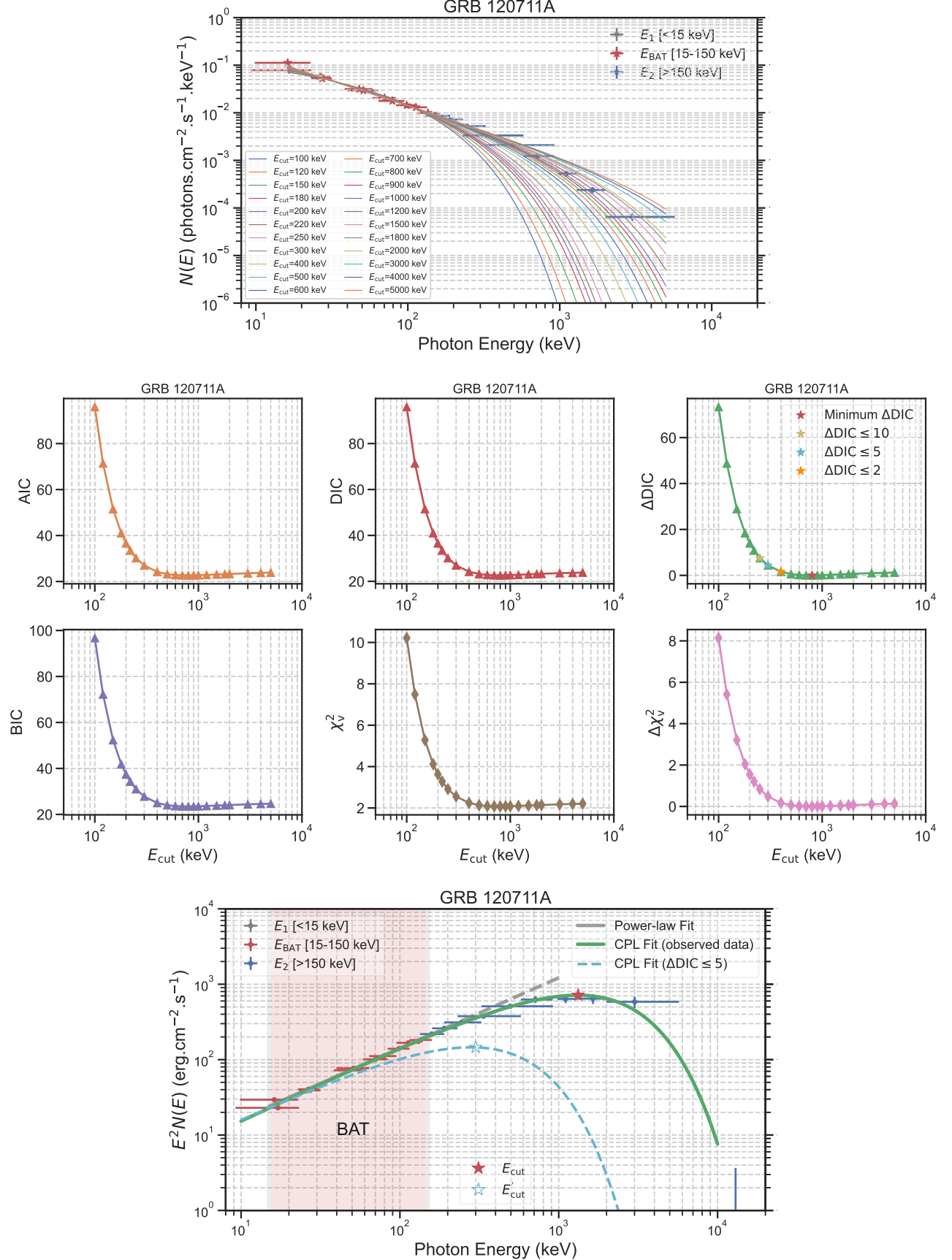


Figure 11. Same as Figure 3 but for GRB 120711A. Note that the best CPL model fit to the original spectral data from GBM observation gives $E_c=1330^{+140}_{-130}$ keV, $A=(1.58^{+0.15}_{-0.14})$, $\alpha=-1.01^{+0.02}_{-0.02}$.

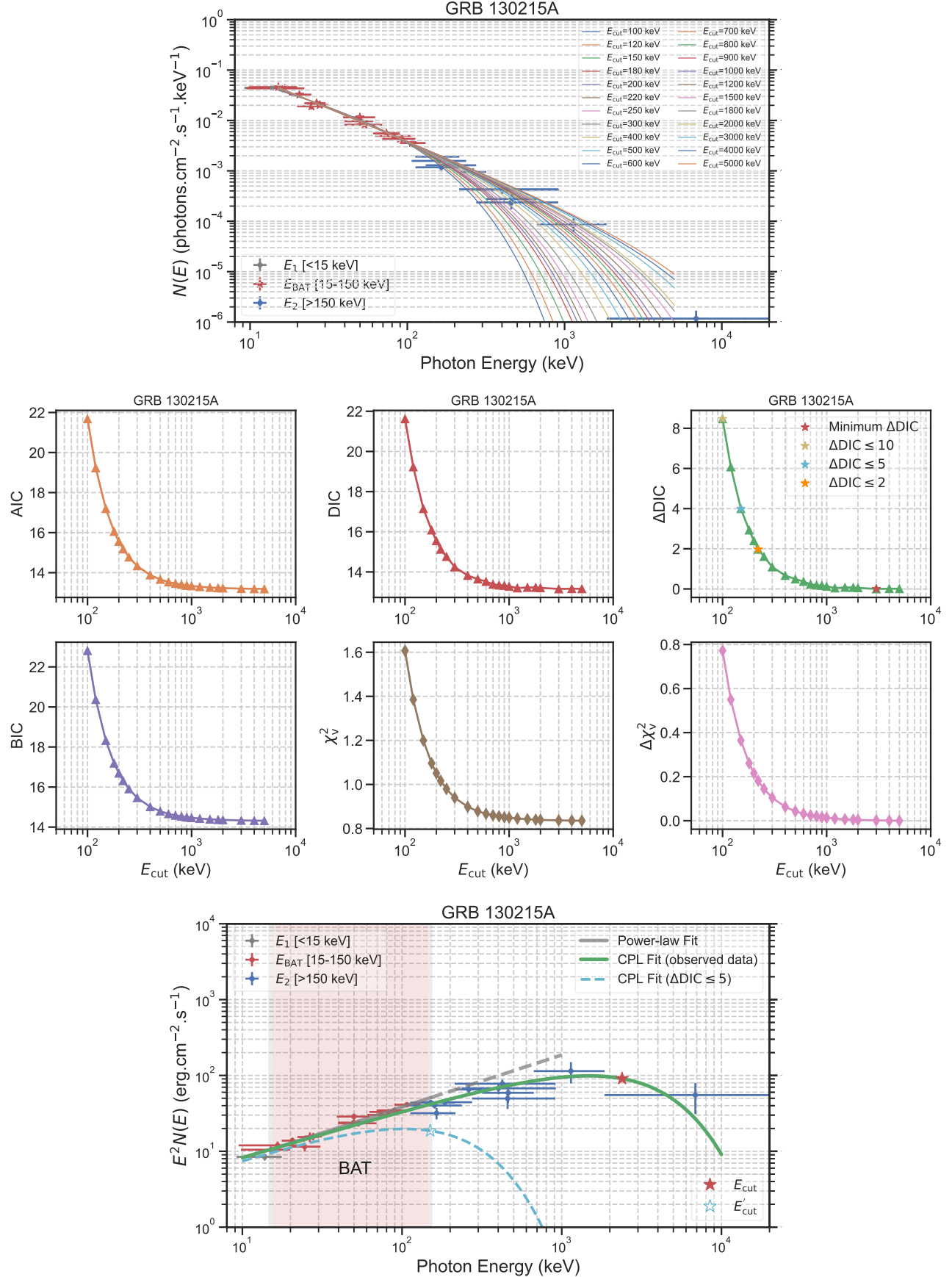


Figure 12. Same as Figure 3 but for GRB 130215A. Note that the best CPL model fit to the original spectral data from GBM observation gives $E_c = 2387^{+1798}_{-970}$ keV, $A = (2.0^{+0.3}_{-0.3})$, $\alpha = -1.38^{+0.04}_{-0.04}$.

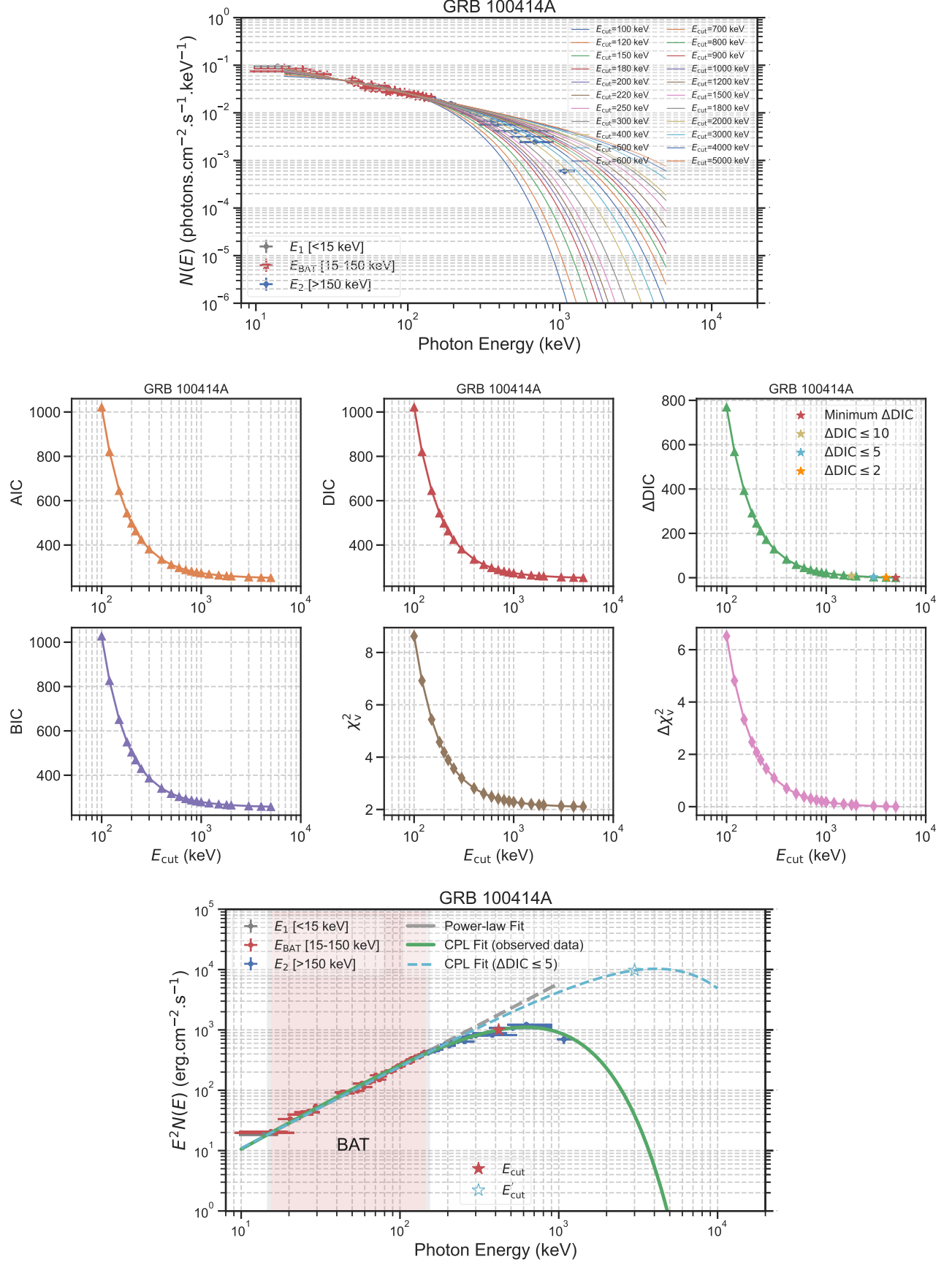


Figure 13. Same as Figure 3 but for GRB 100414A. Note that the best CPL model fit to the original spectral data from GBM observation gives $E_c=418^{+21}_{-20}$ keV, $A=(3.59^{+0.40}_{-0.34}) \times 10^{-1}$, $\alpha=-0.52^{+0.02}_{-0.02}$.

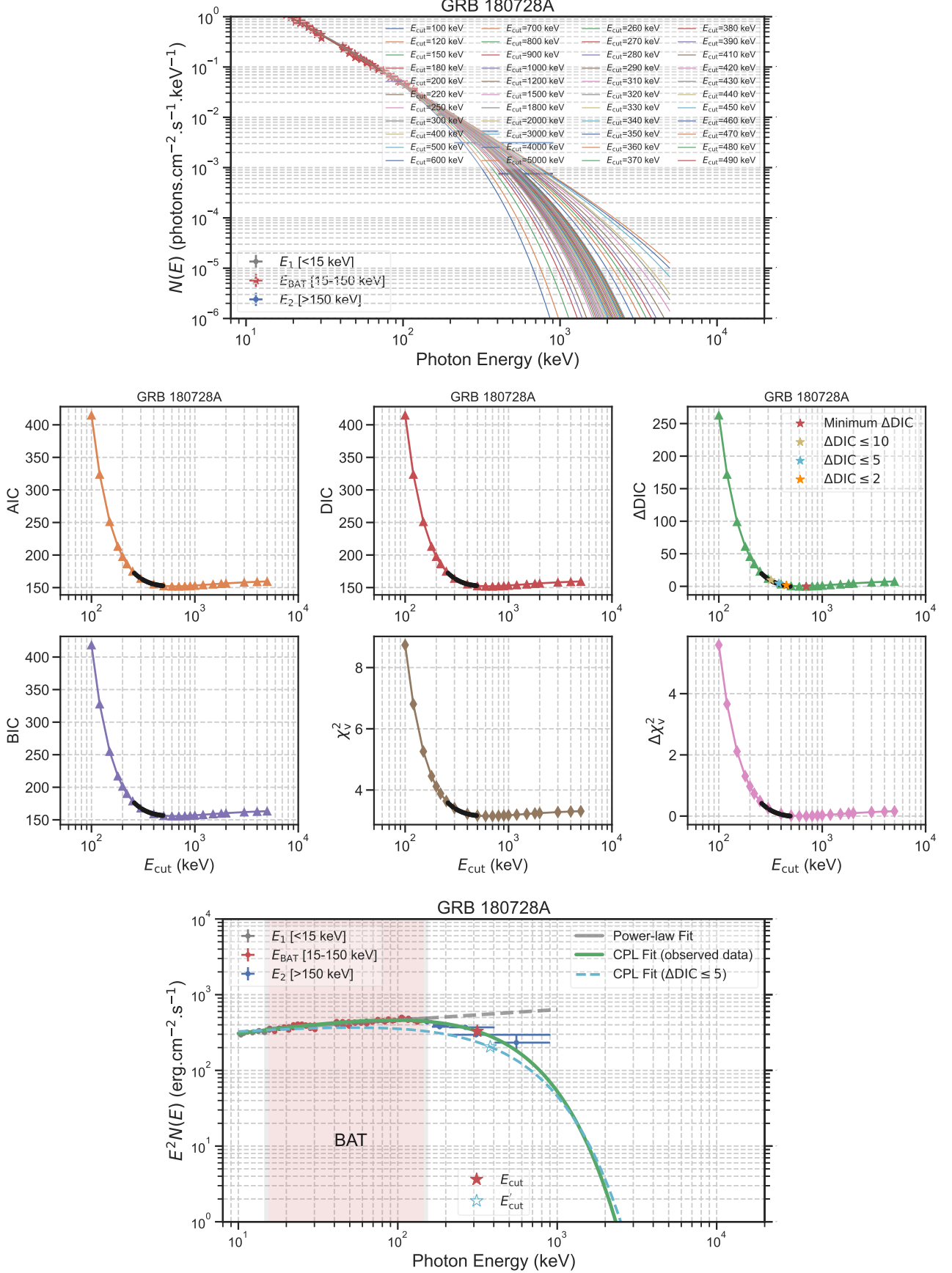


Figure 14. Same as Figure 3 but for GRB 180728A. Note that the best CPL model fit to the original spectral data from GBM observation gives $E_c = 315^{+19}_{-18}$ keV, $A = (1.59^{+0.06}_{-0.05}) \times 10^2$, $\alpha = -1.70^{+0.01}_{-0.01}$.

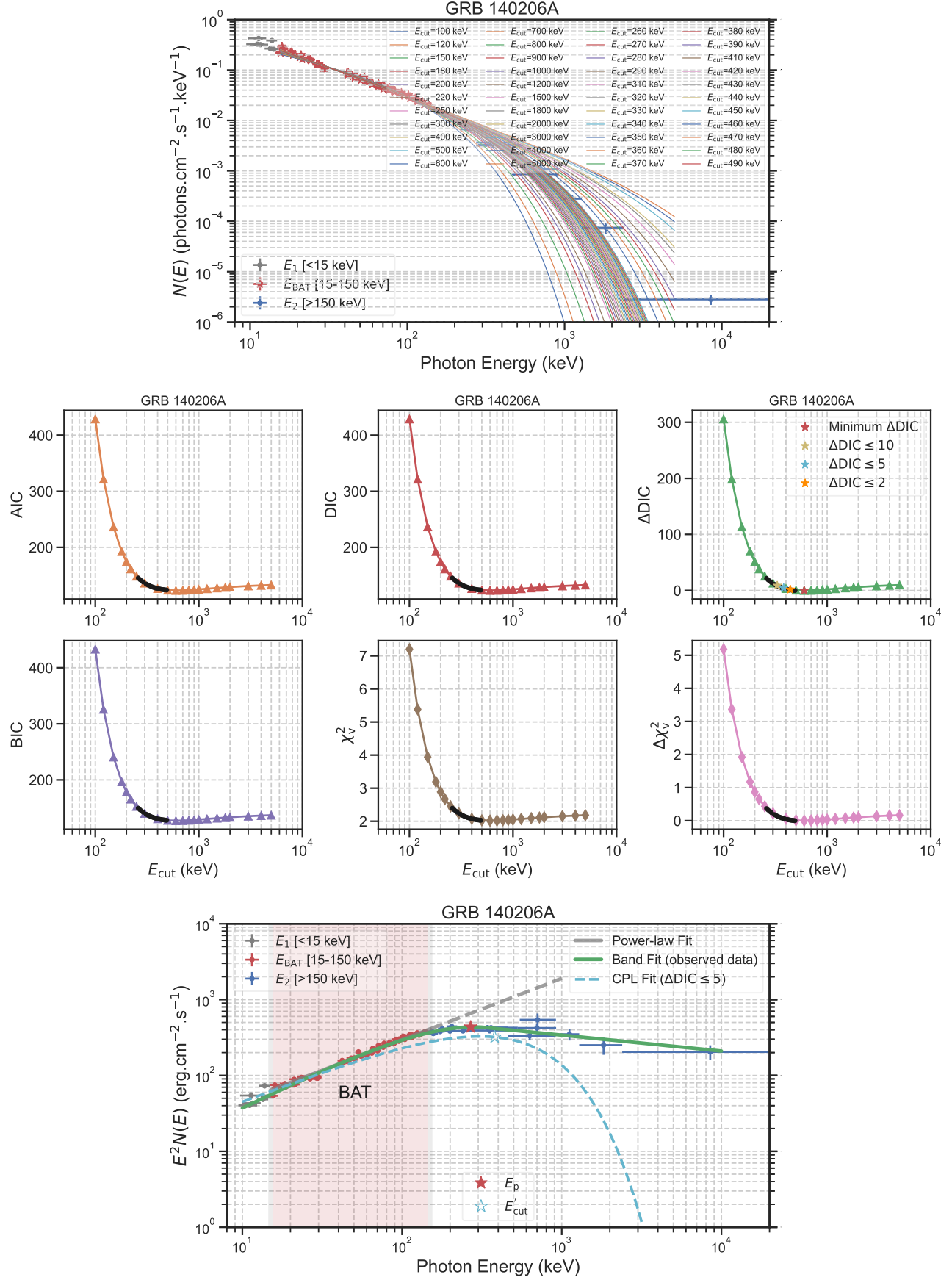


Figure 15. Same as Figure 3 but for GRB 140206A. Note that the best-fit model in this case is the Band function, with fitted model parameters: $E_p=280\pm10 \text{ keV}$, $A=(4.2\pm0.1)\times10^{-2}$, $\alpha=-0.96\pm0.16$, $\beta=-2.21\pm0.05$. Color code and description as in Figure 3.

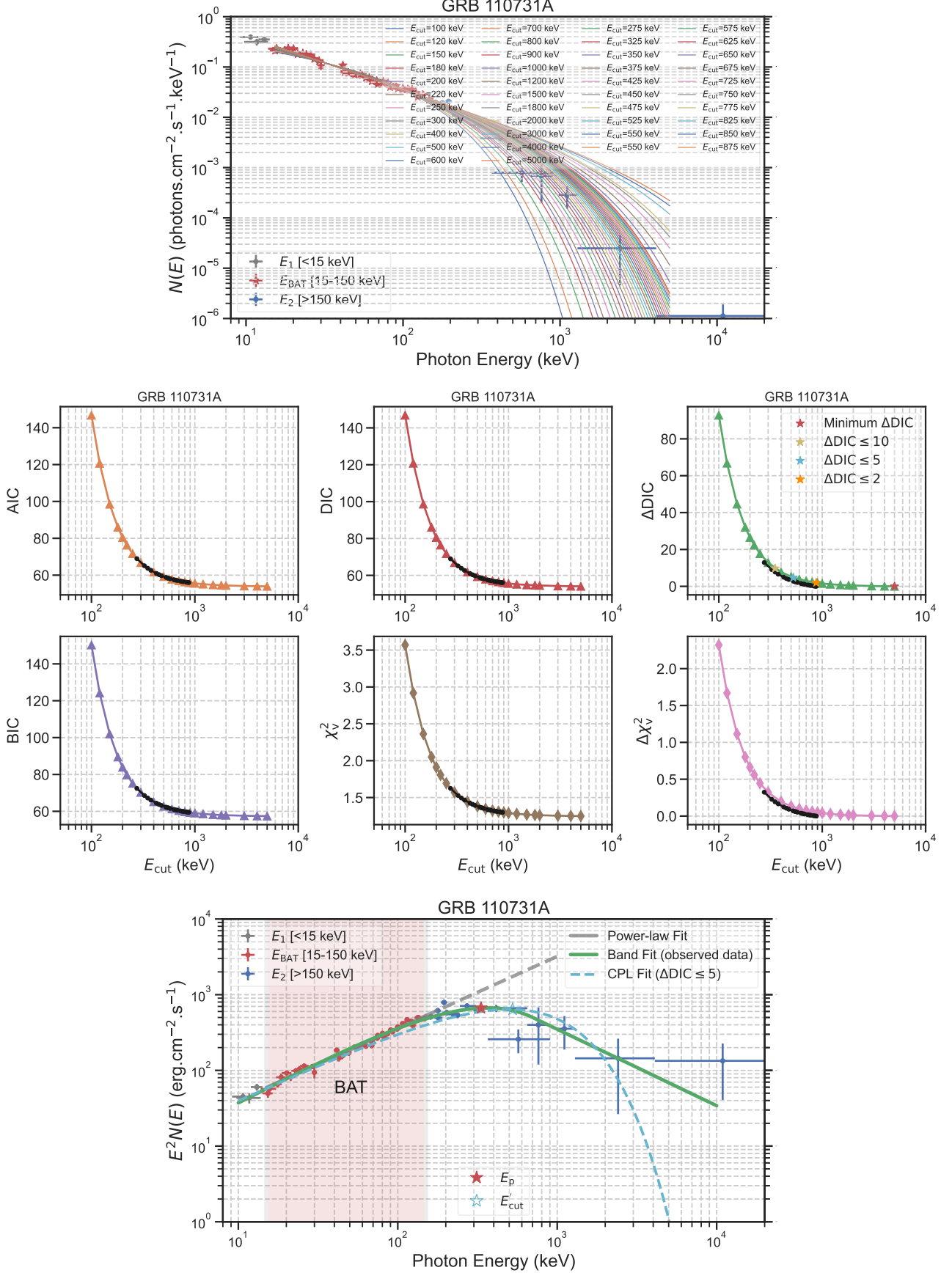


Figure 16. Same as Figure 15 but for GRB 110731A. Note that the best Band model fit to the original spectral data from GBM observation gives $E_p=366\pm27$ keV, $A=(4.8\pm0.2)\times10^{-2}$, $\alpha=-0.90\pm0.03$, $\beta=-3.0\pm0.7$.

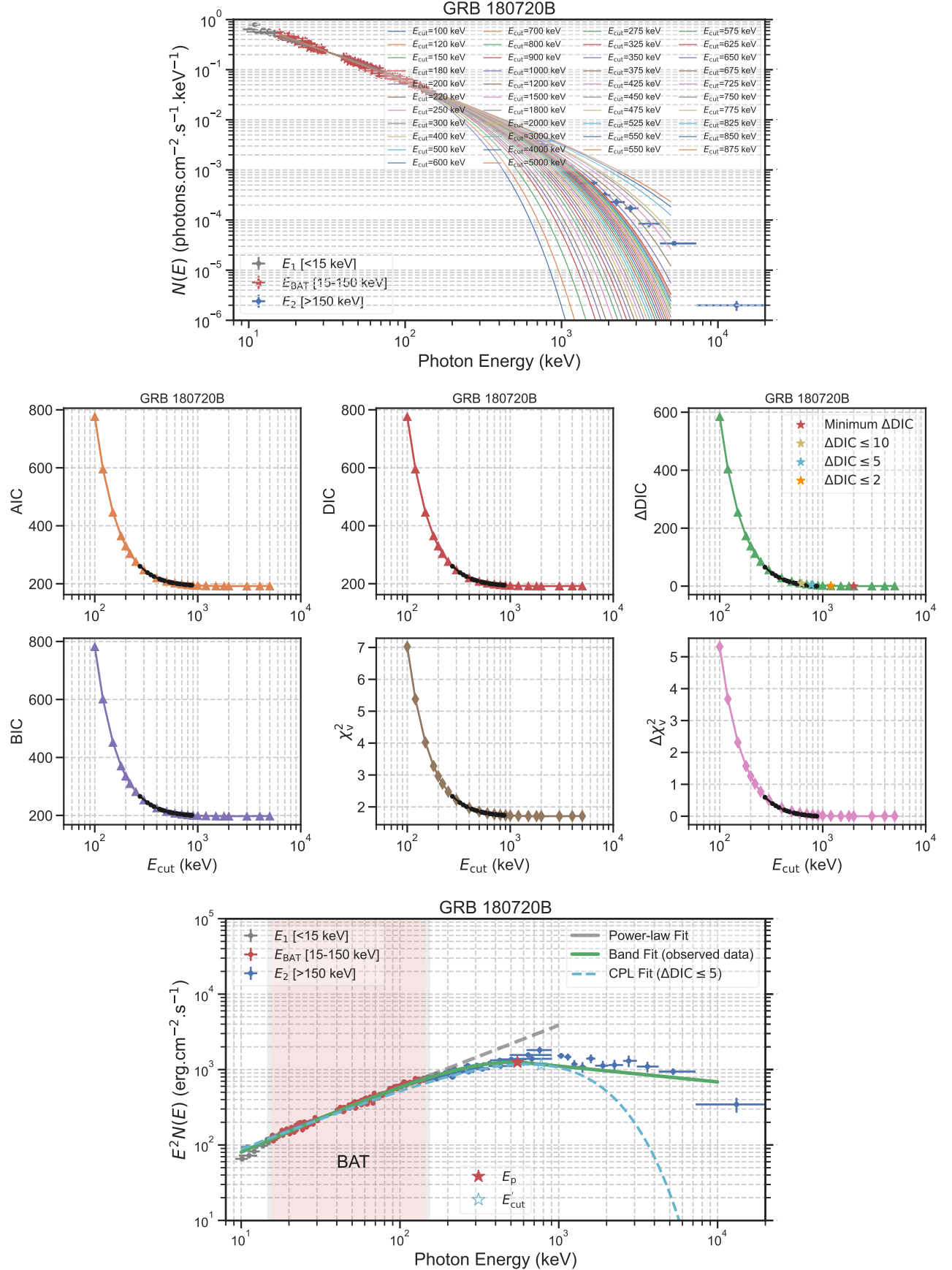


Figure 17. Same as Figure 15 but for GRB 180720B. Note that the best Band model fit to the original spectral data from GBM observation gives $E_p=511\pm26$ keV, $A=(7.0\pm0.1)\times10^{-2}$, $\alpha=-1.07\pm0.01$, $\beta=-2.21\pm0.03$.

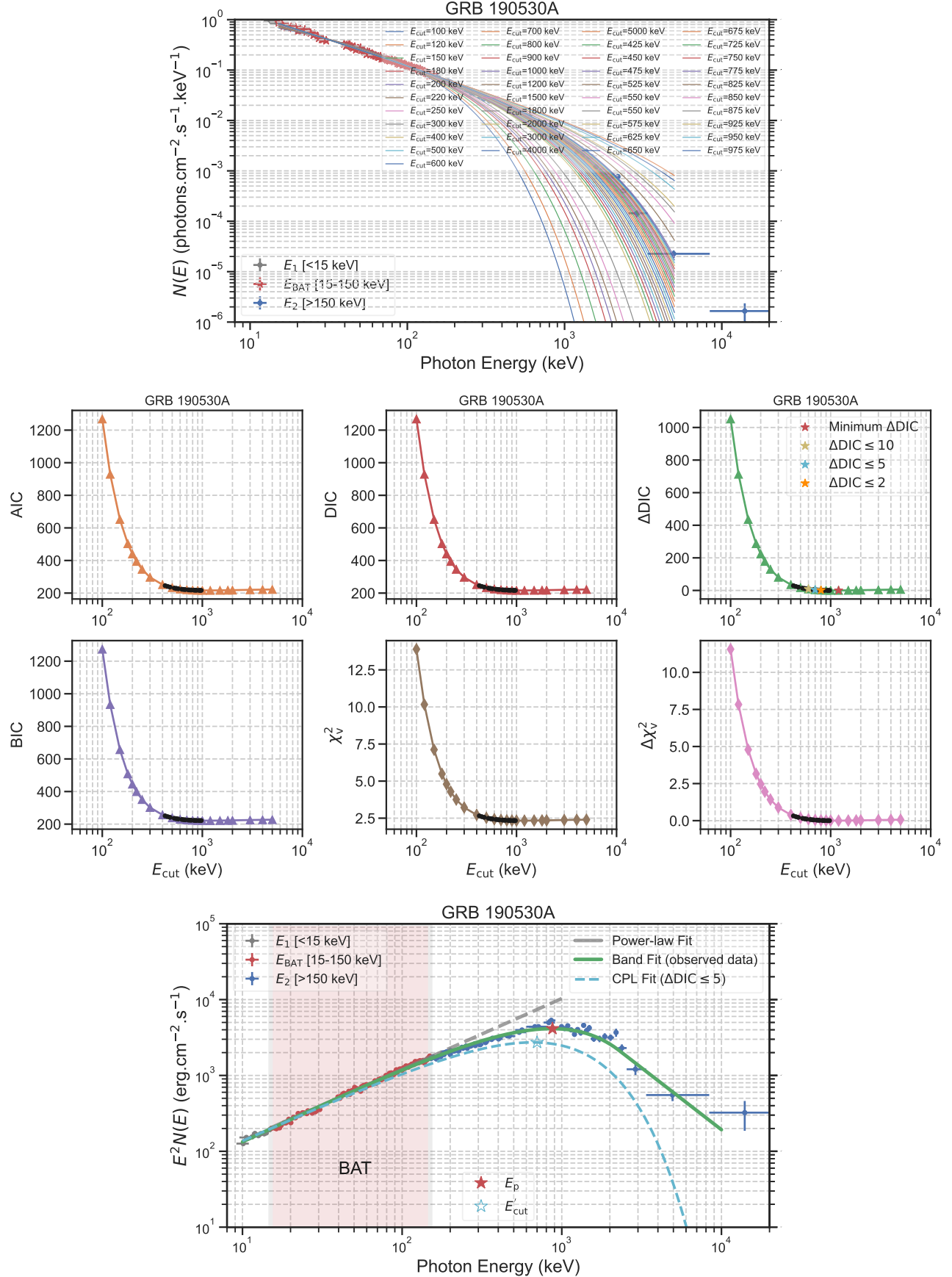


Figure 18. Same as Figure 15 but for GRB GRB 190530A. Note that the best Band model fit to the original spectral data from GBM observation gives $E_p=866\pm 13$ keV, $A=(1.3\pm 0.01)\times 10^{-1}$, $\alpha=-1.01\pm 0.01$, $\beta=-3.63\pm 0.20$.

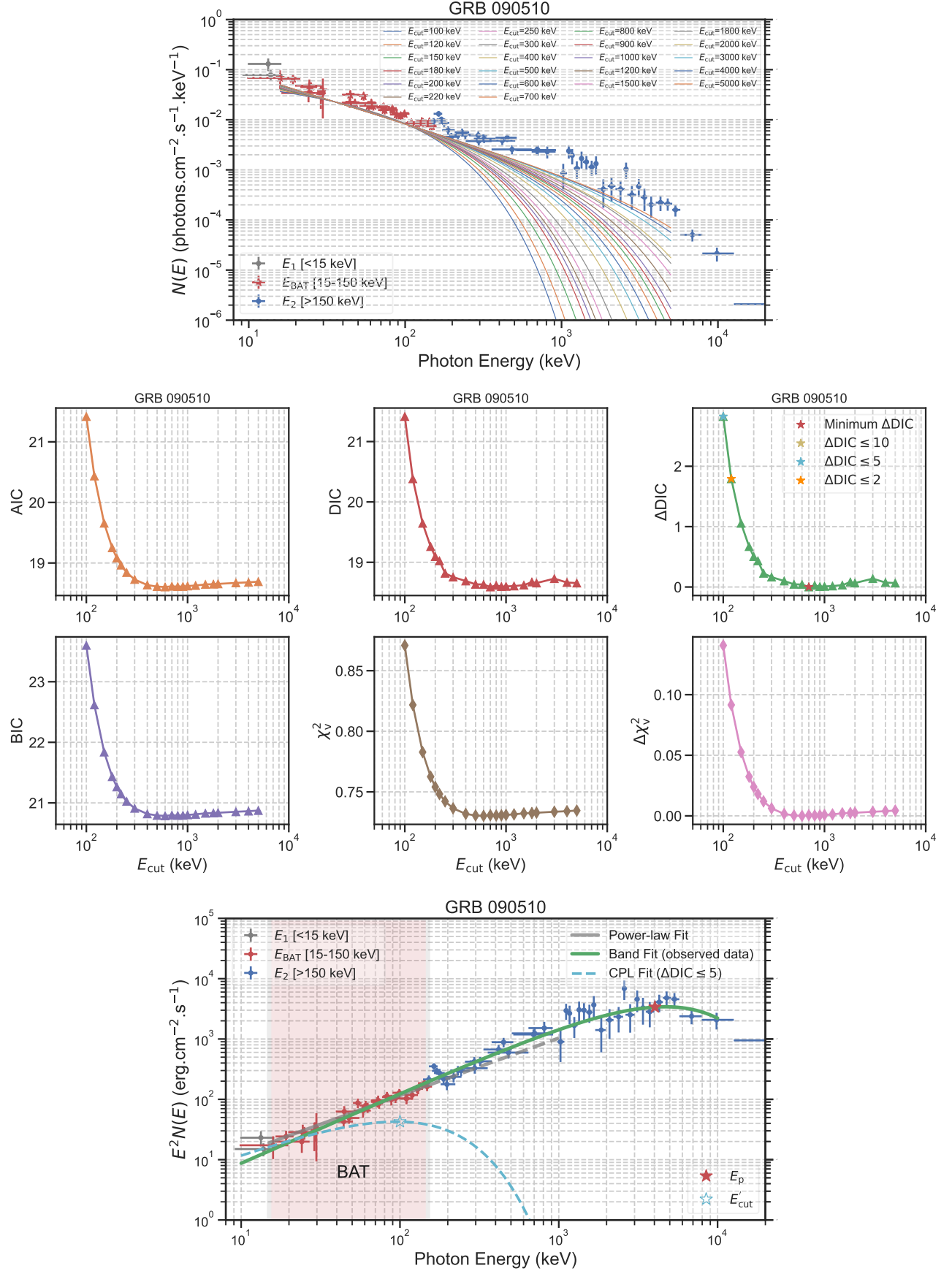


Figure 19. Same as Figure 15 but for GRB GRB 090510. Note that the best Band model fit to the original spectral data from GBM observation gives $E_p = 5200^{+574}_{-584}$ keV, $A = (9.0 \pm 0.4) \times 10^{-3}$, $\alpha = -0.89 \pm 0.04$, $\beta = 3.4 \pm 1.3$.

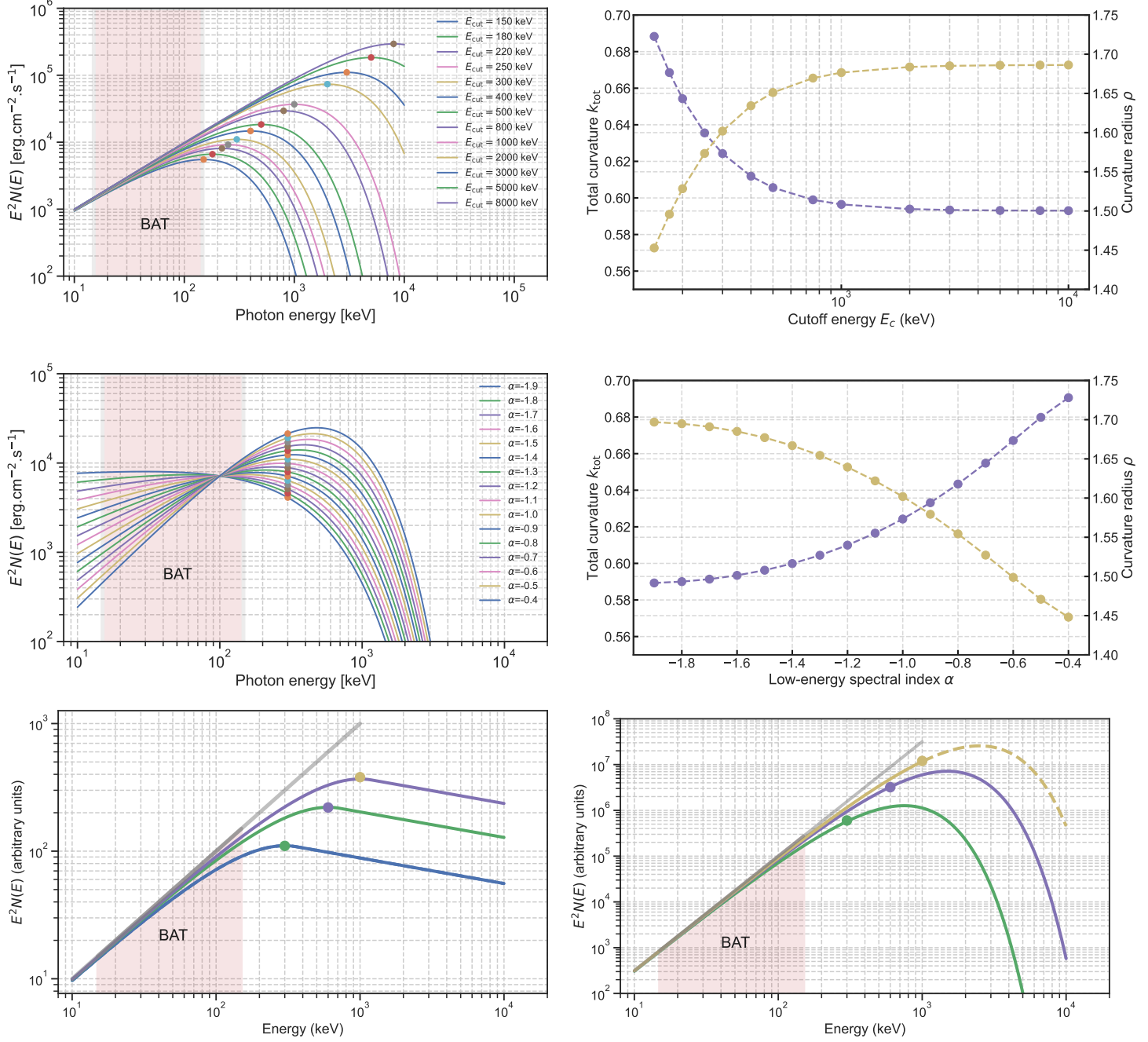


Figure 20. **a,** Spectra of CPL models with the same low-energy power-law index α but different fixed E'_c values, plotted in the νF_ν space. The solid points in different colors represent the corresponding cut-off energies E'_c values. **b,** Total curvature and the associated curvature radius as a function of E'_c . **c,** Same as (a) but for variations in the α index. **d,** Same as (b) but for variations in the α index. **e,** Spectra of Band models with different peak energies ($E_p=300$ keV, 600 keV, and 1000 keV), as well as the baseline power-law model (the same A fixed 1 and α fixed -1). **f,** Same as (e), but for the CPL model.

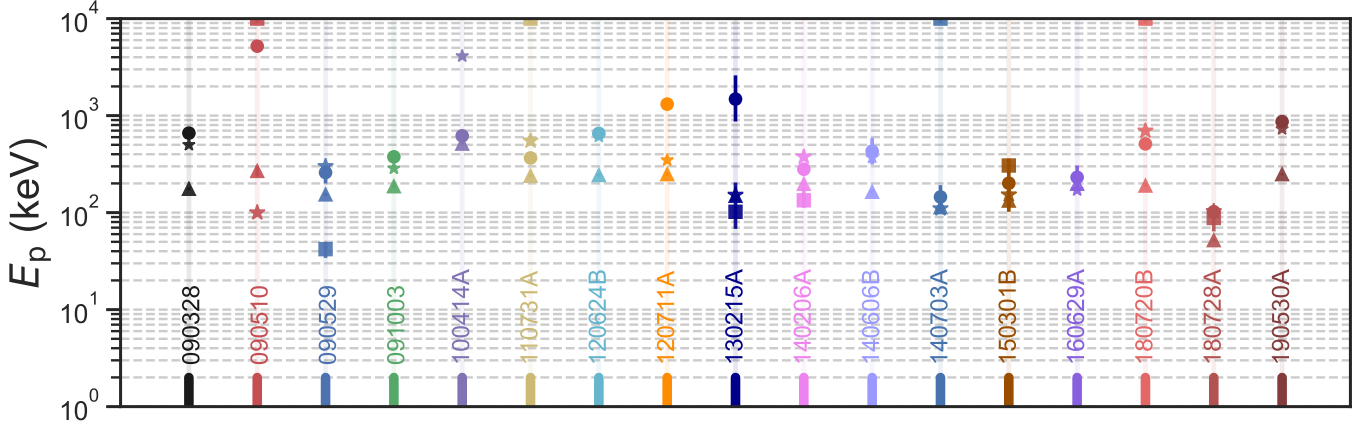


Figure 21. Comparison of several methods for estimating the E_p of *Swift* GRBs. The solid circles represent the true observed E_p values, the stars denote the E_p values estimated using our spectral curvature extrapolation method, the triangles indicate the E_p values derived from the empirical relation proposed by Sakamoto et al. (2009), and the squares show the E_p values provided by the Science Data Centre website based on BAT data fitting. Different colors correspond to different bursts.

APPENDIX

In this appendix, we present the amplitude normalization for different CPL models (Section A1).

A1. AMPLITUDE NORMALIZATION

Details of the amplitude normalization procedure for different E_c values are provided here. According to the definition, we have:

$$N(E) = A \left(\frac{E}{E_{\text{piv}}} \right)^\alpha \exp(-\frac{E}{E_c}), \quad (\text{A1})$$

We consider two specific CPL spectra: one with the intrinsic cutoff energy ($E_{c,0}$), denoted as $N_0(A_0, \alpha_0, E_{c,0})$, and another with a different cutoff energy, denoted as $N_i(A_i, \alpha_i, E_{c,i})$. When $E \ll E_c$, it follows that:

$$\frac{E}{E_c} \approx 0, \quad e^{(-\frac{E}{E_c})} \approx 1. \quad (\text{A2})$$

and we require $N_0 = N_i$, we can derive:

$$A_0 \left(\frac{E}{E_{\text{piv},0}} \right)^{\alpha_0} = A_i \left(\frac{E}{E_{\text{piv},i}} \right)^{\alpha_i}, \quad (\text{A3})$$

since α indices are fixed, one has:

$$\alpha_0 = \alpha_i = \alpha. \quad (\text{A4})$$

Consequently, the final result is:

$$A_i = A_0 \left(\frac{E_{\text{piv},i}}{E_{\text{piv},0}} \right)^\alpha. \quad (\text{A5})$$